ENHANCING CYTOTOXIC T CELL KILLING BY PTEN DEPLETION

A Dissertation

Presented to the Faculty of the Weill Cornell Graduate School

of Medical Sciences

in Partial Fulfillment of the Requirements for the Degree of

Doctor of Philosophy

by

Benjamin Mathias Whitlock

May 2018

ENHANCING CYTOTOXIC T CELL KILLING BY PTEN DEPLETION

Benjamin Mathias Whitlock, Ph.D.

Cornell University 2018

The immunological synapse (IS) is a dynamic structure formed between lymphocytes and antigen presenting cells. Previous work has shown that enhancing PI3K signaling by depletion of the lipid phosphatase PTEN increases the size of the IS. In addition, cytotoxic T lymphocytes (CTLs) lacking PTEN exhibit increased killing capacity *in vitro*. We discovered that CTL force exertion across the IS is coordinated with the release of the toxic proteins perforin and granzyme and is correlated with specific lysis of target cells. We connected these two observations and proposed a model in which T cells use mechanical force at the IS to alter the tension of the target cell plasma membrane, increasing target cell susceptibility to perforin. Adoptive T cell therapies have shown the potential to transform the treatment of some forms of cancer and are of great interest to clinicians. We hypothesized that increasing the killing efficacy of the transferred T cells would increase the effectiveness of these treatments. Accordingly, we assessed the potential of PTEN deficiency to boost anti-cancer responses in a subcutaneous transplantable tumor model. We found that depletion of PTEN in CTLs resulted in reduced tumor rejection relative to wild type control CTLs. Our work indicated that this decrease in tumor rejection stemmed from reduced persistence of PTEN deficient CTLs *in vivo*. We examined the contributions to persistence from migration, survival, and homeostatic proliferation. We found that PTEN deficient CTLs have reduced migration and homeostatic proliferation, which results in diminished persistence *in vivo*. Our work

highlights the importance of migration and homeostatic proliferation in developing an anti-tumor response.

ACKNOWLEDGEMENTS

During my time in graduate school, I have experienced great personal and intellectual growth. This would not have been possible without the immense support and guidance from my advisors Dr. Morgan Huse and Dr. Grégoire Altan-Bonnet. They have nurtured my intellectual development while giving me the opportunity to explore my own interests. I am grateful for everything they have taught me during my graduate studies. I would also like to thank my committee members Dr. Joseph Sun, Dr. Michael Overholtzer, and Dr. David Scheinberg for their direction and advice throughout my doctoral studies.

I would also like to thank all the current and former members of the Huse and Altan-Bonnet laboratories. From the Altan-Bonnet laboratory, I would specifically like to thank Dr. Jennifer Oyler-Yaniv, Dr. Alon Oyler-Yaniv, Dr. Robert Vogel, Dr. Guillaume Voisinne, and Carly Ziegler. From the Huse laboratory, I would like to thank Niels Bantilan, Dr. Thinh Nguyen Duc, Dr. Xin Liu, Dr. Roshni Basu, Dr. Audrey Le Floc'h, Dr. Anne Chauveau, Dr. Jacquelyn Brown, Miguel Francisco M. de Jesus, Dr. Tyler El Rayes, Christina Firl, Dr. Maria Tello Lafoz, Elisa Sanchez, Brian Santich, Dr. Fella Tamzalit, Diana Tran, Mitchell Wang, and Dr. Minggang Zhang. I would also like to thank the laboratories of Drs. Andrea Schietinger, Ming Li, and Joseph Sun for sharing equipment, reagents, and ideas. I would also like to thank our collaborators Weiyang "Susie" Jin and Dr. Lance Kam of Columbia University. It has been a pleasure working and learning alongside all of you for the past seven years.

I have made many friends in and out of the laboratory during my time in New York and I would like to thank all of them for their constant support. My schedule has been difficult and sometimes unpredictable but they have nevertheless been understanding. I could not have completed this without them. I would like to thank my brother Samuel Moore, my mother Penelope Moore, my father David Whitlock, my aunt Dr. Nicola Moore, and my grandmother Dr. Sally Falk Moore for their love, support, and encouragement. I would also like to thank Dr. Alison Thaler for her endless support.

TABLE OF CONTENTS

LIST OF FIGURES

LIST OF ABBREVIATIONS

ACT	adoptive cell therapies
AFM	atomic force microscope
AKT	protein kinase B
APC	antigen presenting cell
Arp2/3	actin related protein-2/-3 complex
Bak	BCL2 Antagonist/Killer 1
Bax	BCL2 Associated X
Bcl-2	B-cell lymphoma 2
BID	BH3 interacting-domain death agonist
Ca^{2+}	calcium
CAR	chimeric antigen receptor
CCL19	C-C motif chemokine ligand 19
CCL21	C-C motif chemokine ligand 21
CCR7	C-C chemokine receptor type 7
CD62L	L-selectin
COG	center of gravity
cSMAC	central supramolecular activation cluster
CTLA-4	cytotoxic T-lymphocyte-associated protein 4
CTLs	cytotoxic T lymphocytes
DAG	diacylglycerol
DD	death domain
Dock2	dedicator of cytokinesis 2
DPP	distance to displaced pillar
dSMAC	distal supramolecular activation cluster
ERK	mitogen-activated protein kinase
F-actin	filamentous actin
FADD	Fas associated death domain
FasL	Fas ligand
FOXO1	forkhead box protein O1
GEF	guanine nucleotide exchange factor
GFP	green fluorescent protein
HBSS	Hank's balanced salt solution
HER-2	human epidermal growth factor receptor 2
HEVs	high endothelial venules
i.v.	intravenous
ICAM-1	intercellular adhesion molecule 1
IFNγ	interferon gamma
IL-2	interleukin-2
IL-7	interleukin-7

IL-7Rα	interleukin-7 receptor alpha
IL-15	interleukin-15
IP_3	inositol 1,4,5-trisphosphate
IS	immunological synapse
ITAMs	immunoreceptor tyrosine-based activation motif
KLF2	Krüppel-like Factor 2
LAG-3	lymphocyte-activation gene 3
LAT	linker for activation of T cells
Lck	lymphocyte-specific protein tyrosine kinase
LCMV	lymphocytic choriomeningitis
LDH	lactate dehydrogenase
LG	lytic granules
LPS	lipopolysaccharides
MCA	methylcholanthrene
MEK	mitogen-activated protein kinase kinase
MHC	major histocompatibility complex
MMP	matrix metalloproteinase
mTOR	mammalian target of rapamycin
mTORC1	mammalian target of rapamycin complex 1
mTORC2	mammalian target of rapamycin complex 2
NFAT	muclear factor of activated T-cells
NFκB	nuclear factor kappa-light-chain-enhancer of activated B cells
NK	natural killer
NMII	nonmuscle myosin II
Nur77	nerve growth factor IB
OT-1	TCR specific for the OVA peptide
OVA	ovalbumin257–264 peptide
PBMC	peripheral blood mononuclear cell
PD-1	programmed cell death protein 1
PD-L1	programmed death-ligand 1
PDK1	phosphoinositide-dependent kinase-1
PDMS	polydimethylsiloxane
pHluorin	pH-sensitive GFP
PI	propidium iodide
PI3K	phosphoinositide 3-kinase
PIP_2	phosphatidylinositol-4,5-bisphosphate
PIP_3	phosphatidylinositol-3,4,5-trisphosphate
PKCθ	protein kinase C theta
PLCγ	phospholipase gamma
PNAd	peripheral node addressin
poly(I:C)	Polyinosinic:polycytidylic acid
pSMAC	peripheral supramolecular activation cluster

PTEN	phosphatase and tensin homolog
RAG	Recombination-activating gene
$RAG^{-/-}$ $\gamma_C^{-/-}$	RAG and common gamma chain double knockout
RASGRP1	RAS guanyl-releasing protein 1
s.c.	subcutaneously
S1P	sphingosine-1-phosphate
S1PR1	sphingosine-1-phosphate receptor 1
shDock2	shRNA targeting Dock2
shMyH9	shRNA targeting the myosin heavy chain MyH9
shNT	nontargeting shRNA
shPTEN	shRNA targeting PTEN
shRNA	short hairpin RNA
SLP76	lymphocyte cytosolic protein 2
tBID	truncated BID
TCR	T cell receptor
TIM-3	hepatitis A virus cellular receptor 2
TLR3	Toll like receptor 3
TNFα	tumor necrosis factor alpha
Tregs	regulatory T cells
VISTA	V-domain Ig suppressor of T cell activation
WASP	Wiskott–Aldrich syndrome protein
WAVE2	Wiskott-Aldrich syndrome protein family member 2
WT	wild-type
ZAP70	zeta-chain-associated protein kinase 70

CHAPTER 1: INTRODUCTION

1.1. Innate and adaptive immunity

Animals have evolved an immune system to protect against foreign pathogens. The immune system is divided into two branches, which work together to establish host immunity. The first arm of the immune system is the innate immune system, which provides an initial defense against pathogens and can be triggered very quickly but is limited in the scope of molecules it recognizes. The second arm is the adaptive immune system, which is slower to establish a response but can tailor that response to a specific antigen. Innate immune cells have pattern recognition receptors that identify foreign cells and proteins. These cells are important for presenting foreign molecules to cells in the adaptive immune system.

The adaptive immune system is made up of B cells and T cells. The primary role of B cells is to produce antibodies. These antibodies bind to molecules and identify them as foreign to other immune cells. There are two main subtypes of T cells, $CD4^+$ and $CD8^+$ T cells, which are named for the co-receptor the cells express. These subtypes have very distinct roles in driving host immunity. $CD4^+$ T cells differentiate into T-helper cells and $CD8^+$ T cells differentiate into cytotoxic T lymphocytes (CTLs). CTLs are capable of killing malignant or infected cells in addition to producing inflammatory cytokines such as interleukin-2 (IL-2), interferon gamma (IFNγ), and tumor necrosis factor alpha (TNFα)[1].

1.2. T cells

T cells are defined by expression of the T cell receptor (TCR). The TCR is a multisubunit receptor consisting of α-, β-, γ-, δ-, ε-, and ζ-chains. These subunits form a complex that recognizes an antigenic peptide in the major histocompatibility complex (MHC) on an antigen-presenting cell (APC). There are two categories of MHC molecules, which are called class I and class II (referred to as MHC I and MHC II, respectively). The specificity of an αβ T cell for MHC I or MHC II is determined by the co-receptor it expresses. $CD8^+$ T cells recognize peptides presented by MHC I and $CD4^+$ T cells recognize peptides presented by MHC II.

T cell development is a tightly regulated process that has been carefully delineated. T cells differentiate from thymic progenitors that originate in the bone marrow[2]. In the thymus, these cells go through several stages of differentiation to become T cells. T cells undergo programmed rearrangement of the β chain of the TCR to increase diversity of the TCRs[2]. During this process, some TCRs become non-functional and unable to recognize pMHC complexes. These cells undergo programmed cell death during beta selection[2]. Next, cells undergo rearrangements of their α chain and subsequent positive selection[2]. The surviving cells then go through negative selection. This removes T cells with receptors that bind with high affinity to MHC complexes containing host peptides[2]. Negative selection ensures that T cells are removed if they express a TCR that would generate auto-immunity. This process is not completely efficient and some self-reactive T cells survive negative selection. Some of these T cells will differentiate into regulatory T cells (Tregs), which play a crucial role in immune tolerance[3]. After all of these

checkpoints, naïve T cells leave the thymus where they begin the process of surveying the host looking for infected or malignant cells.

1.2.1. T cell signaling

Following the formation of a TCR-pMHC interaction and recognition of an antigenic peptide, many downstream signaling pathways are activated. These signaling events trigger rapid changes in T cell morphology and function. TCR signaling begins with lymphocyte-specific protein tyrosine kinase (Lck), a Src family kinase, phosphorylating the immunoreceptor tyrosine-based activation motifs (ITAMs) on the TCR[4]. ITAMs are signaling motifs contained within the cytoplasmic tails of the CD3 γ-, δ-, ε-, and ζ-chains[5]. Phosphorylated ITAMs recruit the tyrosine kinase zeta-chain-associated protein kinase 70 (ZAP70) to the TCR, where it phosphorylates the scaffolding proteins linker for activation of T cells (LAT) and lymphocyte cytosolic protein 2 (SLP76), inducing them to form a complex. This LAT-SLP76 complex then recruits various downstream signaling proteins including phospholipase gamma (PLCγ), which produces diacylglycerol (DAG) and inositol 1,4,5-trisphosphate (IP_3). IP_3 signaling drives an increase in the level of intracellular calcium (Ca^{2+}), which results in nuclear factor of activated T cells (NFAT) localizing to the nucleus. DAG, in turn allows RAS guanyl-releasing protein 1 (RASGRP1) to be activated leading to the activation of Ras and downstream signaling proteins including mitogen-activated protein kinase (ERK) and mitogen-activated protein kinase kinase (MEK). DAG also induces nuclear factor kappa-light-chain-enhancer of activated B cells (NFκB) signaling through protein kinase C theta (PKCθ)[6]. Following these stages of activation, T cells upregulate activation markers such as CD69 and secrete cytokines

including but not limited to IL-2, IFNγ, and TNFα. These pro-inflammatory cytokines help coordinate an immune response among many cell types.

Activation of RAS also leads to the activation of the phosphatidylinositol-4,5-bisphosphate 3-kinase (PI3K) signaling pathway (Figure 1.1). In the first part of the pathway, PI3K phosphorylates the lipid phosphatidylinositol-4,5-bisphosphate (PIP_2), generating phosphatidylinositol-3,4,5-trisphosphate (PIP_3)[7]. Phosphatase and tensin homolog (PTEN) attenuates PI3K signaling by dephosphorylating PIP_3 to yield PIP_2. PIP_3 binds to and recruits protein kinase B (AKT), localizing it to the plasma membrane and allowing it to be phosphorylated by the regulatory Ser/Thr kinase phosphoinositide-dependent kinase-1 (PDK1). Once phosphorylated, AKT activates a number of pathways controlling cell growth and proliferation. In another arm of the PI3K signaling pathway, PIP_3 recruits the guanine nucleotide exchange factor (GEF) dedicator of cytokinesis 2 (Dock2) to the plasma membrane[8]. This branch of the pathway will be discussed below.

AKT signaling acts through a number of downstream proteins including the mammalian target of rapamycin (mTOR)[7]. mTOR is a complex of several proteins and has two main components named complex 1 and complex 2 (mTORC1 and mTORC2 respectively). mTORC2 has been found to activate AKT, which in turn signals through mTORC1[9]. These complexes play an important role in nutrient sensing and cell growth. AKT also regulates forkhead box protein O1 (FOXO1), which is responsible for controlling expression interleukin-7 receptor alpha (IL-7Rα)[10,11]. An increase in AKT signaling increases mTORC1 and reduces FOXO1 signaling, which reduces expression of the transcription factor Krüppel-like Factor 2 (KLF2). KLF2 is responsible for

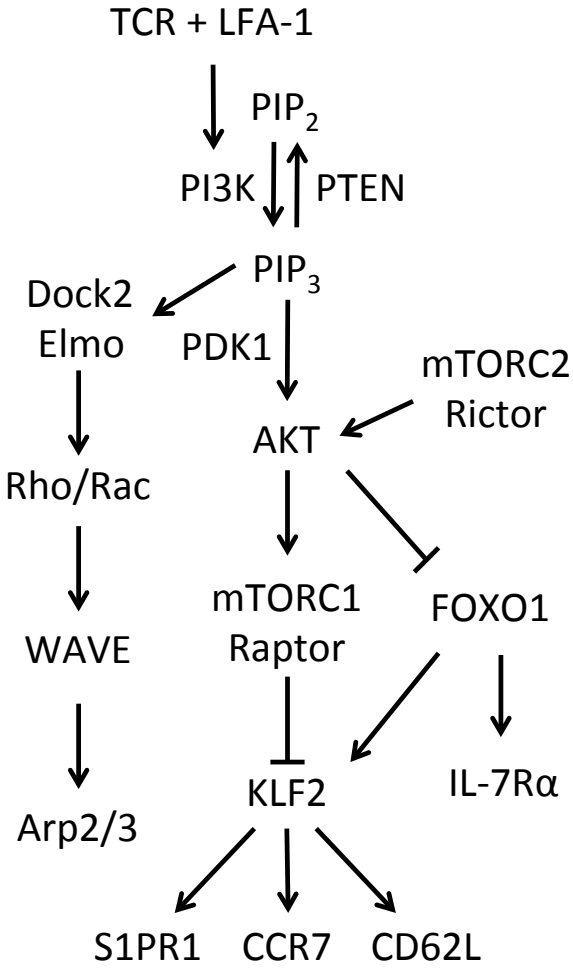

Figure 1.1 Cartoon of the PI3K signaling pathway
T cell activation through TCR and LFA-1 results in the phosphorylation of PIP_2 to PIP_3 by PI3K. PIP_3 accumulation results in several down stream signaling processes. PIP_3 recruits AKT to the plasma membrane, which results in its phosphorylation by PDK1. mTORC2 signals through AKT and increases AKT signaling. AKT phosphorylates FOXO1, which prevents it from localizing to the nucleus and reduces expression of IL-7Rα. AKT also activates mTORC1 and the scaffold Raptor. Increased mTORC1 signaling has been shown to reduce KLF2 expression, which reduces expression of S1PR1, CCR7, and CD62L. PIP_3 also recruits Dock2 and its scaffold Elmo to the plasma membrane. Elmo allows Rac/Rho small GTPases to bind and signals through WAVE complex to Arp2/3 to control actin growth.

regulating the expression C-C chemokine receptor type 7 (CCR7), L-selectin (CD62L), and sphingosine-1-phosphate receptor 1 (S1PR1), which are important regulators of T cell trafficking that will be discussed below.

1.2.2. Immunological synapse

Upon binding of the TCR to pMHC on an APC, T cells undergo dramatic changes in their cytoskeleton creating a structurally stereotyped interface with the APC. This interaction, called the immunological synapse (IS) is an annular structure that resembles a “bulls-eye” with a ring of actin making up the perimeter (Figure 1.2). The IS has been shown to be important for the targeted release of some cytokines and lytic granules (LG)[13,14].

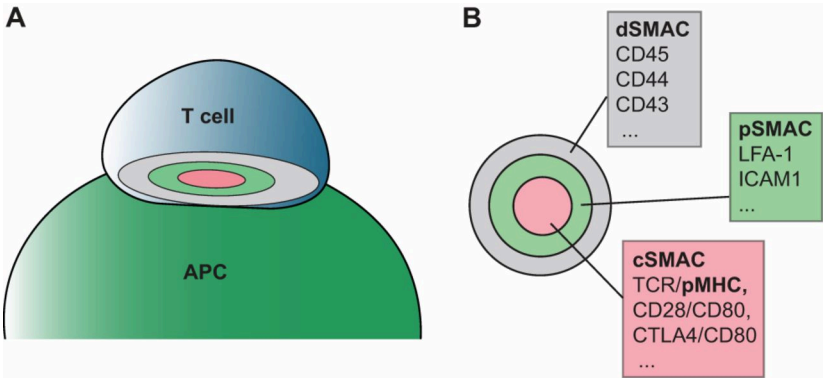

Figure 1.2 Cartoon of the IS between a T cell and an APC
(A) A diagram of a T cell forming a conjugate with an APC. The IS is depicted as a “bulls-eye” structure on the interface. (B) The IS is divided into the dSMAC, pSMAC, and cSMAC. During the formation and maturation of the IS, various proteins are segregated into the different regions. This figure was adapted from Yu, Y. et al.[12].

Following TCR activation, actin polymerization occurs rapidly forming the IS. Previous work has demonstrated that the formation of this annular actin structure depends on PIP_3 accumulation following TCR activation[8]. PIP_3 recruits the GEF Dock2, which induces the activation of the Rho family

GTPase Rac. Activated Rac then signals through the Wiskott-Aldrich syndrome protein family member 2 (WAVE2) to facilitate lamellipodial growth[8,15]. Rac does not interact with WAVE2 directly but interacts with the WAVE complex containing WAVE2, Sra, Nap, and Brk1[15]. WAVE2 then promotes lamellipodial growth through the Arp2/3 protein complex. Arp2/3 initiates the formation of y-branches of actin at the lamellipodia[16,17]. The observation that PIP_3 controls actin dynamics by signaling through Dock2 and Rho/Rac to Arp2/3 does not rule out the possibility that PIP_3 could signal through other molecules that have not been identified.

Segregation of proteins into different regions of the IS called the central, peripheral, and distal supramolecular activation cluster (cSMAC, pSMAC, and dSMAC respectively) has been observed in mature T cell-APC synapses[18]. The cSMAC, which is located at the center of the IS, contains the TCR, CD28, and PKCθ[18,19]. The pSMAC, which surrounds the cSMAC, contains lymphocyte function-associated antigen 1 (LFA-1) and Talin[18]. CD45 is initially localized to the pSMAC, but is then gradually excluded based on the size of its large ectodomain[20]. The dSMAC surrounds the pSMAC in the mature IS and contains the F-actin ring and CD45. CD43 was also found to localize to the dSMAC[21]. Most of the work characterizing the migration of proteins to the different regions of the IS has been performed on lipid bilayers containing stimulatory ligands. In these experiments, T cells form a single IS that resembles a “bulls-eye.” However, the direct implications of this work are unclear as synapses T cell-APC conjugates have been shown to form multiple regions resembling the cSMAC[19,22]. Thus, lipid bilayers are not able to fully recapitulate a proper T cell-APC conjugate. More research utilizing high-

resolution microscopy is needed to examine the precise structure of the T cell-APC IS and to understand its function.

1.2.3. T cell motility

Actin plays a very important role in T cell motility. It allows T cells to migrate through lymphoid organs and the periphery. As T cell move, they develop the classical “hand-mirror” morphology with a leading edge or lamellipodia, consisting of highly branched actin[23]. Lymphocyte motility is driven by the formation of a branched network of actin through the actin related protein-2/-3 complex (Arp2/3), which facilitates actin nucleation events[17]. These nucleation events occur at 70° making a y-shape branch[17]. This process is highly regulated by members of the WAVE and Wiskott–Aldrich syndrome protein (WASP) protein families, which were previously described. The lamellipodial protrusions containing branched actin are also involved in scanning the environment for antigens. Following antigen recognition, the motility of the T cell is reduced and the migration of T cells is halted. This stop signal has been found to be calcium dependent[24].

1.2.4. T cell migration

T cell homing and migration are complex processes that combine chemokine signaling, integrins, and adhesion receptors. Naïve T cells circulate among lymph nodes through lymphatic vessels and blood[25]. T cells use CD62L to roll on high endothelial venules (HEVs) and to resist hemodynamic flow (Figure 1.3). Upon activation, T cells shed CD62L by cleavage with matrix metalloproteinase (MMPs)[26]. CD62L recognizes mucin like glycoproteins called peripheral node addressin (PNAd). These proteins include which include CD34, podocalyxin, endomucin, nepmucin, and glycosylation-

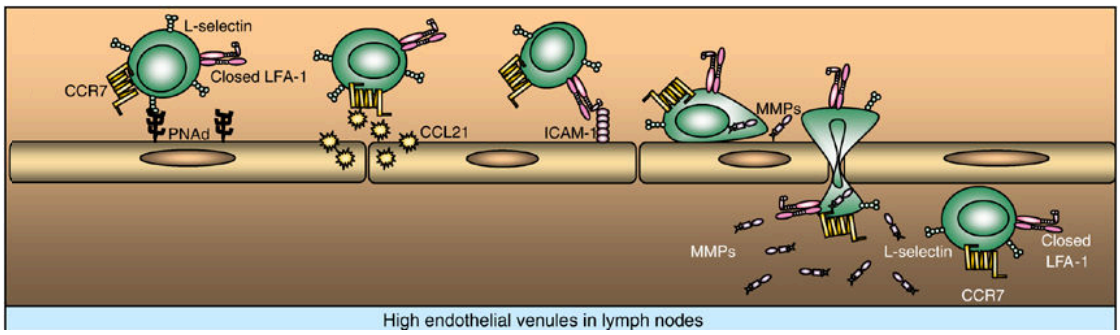

Figure 1.3 T cell migration on HEVs
T cells migrate through the circulatory system by rolling on HEVs. Rolling is facilitated by CD62L binding to molecules on the HEVs including PNAd. Epithelial cells secrete CCL19 and CCL21, which upregulate LFA-1 on the T cell. LFA-1 on the T cell surface binds to ICAM-1 on the epithelial cells and stops the T cell from rolling. T cells begin extravasating in between the epithelial cells. During this process, MMPs cleave CD62L on the T cells. This figure was adapted from Lewis, M. et al.[27].

dependent cell adhesion molecule 1, and endothelial-expressed P-selectin glycoprotein ligand 1[25,28]. T cells rolling on HEVs express CCR7 and thus respond to the C-C motif chemokine ligand 19 and 21 (CCL19 and CCL21 respectively). These chemokines are produced by the endothelial cells on HEVs[29]. These signals upregulate LFA-1 on the T cells resulting in increased adhesion to the HEVs, which express LFA-1's binding partner intercellular adhesion molecule 1 (ICAM-1)[29]. Thus begins the extravasation process whereby T cells leave the circulatory system through the HEVs and enter the lymph node[25,28]. T cells extravasate from the blood into the paracortex of lymph nodes. Here naïve T cells scan dendritic cells in search of their cognate peptide. If antigens are not detected, T cells will migrate to another lymph node through the lymphatic vessels after 6-12 hours[28,30]. Memory T cells reside close to HEVs, which positions them in a good location for encountering APCs cells traveling through the lymphatics[31]. In the paracortex, naïve T cells upregulate S1P1R1, which is the receptor that recognizes sphingosine-1-

phosphate (S1P)[25]. Experiments utilizing pertussis toxin (an inhibitor of G-protein coupled receptors) and the small molecule FTY720, which induces S1P1R1 downregulation, have demonstrated the importance of S1P signaling in maintaining T cells in the lymph node[32,33]. When S1P signaling is blocked with either of these agents, lymphocytes are unable to egress and, as a result, accumulate in the lymph nodes.

The migration of T cells towards APCs expressing their cognate antigen is two sided as APCs also migrate in search of T cells. When a dendritic cell is primed in the periphery, it matures, upregulating CCR7 and traveling through lymphatics to the draining lymph node where it comes into contact with T cells. In lymph nodes, a single APC is capable of scanning at least 500 T cells per hour[34]. This suggests that in an hour 200 APCs are sufficient to identify a single antigen specific T cell in 10^5 cells[34]. Over several days, T cells are capable of scanning orders of magnitude more APCs. An important consideration in these calculations is that scanning cannot occur too fast or the T cell will be unable to properly recognize its cognate antigen. As a result, T cells balance their ability to scan a wide variety of cells quickly with the need to spend enough time on each contact to allow the T cell to become activated[35].

This scanning process is enabled by several characteristics of T cell signaling. This process is aided by the fact that TCRs are highly sensitive and a T cell is capable of recognizing a single pMHC molecule *in vitro*[36]. T cell signaling has been shown to be digital in nature[37]. These characteristics allow T cells to scan a large number of antigens while maintaining their high specificity for their cognate peptide. The process of naïve T cell migration

through secondary lymphoid organs has been characterized as a random walk[38]. This differs from the migration pattern of effector or memory T cells, which undergo chemotaxis towards an area of injury or inflammation[39].

As cancerous cells proliferate and establish a tumor, these cells require additional nutrients. To resolve this problem, tumors undergo angiogenesis to generate their own vasculature. This increases the ability of lymphocytes to infiltrate tumors. One way that tumors evade detection by the immune system is to evolve ways of preventing lymphocyte extravasation from blood. They achieve this by down-regulating ICAM-1 and other integrins[40]. As a solid tumor grows, the environment in its interior becomes hostile for lymphocytes[40]. This results in tumor infiltrating lymphocytes dying and becoming dysfunctional[41,42]. How to increase lymphocyte migration to tumors and to prevent or reverse their dysfunction is an active area of research.

T cells that migrate to the tumor and survive its inhospitable environment are exposed to a number of signals to reduce their activity. Parallels have been drawn between dysfunctional T cells found in solid tumors and T cell exhaustion that occurs from chronic infections such as HIV[41,43]. T cells in mice infected with lymphocytic choriomeningitis virus (LCMV) clone 13 become exhausted and have reduced proliferation and cytokine production upon restimulation[42,44,45]. These cells express high levels of the inhibitory receptor programmed cell death protein 1 (PD-1). This is thought to occur in response to chronic antigen stimulation through the TCR and perpetual exposure to an inflammatory environment[42]. It is conceivable that reversal of this dysfunctional phenotype would result in an increased immune response against the infection or cancer. Thus, this is an active area of research. Some

approaches that are thought to reverse the tolerogenic environment of the tumor will be discussed below.

1.2.5. Apoptosis

The ability of cells to undergo programmed cell death is critical for homeostasis. The acquired ability of cells to evade apoptosis and to become resistant to programmed cell death is one of the hallmarks of cancer[46]. The process of undergoing apoptosis is tightly regulated with many checkpoints to ensure that it does not happen unintentionally.

One way cells undergo apoptosis is in response to Fas signaling, which is initiated after trimeric FasL engages trimeric Fas (Figure 1.4)[47]. Binding of Fas ligand (FasL) exposes the death domain (DD) protein motif on the intracellular tail of Fas[47]. This results in the recruitment of Fas associated death domain (FADD), which in turn recruits pro-caspase-8 to the receptor. Pro-caspase-8 is then cleaved into its active form of caspase-8. The next step varies between cell types, which undergo either Type I or Type II apoptosis. In Type I cells, caspase-8 directly cleaves pro-caspase-3 to caspase-3, and induces cell death. In Type II cells, caspase-8 cleaves BH3 interacting-domain death agonist (BID) into truncated BID (tBID). In healthy cells, BID is located on the mitochondrial membrane and is a pro-apoptotic member of the B-cell lymphoma 2 (Bcl-2) family of proteins. tBID interacts with Bcl-2 associated X (Bax) and Bcl-2 antagonist/killer 1 (Bak), triggering their insertion into the mitochondrial membrane, which permeabilizes it. In cells that do not undergo apoptosis, pro-survival Bcl-2 family proteins sequester Bax and Bak on the mitochondrial surface and prevent them from puncturing the mitochondrial membrane[48]. These pro-survival proteins include Bcl-2, BCL2 Like 1 (Bcl-XL),

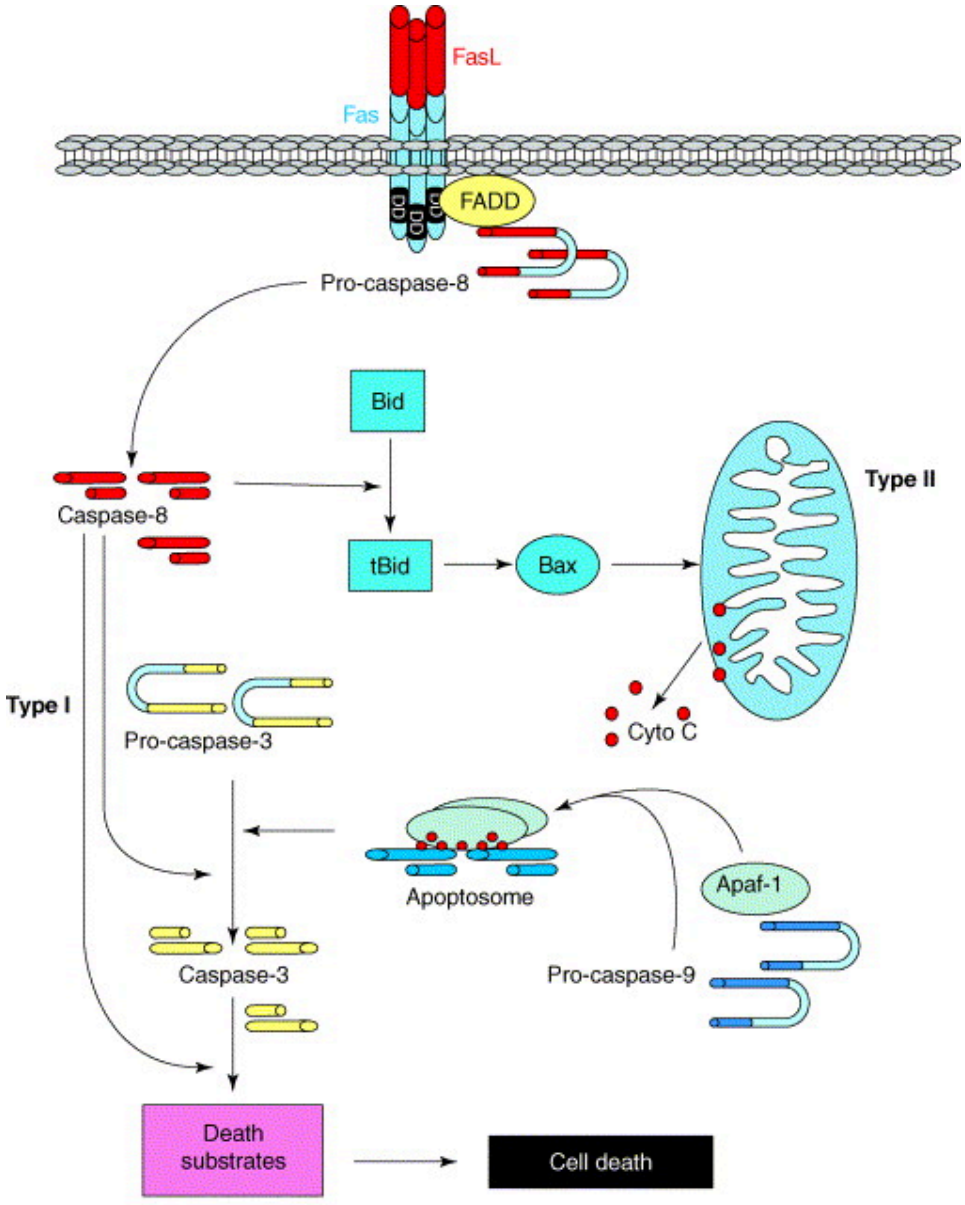

Figure 1.4 Cartoon of Fas induced apoptosis
Apoptosis can be triggered by binding of FasL to Fas. That results in exposure of DD and binding of FADD, which then cleaves pro-caspase-8. In cells undergoing Type I apoptosis, caspase-8 can cleave pro-caspase-3, which is a hallmark of apoptosis. In cells undergoing Type II apoptosis, caspase-8 cleaves BID to tBID. This activates Bax and Bak resulting in the permeabilization of the mitochondrial membrane and the release of cytochrome C. Cytochrome C then forms the apoptosome with Apaf-1, which then cleaves caspase-3 to induce apoptosis. This figure was modified from Houston, A. et al.[47].

and myeloid cell leukemia sequence 1 (MCL-1). Following permeabilization of the outer mitochondrial membrane, cytochrome C is released. This event is considered to be the point of no return for cells undergoing apoptosis. The release of cytochrome C leads to the formation of the apoptosome, a 7 subunit protein complex consisting of cleaved cytochrome C and apoptotic protease activating factor 1 (Apaf-1). The apoptosome then cleaves pro-caspase-9 into caspase-9, which cleaves and activates pro-caspase-3, which leads to cell death.

1.2.6. Lymphocyte cytotoxicity

As $CD8^+$ T cells differentiate into CTLs, they upregulate proteins responsible for killing, namely FasL, perforin, and a number of granzymes. These proteins are contained within LGs, which are secretory lysosomes. LGs are also expressed and released by natural killer (NK) cells, which use the same cytotoxic machinery as CTLs. The contents of LGs are released following TCR stimulation of CTLs. Here we present the mechanics of how the release of FasL, granzymes, and perforin are coordinated to induce apoptosis.

One way that cytotoxic lymphocytes induce death in target cells is through Fas. Ligation of FasL to Fas induces signaling that leads to apoptosis. Cell death through Fas signaling occurs more slowly than granzyme and perforin mediated cytotoxicity but is still an important mechanism for inducing cell death[49]. There are five granzymes in humans and ten in mice[50]. Granzymes are serine proteases that have many targets within cells. Granzyme B is the most highly expressed and most studied granzyme[51]. In CTLs, granzyme B is one of the most highly expressed proteins and is expressed at similar levels to actin. Targets of granzyme B include but are not

limited to caspase-3, caspase-7, caspase-9, and caspase-10. There have been reports that granzyme B cleaves BID into tBID; however, these reports have been disputed[52,53]. Granzymes have also been shown to play a role in host defense against intracellular pathogens[54,55]. Granzyme A induces cell death by triggering DNA damage[51]. The other granzymes induce cell death through a variety of other mechanisms, many of which are not known. Cells treated with granzymes do not undergo apoptosis as granzymes are unable to penetrate the plasma membrane. Cytotoxic lymphocytes puncture the plasma membrane using perforin, a protein that forms pores in a calcium dependent manner. Perforin is stored in an inactive form in LGs at low pH. Upon lymphocyte activation, perforin is released and forms pores 12-17nm in diameter on the target cell membrane[56].

The current model for perforin and granzyme mediated death begins with the cytotoxic lymphocyte releasing the contents of LGs into the space between itself and target cell (Figure 1.5)[57]. Perforin forms holes in the plasma membrane, which trigger an influx of Ca^{2+} in the target cell[57,58]. Perforin has been found to form pores within minutes of cytotoxic lymphocyte-target cell interactions[59]. The influx of Ca^{2+} initiates membrane repair mechanisms, which involve endocytosis of the target cell plasma membrane for repair[57]. This brings perforin and granzyme from the extracellular space into the target cell in endosomes. Inside endosomes, perforin makes holes in the membrane releasing granzymes into the cytoplasm. Once in the cytoplasm, granzymes induce cell death through caspase dependent and independent mechanisms as discussed above[60].

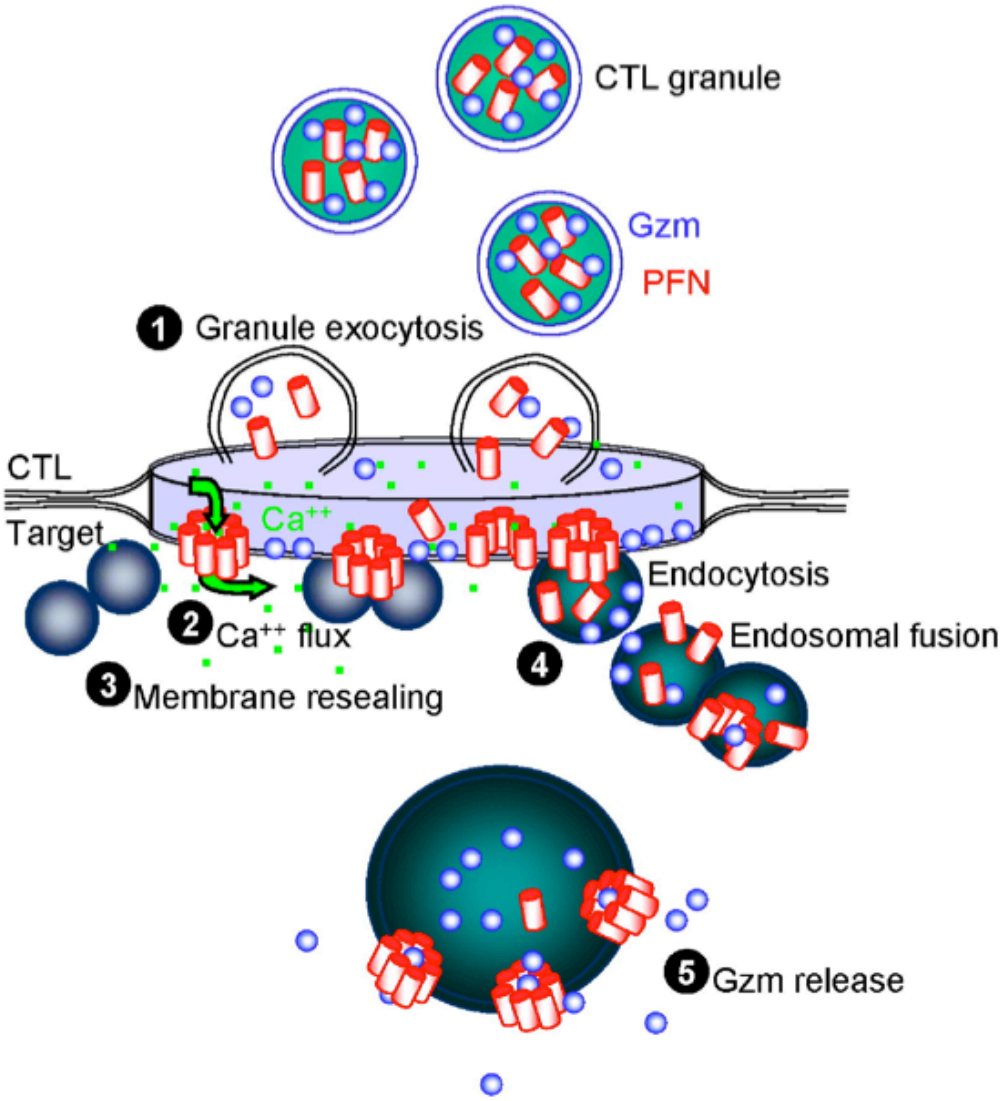

Figure 1.5 Cartoon of perforin and granzyme release and entry into target cells

(1) Lytic granules are secreted from the cytotoxic lymphocyte into the space between the lymphocyte and target cell through the immunological synapse. Perforin forms holes in the target cell plasma membrane, which triggers an influx of Ca^{2+} (2). This influx of calcium initiates membrane repair mechanisms that result in membrane resealing (3). This then results in endocytosis of the plasma membrane, creating endosomes containing perforin and granzyme (4). Inside the endosomes, perforin makes holes in the endosome membrane releasing granzyme, which triggers apoptosis. This figure was modified from Keefe, D. et al.[57].

Researchers have examined the roles of granzyme A, granzyme B, and perforin in spontaneous and subcutaneous tumor growth experiments. Perforin is indispensible for tumor rejection; however both granzyme A and granzyme B are not required[61]. This suggests that there is some overlapping function for granzymes and that if one granzyme is missing others are able to compensate for it. Experiments to assess cytotoxicity of cells isolated from mice knocked out for every granzyme have not been performed. However, mice lacking perforin have a dramatic defect in cytotoxicity of CTLs and NK cells[61,62].

Perforin deficient mice also experience increased rates of tumor development in the methylcholanthrene (MCA) induced tumor model[63]. These experiments demonstrate the unique role perforin plays in cytotoxicity. Perforin appears to have an additional role in regulation of the immune system as patients with familial hemophagocytic lymphohistiocytosis have nonsense mutations in the perforin gene[64]. The importance of perforin to suppress the immune system has also been shown for mice infected with LCMV clone 13. Perforin deficient mice infected with LCMV clone 13 experienced decreased survival due to over expansion of $CD8^+$ T cells[65]. This stems from uncontrolled inflammation produced by viral specific $CD8^+$ T cells. Treating mice with antibodies to deplete $CD8^+$ T cells and to block cytokines prolongs survival[66]. Furthermore, mice deficient for both perforin and Fas show an increase in lymphoproliferative disease relative to mice deficient for Fas and heterozygous for perforin[65]. These results highlight a key role for perforin and Fas outside of lymphocyte cytotoxicity in maintaining immune homeostasis.

1.2.7. Mechanobiology of T cell activation

Recent work has provided insight into how the TCR can distinguish single amino acid substitutions in short peptides. Previous research has shown that the ζ-chain of the TCR undergoes conformational changes to expose phosphorylation sites in its ITAM domains[67]. Other work has shown that the TCR is an anisotropic mechanosensor that requires force orthogonal to the IS for the induction of calcium signaling[68]. The model that these two observations suggest is that force is required to expose ITAM domains on the TCR, which leads to the induction of membrane proximal signaling. Furthermore, the TCR-pMHC interaction has been shown to function as a catch bond[69]. A catch bond is a type of bond in which application of a force increases the lifetime of the interaction. It was shown that the capacity to form a catch bond plays a critical role in enabling the TCR to discriminate between high and low affinity agonists[69]. Together these studies demonstrate the important role of mechanobiology in TCR activation and signaling.

The IS has been shown to be a dynamic and physical structure that is capable of exerting mechanical force[70,71]. Naïve T cells have been shown to exert mechanical force on polydimethylsiloxane (PDMS) pillars coated with activating proteins[71]. It is conceivable that T cells could exert forces as a way of sensing the mechanical properties of activating surfaces. This is supported by previous research demonstrating that T cells are more strongly activated on softer rather than stiffer PDMS surfaces, as measured by cytokine production and proliferation[72]. Activating peripheral blood mononuclear cells (PBMCs) on softer surfaces with CD3/CD28 antibodies tended to increase shedding of CD62L, which is a consequence of T cell activation[72]. This is intriguing

because the opposite phenomenon has been observed for naïve mouse T cells activated on polyacrylamide surfaces with CD3/CD28[73]. Possible explanations for this discrepancy include a difference between human and mouse cells. It is also possible T cells respond differently to antibodies on PDMS and polyacrylamide surfaces. Further research is needed to understand the precise role of surface tension on T cell activation. Yet, these studies are intriguing and support the concept that signaling and cell biology are not merely biochemical reactions. These observations show that mechanical properties of biology are important factors that have been largely overlooked in immunology until recently.

1.3. Immune system and cancer

The connection between the immune system and tumor development has been active area of research for decades. The idea that the immune system is capable of surveying a host and eliminating cancer was first coined cancer immunosurveillance by Sir Macfarlane Burnet in 1957[74]. This idea was quickly abandoned for lack of evidence. The first evidence of this phenomenon came from carcinogen induced cancer models[75]. This concept has evolved into the model of immunoediting[75,76]. This term encapsulates immunosurveillance as well as conveying the notion that the immune system alters the tumor and shapes its development. The theory of cancer immunoediting describes three components of the process, termed the three E's of immunoediting[76]. In the first stage, the immune system actively eliminates transformed cells preventing the formation of a tumor[76]. In the second stage, the transformed cells come to an equilibrium with the immune system[76]. In the third stage, the transformed cells escape containment by the

immune system and grow out, forming a tumor[76]. Since the emergence of the immunoediting model, there has been a tremendous amount of research examining the precise relationship between the immune system and cancer. As part of this research, the immune system has been identified as playing a distinct role in the formation of tumors.

The tumor microenvironment is a dynamic landscape with many different immune cell infiltrates including different types of T cells, macrophages, and myeloid cells. These cells can promote both an anti-tumor immune response and tumorigenesis[77]. For instance, macrophages can have an M1 or M2 phenotype, and they play different roles in tumor progression. M1 macrophages produce pro-inflammatory cytokines and act as APCs, whereas M2 macrophages promote tumorigenesis and produce anti-inflammatory cytokines[77]. T cells also have both tumorigenic and anti-tumor effects. Both $CD4^+$ T cells and $CD8^+$ CTLs are present in tumors. One subtype of $CD4^+$ T cell found in tumors is Tregs. In healthy individuals, Tregs provide immunosuppressive functions[78]. Without Tregs, mice and patients develop severe autoimmunity. However, in the tumor microenvironment, Tregs have a complex and poorly understood role. The presence of Tregs in tumors has been correlated with a poor prognosis in the case of breast and hepatocellular carcinomas[79,80]. Alternatively, the presence of high numbers of Tregs in colorectal cancer is an indicator of a good prognosis[81]. As CTLs infiltrate the tumor, they are exposed to the immunosuppressive environment created by macrophages, Tregs, and other cells. They are also exposed to chronic stimulation through their TCR and pro-inflammatory cytokines. Chronic overstimulation of the TCR in the tumor environment causes CTLs to become

dysfunctional and express various inhibitory markers such as PD-1, TIGIT, and others[41,42]. There is a concerted effort in the scientific community to reverse these immunosuppressive effects and to use the immune system as a cancer treatment. Some of these approaches will be discussed next.

1.4. Cancer Immunotherapies

Attempts to harness the immune system to treat illnesses predate a simple understanding of the immune system with vaccines. More recently, physicians have been using the adaptive immune system in their fight against cancer. In the last several years there have been a number of significant breakthroughs, which have generated a great deal of interest.

1.4.1. Checkpoint blockade

The development of checkpoint blockade emerged from the discovery of CD28 and co-stimulation[82]. When T cells encounter an APC, they receive stimulation through their TCR. When a naïve T cell encounters an APC, its activation depends on receiving a second signal through CD28. Co-stimulatory ligands for CD28 include B7-1 and B7-2. Inhibitory receptors for B7-1 and B7-2 have also been discovered, which include cytotoxic T-lymphocyte-associated protein 4 (CTLA-4)[83]. Treating T cells with antibodies to block CTLA-4 was found to increase their proliferation; whereas treating T cells with antibodies to crosslink CTLA-4 reduced their proliferation[83,84]. *In vitro*, CTLA-4 has been shown to compete with CD28 for B7 molecules on the surface of the APC, which results in reduced co-stimulation of T cells[83]. Further studies showed that treatment of tumor bearing mice with CTLA-4 blocking antibodies resulted in a significant improvement in the anti-tumor responses[85]. PD-1 is structurally and functionally similar to CTLA-4 and has been shown to be a

negative regulator of T cell activation[86]. PD-1 is thought to attenuate TCR signaling by inhibiting the phosphorylation of ZAP70, CD3ζ, and CD28[87,88]. This work has led to many clinical trials, which found that treatment of cancer patients with blocking antibodies for CTLA-4 and PD-1 resulted in a remarkable increase in survival. Clinical trials have been performed with a variety of cancers but the most success has been for patients with metastatic melanoma[89]. While the mechanism for how CTLA-4 and PD-1 blockade work *in vitro* is well understood, it is unclear how precisely they work *in vivo*[90]. Understanding this is critical for improving and developing new cancer therapies.

Following the discovery and success of monoclonal antibodies targeting the receptors CTLA-4 and PD-1, there has been a great interest in developing similar molecules to other receptors[89,91,92]. Additional targets include Programmed death-ligand 1 (PD-L1), V-domain Ig suppressor of T cell activation (VISTA), Hepatitis A virus cellular receptor 2 (TIM-3), and Lymphocyte-activation gene 3 (LAG-3)[93]. There are also efforts to determine whether the checkpoint blockade approach can be applied to other types of cancer besides metastatic melanoma[94].

One challenge that has emerged with new cancer therapies is that it is difficult to determine which treatment is best for each patient. This necessitates the discovery of good biomarkers that could identify the right drug for a patient. This is especially true given the low response rates of some forms of cancer to checkpoint blockade including non-small cell lung cancer and renal cell carcinoma with response rates under 20% and 30% respectively[92]. Biomarkers include PD-L1 expression, mutational burden, and

the number of T cell infiltrates in the tumor[92]. However, the utility of these biomarkers is limited by tumor heterogeneity, inconsistent lymphocyte infiltration, insufficient biopsies, and other reasons. Furthermore, the fact that we do not understand the precise mechanism for checkpoint blockade further limits our ability to identify biomarkers to predict responses.

1.4.2. Adoptive cell therapies

Adoptive cell therapies (ACT) are another promising strategy for using the immune system to treat cancer. These treatments rely on isolating lymphocytes from the peripheral blood of patients and expanding them *ex vivo*[95–98]. While they are being expanded, lymphocytes are sometimes treated to express proteins to modulate their function such as chimeric antigen receptors (CARs). The CAR is a fusion protein consisting of an extracellular domain of a single chain antibody targeting a specific antigen, a transmembrane domain, and various intracellular signaling domains[99]. There is some variety with respect to which signaling domains are used and optimizing the motifs is an area of active research. The CARs that have had the most success are the ones targeting B cell malignancies via the CD19 antigen, which is very specifically expressed on B cells[99]. On-target off-tumor side effects are a concern when the CAR antigen is widely expressed on non-cancerous cells, even at low levels. At least one patient has died from cytokine release syndrome likely due to on-target but off-tumor side effects following treatment with a CAR against human epidermal growth factor receptor 2 (HER-2)[100]. Furthermore, as blood cancers are liquid tumors, they do not have the same immunosuppressive environment of solid tumors, which was

previously discussed. These factors hint that it might be difficult to design CAR treatments that would be effective in solid tumors.

Other types of ACT involve expanding patients' lymphocytes and transferring them back into the patient without transfecting them to express novel receptors. Steven Rosenberg at the National Institutes of Health has pioneered some of this work. He has performed clinical trials where polyclonal tumor infiltrating lymphocytes were taken from patients, expanded, and transferred back into the patients. Upon transfer, patients can experience a dramatic reduction in tumor mass[98]. This approach has many benefits over CAR therapies including success in solid tumors. However, one of the limitations of this approach is that there is a large amount of patient-to-patient variability. This makes a standard protocol difficult to develop as every patient has a unique repertoire of T cells and a unique cancer.

One of the primary drawbacks to ACTs is the significant toxicity observed in the clinical trails[101]. This has led to several trials being halted. One of the ways to reduce the toxicity of ACT, in principle, is by using molecular switches to turn on or off the transferred cells. For instance, synthetic Notch receptors have been used to turn on expression of a CAR only when a cell has encountered a second signal[102]. While cancer treatments involving these molecular switches will be more complicated for physicians to administer, they also provide increased flexibility and likely improved safety, which are both lacking for traditional CARs. There are also switches that turn on suicide genes to halt the progression of cytokine release syndrome[101].

1.5. Conclusion

The development of successful ACTs relies on a detailed understanding of T cell activation, migration, and cytotoxicity. Here we examine the mechanism behind the increase in CTL cytotoxicity observed upon PTEN depletion. PTEN depletion increases CTL force exertion in response to antigen in the plane of the IS and orthogonal to the IS. We connect this increase in force exertion with faster perforin pore formation. We demonstrate that tenser plasma membranes results in increased susceptibility of cancer cells to perforin and CTL lysis. We further implicate force in cytotoxicity by establishing a spatiotemporal relationship between force exertion and degranulation events.

Given the increased cytotoxicity of PTEN depleted cells *in vitro*, we next examined whether PTEN depletion could be used as a way to enhance tumor rejection in a transplantable melanoma model of ACT. PTEN depleted cells were found to have reduced anti-tumor effects *in vivo*. Tumor rejection requires both CTL persistence and cytotoxicity. PTEN depleted cells were found to have a defect in persistence, which we investigated to understand how migration, survival, and proliferation contribute to persistence. T cells depleted for PTEN were found to have defective migration, reduced homeostatic proliferation, and increased survival. This work highlights the importance of homeostatic expansion and migration as critical components of ACT and illuminates them as functional targets for improving ACTs in the future.

CHAPTER 2: CYTOTOXIC T CELLS USE MECHANICAL FORCE TO POTENTIATE TARGET CELL KILLING*

2.1. Introduction

Cells exchange information through adhesive and highly dynamic cell-cell interactions. Within these contacts, communicative chemical processes are exposed to micrometer scale membrane and cytoskeletal movements capable of imparting substantial mechanical force. It is known that cells use applied force to sense the physical properties of their environment and translate this information into afferent chemical signals that flow into the cell. This process, called mechanotransduction, plays critical roles in the activation and differentiation of multiple cell types[103,104]. In principle, force could also modulate intercellular communication, particularly in close cell-cell interactions where movement on one side of the interface induces physical changes on the other side. Whether cell-derived forces actually contribute to the transmission of efferent signals in this manner, however, remains unclear.

Cell-cell contacts in the immune system represent an interesting experimental context for exploring this question because they are structurally dynamic and also mediate a substantial amount of information transfer. One of

---

* †Basu, R., †Whitlock, B.M., †Husson, J., Le Floc'h, A., Jin, W., Oyler-Yaniv, A., Dotiwala, F., Giannone, G., Hivroz, C., Lieberman, J., Kam, L.C., Huse, M. (2016). Cytotoxic T Cells Use Mechanical Force to Potentiate Target Cell Killing. *Cell*, *165*(1), 100–110. http://doi.org/10.1016/j.cell.2016.01.021

the most important of these interactions is the IS used by CTLs to instruct infected or transformed target cells to die. Target cell killing is crucial for adaptive immune responses against intracellular pathogens, and it also plays a central role in several cell-based anti-cancer immunotherapies[97]. IS assembly is triggered by the recognition of pMHC on a potential target by TCRs on the CTL. Once the IS forms, CTLs secrete a toxic mixture of proteins into the synaptic space that includes perforin and several granzyme proteases[105]. Perforin is a hydrophobic molecule that forms calcium (Ca^{2+})-dependent pores in the target cell membrane. This induces a repair response that enables granzymes to access the target cell cytoplasm, where they induce apoptosis[57,58].

Perforin and granzymes are stored in secretory lysosomes called lytic granules, which cluster around the centrosome in activated CTLs. During IS formation, the centrosome reorients to the center of the contact, placing the granules in close apposition to the synaptic membrane[14]. This polarization event is thought to enhance the potency and the specificity of killing by promoting directional release of granule contents toward the target. Recent results, however, indicate that CTLs kill quite effectively in the absence of centrosome reorientation, suggesting there are additional mechanisms by which the IS potentiates cytotoxicity[106].

IS formation also involves intense remodeling of filamentous actin (F-actin), which controls both the growth and the organization of the interface[107]. Recently, we demonstrated that PI3K activity stimulates actin polymerization within the IS by recruiting Dock2, an exchange factor for the Rho GTPase Rac[8]. CTLs lacking Dock2 form miniaturized synapses that are

structurally unstable. Conversely, depletion of PTEN, a lipid phosphatase that antagonizes PI3K, markedly enhances IS growth. Interestingly, whereas Dock2-deficient CTLs kill target cells poorly, PTEN-deficient CTLs exhibit dramatically enhanced cytotoxicity[8]. These results establish an intriguing link between target cell killing and F-actin remodeling at the IS. The mechanistic basis for this relationship, however, has remained unclear.

Synaptic F-actin is highly dynamic, exhibiting constant retrograde flow toward the center of the IS as well as bursts of anterograde flow in the opposite direction[70,108,109]. These and other effects enable the T cell to impart nanonewton scale forces against the target cell[71,110]. In the present study, we combined specific perturbations of PI3K-Dock2 signaling with single cell biophysical approaches to investigate the impact of synaptic forces on CTL function. We found that force exertion at the IS potentiates killing by straining the target cell surface and thereby enhancing the pore forming activity of perforin. These results demonstrate that T cells mix physical and chemical outputs to enhance their effector responses and reveal an unexpected role for cellular mechanics in intercellular communication.

2.2. Results

2.2.1. Cytotoxicity Correlates with Synaptic Force Exertion

The killing phenotypes observed in PTEN- and Dock2-deficient CTLs implied an important role for PI3K-dependent F-actin remodeling in cellular cytotoxicity. To investigate this relationship, we first examined the distribution of lytic granules in CTL-target cell conjugates. CTLs expressing the OT-1 TCR, which recognizes the ovalbumin$_{257–264}$ peptide (OVA) bound to the class I MHC molecule H2-K^{b}, were transduced with short hairpin RNA (shRNA)

against PTEN (shPTEN) or Dock2 (shDock2) or with nontargeting control shRNA (shNT) (Figure 2.1). They were then mixed with OVA-loaded EL4 target cells and the resulting conjugates fixed and stained to visualize lytic granules (Figure 2.2A). Suppression of Dock2 or PTEN had no effect on granule polarization to the IS (Figure 2.2B), indicating that intracellular trafficking of cytotoxic cargo does not involve PI3K-Dock2 signaling. We also quantified granule release (called degranulation) from CTLs by measuring surface exposure of the granule resident protein Lamp1 after stimulation with target cells. This response was unaffected by depletion of PTEN or Dock2 (Figure 2.2C), consistent with previous results[8]. Finally, we examined TCR-induced calcium (Ca^{2+}) flux, a requisite step for granule clustering and exocytosis, by imaging CTLs on glass surfaces coated with H2-K^b-OVA and ICAM-1 (a ligand for the $\alpha_L\beta_2$ integrin LFA-1)[111,112]. Dock2- and PTEN-deficient CTLs displayed robust Ca^{2+} responses that were comparable to those of shNT expressing controls (Figures 2.2D and 2E). Taken together, these data

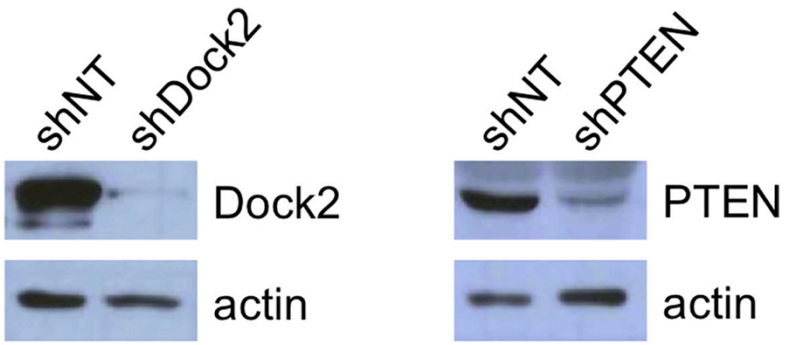

Figure 2.1 shRNA-Mediated Suppression of Dock2 and PTEN
Representative western blots showing typical levels of Dock2 and PTEN depletion in OT1 CTLs expressing shDock2 and shPTEN, respectively, relative to controls expressing shNT. Actin served as a loading control. Data are representative of at least 5 independent experiments. Audrey Le Floc'H performed these experiments.

Figure 2.2 PTEN and Dock2 Are Not Required for Lytic Granule Polarization and Ca^{2+} Flux

(A and B) OT1 CTLs expressing the indicated shRNAs were mixed with OVA-loaded EL4 cells, fixed, and stained for pericentrin and Lamp1 to visualize the centrosome and lytic granules, respectively. (A) Left: brightfield image of a representative CTL-target cell conjugate. Right: corresponding fluorescence image, with white lines indicating CTL boundaries. (B) Left: polarization index was calculated using the center of gravity (COG) of the lytic granules. Right: quantification of lytic granule polarization index (n ≥ 37 per sample). Differences were not significant (two-tailed Student's t test). (C) OT1 CTLs expressing the indicated shRNAs were mixed with OVA-loaded EL4 cells and degranulation assessed by surface exposure of Lamp1. (D) CTLs expressing the indicated shRNAs were loaded with Fura2-AM and imaged on glass surfaces coated with H2-Kb-OVA and ICAM1. Left: representative time-lapse montages of CTLs contacting the stimulatory surfaces. Images are pseudocolored with warmer colors (e.g., orange, red) indicating higher concentrations of intracellular Ca2+. Time in MM:SS is indicated above the montages. Right: mean normalized Fura ratio graphed against time. n ≥ 21 cells per sample. All scale bars, 10 μm. Error bars denote SEM. Data are representative of at least two independent experiments. Audrey Le Floc'H and Morgan Huse performed these experiments.

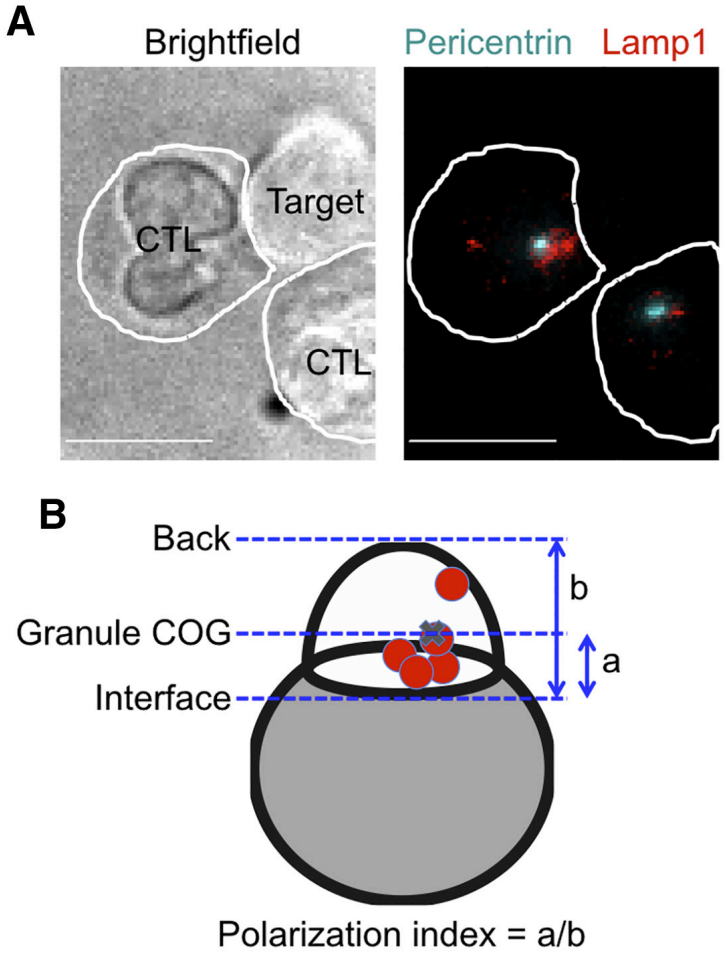
A
Brightfield
Pericentrin
Lamp1
Target
CTL
CTL
B
Back
Granule COG
Interface
b
a
Polarization index = a/b
Polarization index
1.0
0.8
0.6
0.4
0.2
0
sh NT
sh PTEN
sh Dock2

Figure 2.2 (continued)

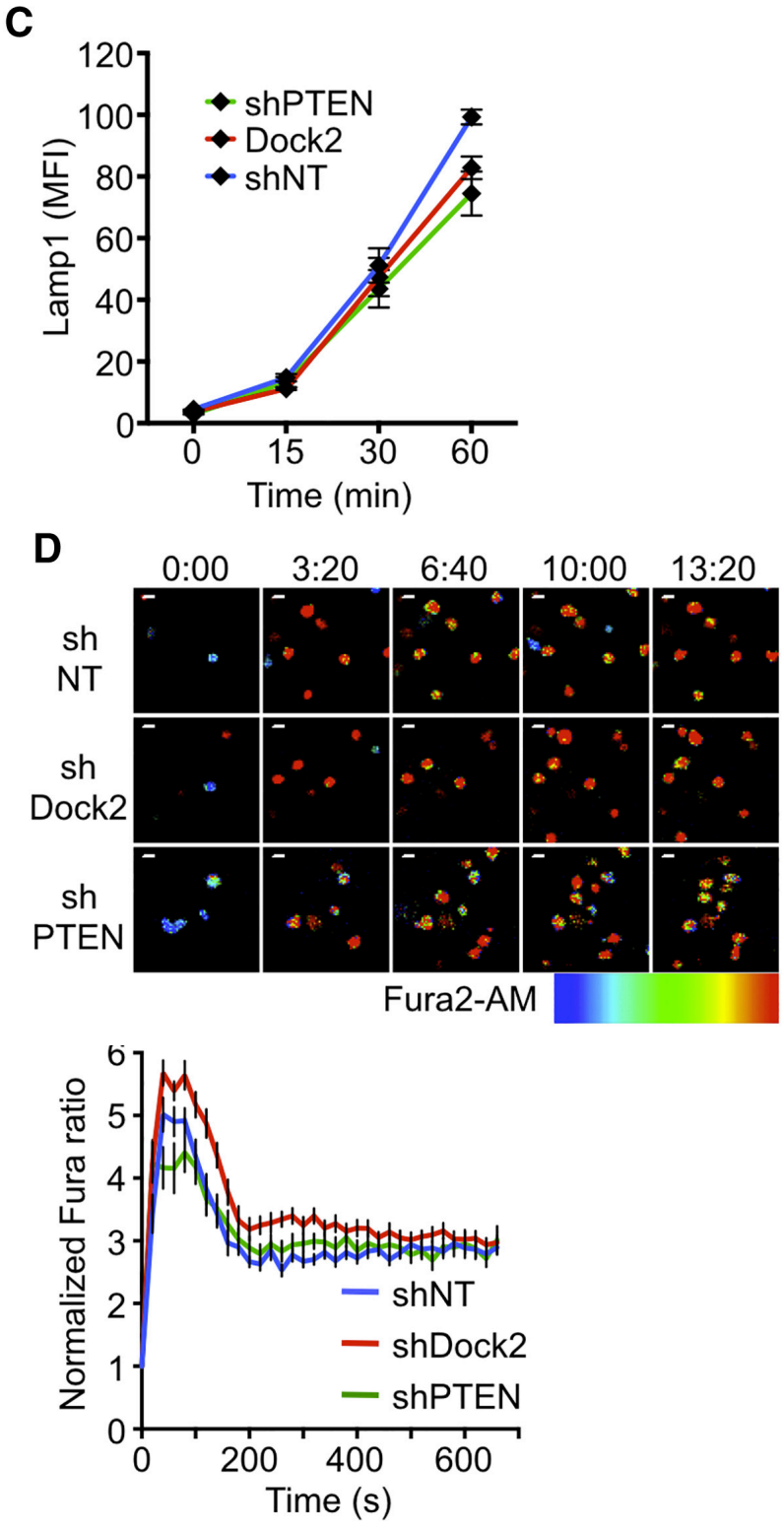

indicate that suppression of PTEN and Dock2 does not affect granule polarization and fusion at the IS, implying that these perturbations influence cytotoxicity via a different mechanism.

Force exertion across the IS could, in principle, provide a physical avenue for control of target cell killing. To investigate this possibility, we first asked whether PI3K-Dock2 signaling, which controls cytotoxic efficiency, might also regulate IS mechanics. Accordingly, we compared synaptic force exertion in OT-1 CTLs transduced with shNT, shPTEN, and shDock2. To measure forces perpendicular to the IS, we used micropipettes to place individual CTLs in contact with polystyrene beads coated with H2-K^b-OVA and ICAM-1 (Figure 2.3A). Subsequent bead displacements toward or away from the CTL were translated into force measurements using the known stiffness of the micropipette holding the bead. Contact with stimulatory beads induced a rapid CTL spreading response not unlike IS formation with a target cell. Spreading was frequently accompanied by transient pushing of the bead away from its initial position. This was followed in almost all cases by a pronounced pulling phase in which the bead became engulfed by the CTL (Figure 2.3B). Analysis of kymographs derived from each experimental trial enabled us to determine the rate of bead movement during the pulling phase of the response (Figure 2.3C), which is proportional to the pulling force. This parameter, called the loading rate, was significantly enhanced in CTLs lacking PTEN and markedly reduced in CTLs lacking Dock2 (Figure 2.3D). These results indicate that PI3K-Dock2 signaling drives force exertion perpendicular to the CTL-target cell interface.

Figure 2.3 PI3K Signaling Controls Force Exertion Perpendicular to the IS

(A) Schematic diagram of the micropipette-based system. (B) Time-lapse montage of a representative micropipette experiment. Dashed white line denotes the initial position of the bead. Time is indicated in M:SS in the bottom left corner of each image. (C) Kymograph of the experiment shown in (B). The loading rate can be derived from the slope of the red line. (D) Average loading rate during the pulling phase of the response, calculated for cells expressing the indicated shRNAs. Error bars denote SEM. n ≥ 10 cells per condition. $^{*}p < 0.05$, $^{**}p < 0.01$, calculated by two-tailed Mann-Whitney test. All scale bars, 5 μm. Data are representative of at least two independent experiments. Audrey Le Floc'H and Julien Husson performed these experiments.

A

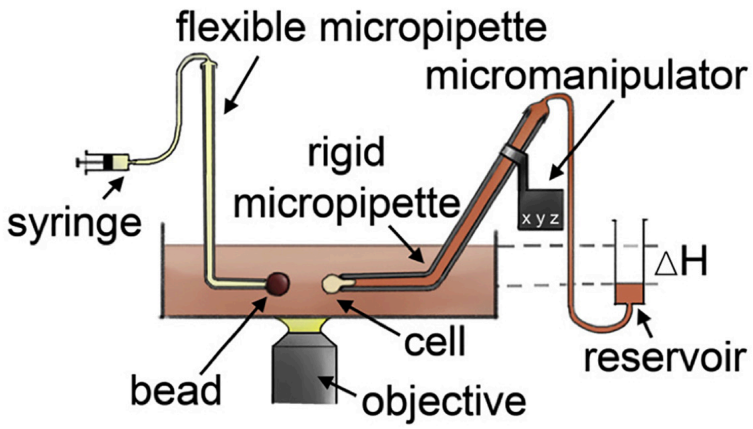
flexible micropipette
micromanipulator
rigid
micropipette
syringe
xyz
ΔH
cell
reservoir
bead
objective

B

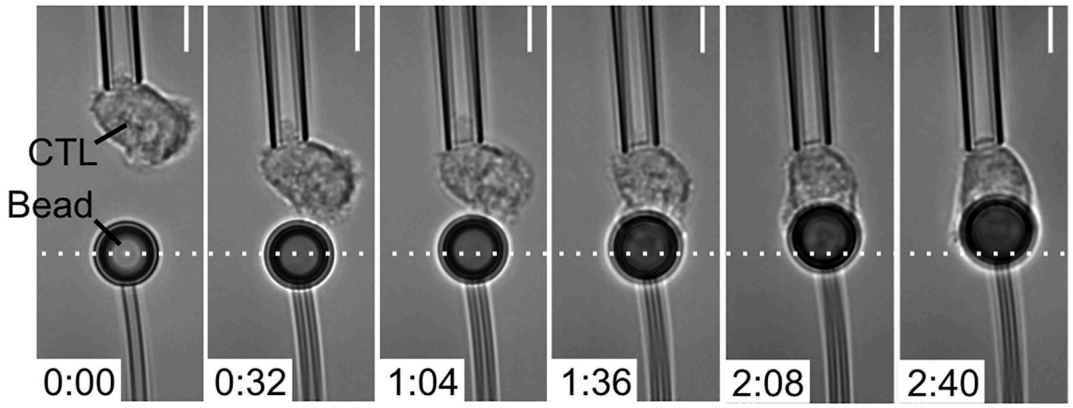
CTL
Bead
0:00
0:32
1:04
1:36
2:08
2:40

C

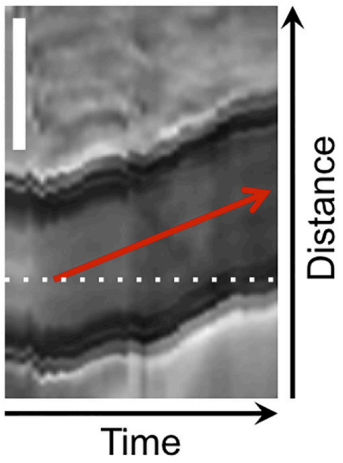
Distance
Time

To measure forces in the plane of the IS, we imaged OT-1 CTLs on arrays of polydimethylsiloxane (PDMS) micropillars bearing immobilized H2-K^b-OVA and ICAM-1 (Figure 2.4A)[71]. Because the dimensions (6 μm tall, 0.7 μm diameter) and composition of these pillars were known, observed pillar deflections could be converted into force vectors. OT-1 CTLs exhibited cell spreading and OVA-induced Ca^{2+} flux upon contact with the arrays, consistent with canonical TCR activation and signaling (Figures 2.4B and 5A). In most cells, spreading was associated with centrifugal pillar deflections, indicative of outwardly oriented forces (Figures 2.4B and 4C). After the size of the interface stabilized, these deflections tended to reverse polarity and point inward. The progression from centrifugal "spreading" to centripetal "squeezing" was reminiscent of the responses displayed by naive $CD4^+$ T cells on pillar arrays[71]. However, OT-1 CTLs exerted substantially more force per pillar than naive cells (Figure 2.4D), and their force profiles were less symmetric[71]. Indeed, instantaneous force exertion tended to be concentrated in "hotspots" characterized by the strong deflection of one to three pillars (Figure 2.4B, green asterisks). Importantly, suppression of PTEN markedly enhanced force exertion on both individual pillars and also the entire array (Figures 2.4E and 5B). Dock2 suppression gave less conclusive results, with some experiments revealing a slight inhibitory effect and others indicating no significant difference (Figures 2.4F and 5B). It is possible that forces in the plane of the IS are less sensitive to reduced PI3K signaling than those in the orthogonal dimension. Nevertheless, when taken together with our micropipette data, these studies indicate that CTLs exert multidimensional PI3K-dependent forces against the target cell.

Figure 2.4 PI3K Signaling and NMII Control Force Exertion Parallel to the IS

(A) Schematic diagram of the micropillar system. (B–F) CTLs expressing shNT, shDock2, or shPTEN were imaged on stimulatory micropillar arrays. (B) Time-lapse montage of a representative CTL-micropillar interaction. Time is indicated in the top right corner of each image. Large pillar deflections are indicated by yellow arrows. Green asterisks denote "hotspots" of strong force exertion. (C) Average projection of pillar deflections along the line connecting each pillar to the cell's center of gravity (COG projection) was determined for the CTL shown in (B) and plotted against time. (D) Aggregate plot of instantaneous force per pillar exerted by the CTL in (B), graphed against time. Pink dots denote pillars in contact with the cell, and blue dots denote pillars outside of the interface. Average force per pillar within the interface is shown in green and background force per pillar in cyan. (E and F) Total force exertion against the pillar array graphed versus time for CTLs expressing the indicated shRNAs. n ≥ 6 cells per sample. (G) CTLs treated with 50 μM blebbistatin (Bleb) or vehicle control (Veh) were imaged on stimulatory micropillar arrays. Total force exertion against the array is graphed as in (E). (H) CTLs expressing the indicated shRNAs were mixed 1:1 with OVA-loaded RMA-s cells. Specific lysis is graphed as a function of OVA concentration. All error bars denote SEM. Data are representative of at least two independent experiments. Benjamin Whitlock, Weiyang Jin, and Morgan Huse performed these experiments.

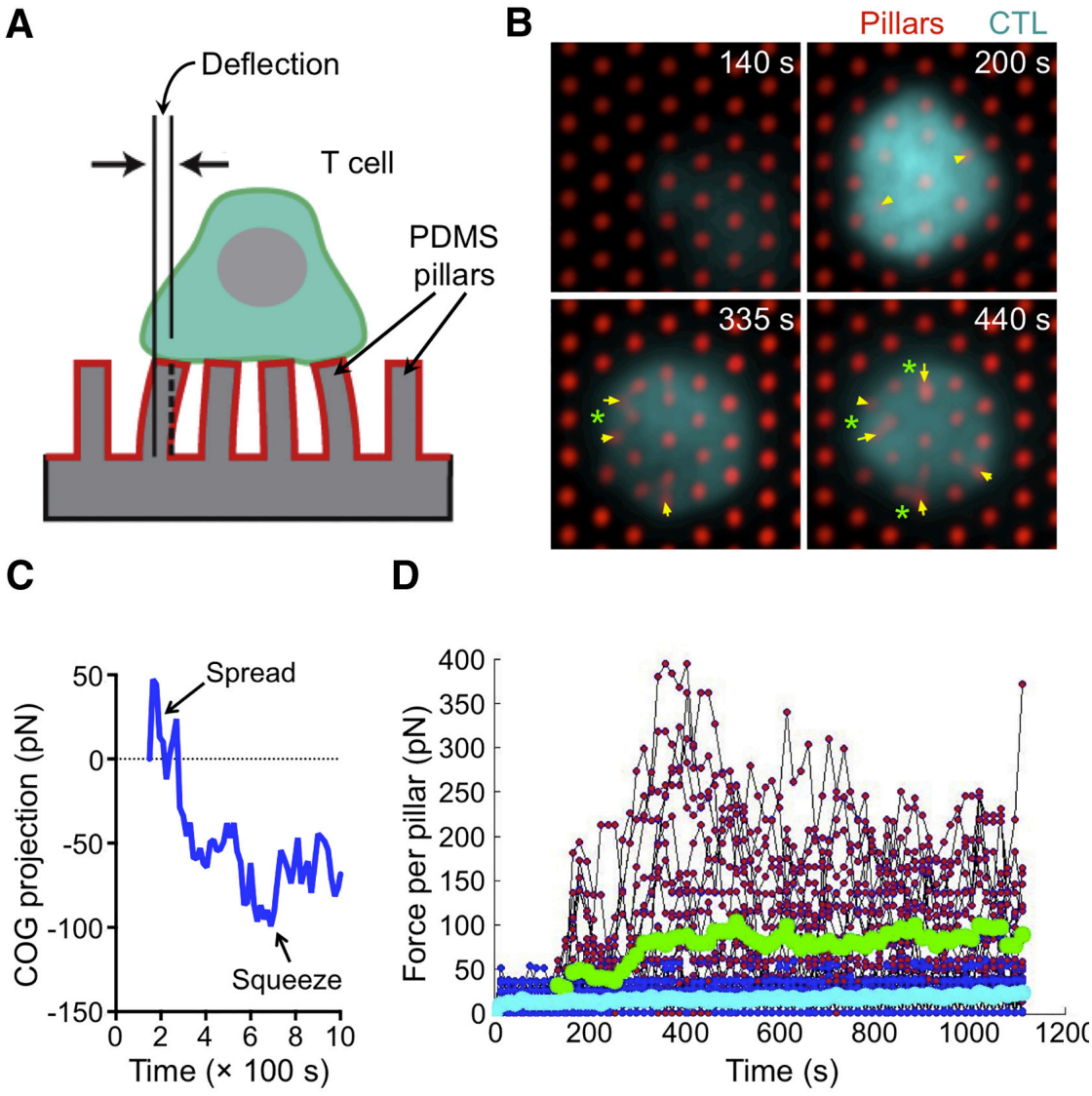
A
Deflection
T cell
PDMS
pillars
B
Pillars
CTL
140 s
200 s
335 s
440 s
C
Spread
Squeeze
COG projection (pN)
50
0
-50
-100
-150
0
2
4
6
8
10
Time (× 100 s)
D
Force per pillar (pN)
400
350
300
250
200
150
100
50
0
0
200
400
600
800
1000
1200
Time (s)

Figure 2.4 (continued)

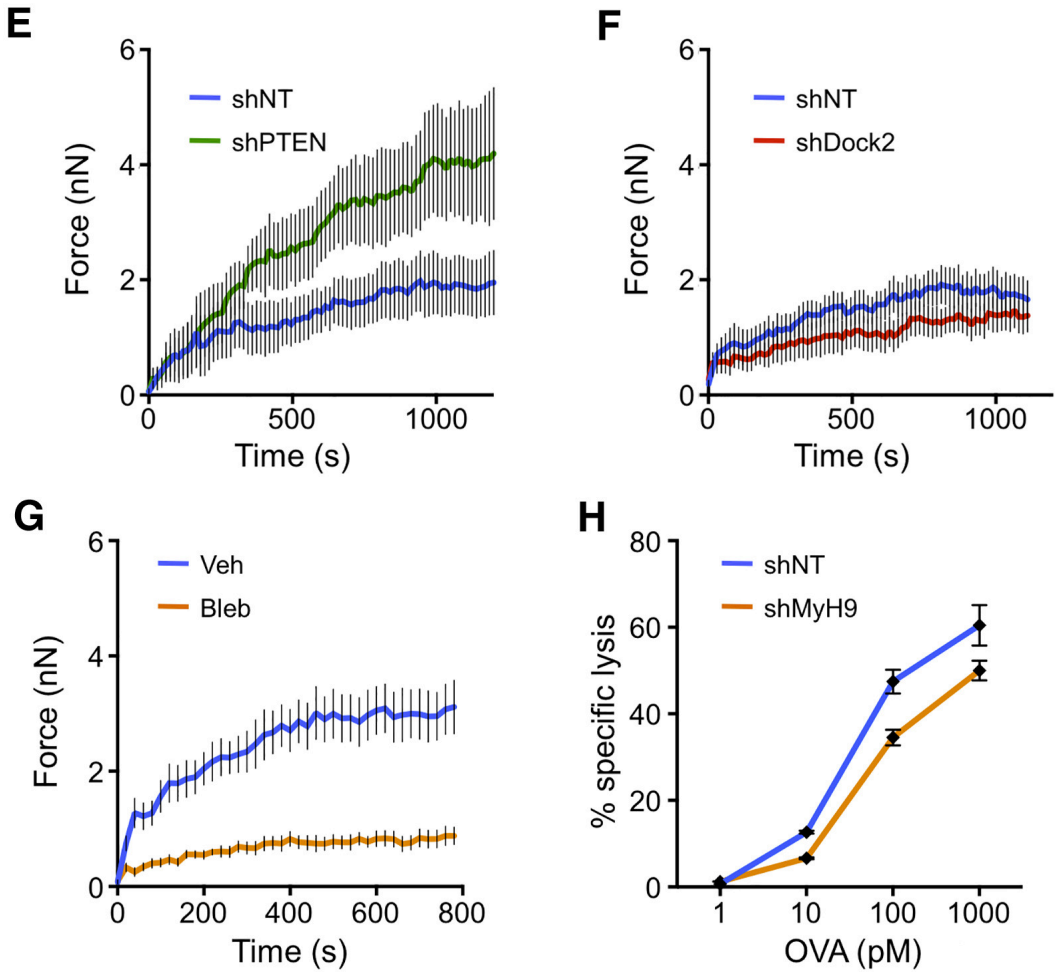

Figure 2.5 Antigen-Induced Forces on PDMS Micropillar Arrays
(A) OT1 CTLs were loaded with Fura2-AM and then imaged on micropillars coated with the indicated ligands (pMHC = H2-Kb-OVA). Representative time-lapse montages are shown of CTLs coming into contact with the surface. Images are pseudocolored with warmer colors (e.g., orange, red) indicating higher concentrations of intracellular Ca2+. Scale bars, 10 μm. (B) CTLs expressing shNT, shDock2, and shPTEN were imaged on micropillar arrays coated with H2-Kb-OVA and ICAM1. Graphs show average force exertion per pillar versus time. n ≥ 6 cells per sample. (C) CTLs treated with 50 μM blebbistatin (Bleb) or vehicle control (Veh) were imaged on stimulatory micropillar arrays. The average COG projection (see Figure 3C) for cells in each condition is plotted against time. Positive values indicate centrifugal "spreading," while negative values indicate centripetal "squeezing." (D) Representative western blot showing typical levels of MyH9 relative to controls expressing shNT. Actin served as a loading control. (E) OT1 CTLs expressing the indicated shRNAs were mixed with OVA-loaded RMA-s target cells and degranulation assessed at various times by surface exposure of Lamp1. Although shMyH9-expressing CTLs displayed increased degranulation in this experiment, the result was not consistent. All error bars denote SEM. Data are representative of at least two independent experiments. Benjamin Whitlock, Weiyang Jin, and Morgan Huse performed these experiments.

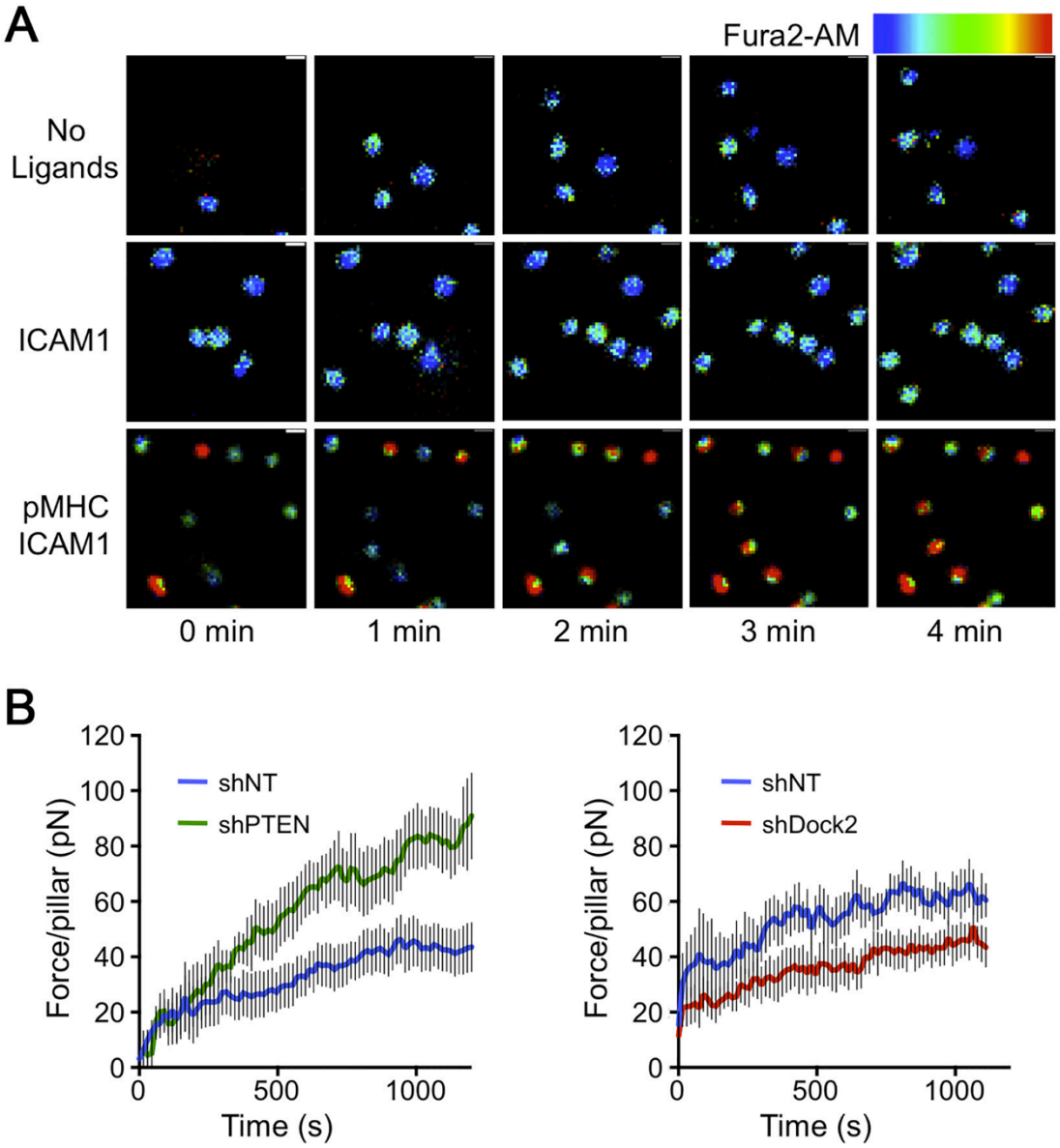
A
Fura2-AM
No Ligands
ICAM1
pMHC ICAM1
0 min
1 min
2 min
3 min
4 min
B
Force/pillar (pN)
Time (s)
shNT
shPTEN
shDock2
0
20
40
60
80
100
120
500
1000

Figure 2.5 (continued)

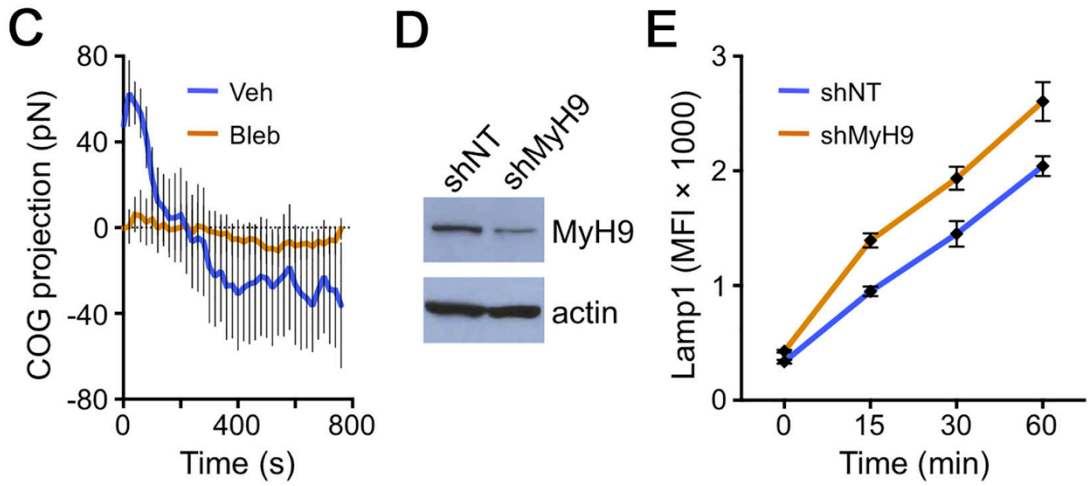

Myosin-based contractility is crucial for the generation of actin-dependent forces in multiple cell types, and clusters of the nonmuscle myosin II (NMII) isoform have been observed within the T cell IS[113–115]. Although the precise function of synaptic NMII remains controversial, it is appropriately positioned to contribute to force exertion[116]. To investigate this possibility, we examined micropillar deflection in the presence of blebbistatin, a small molecule myosin II inhibitor. Blebbistatin treatment dramatically reduced force exertion during both the "spreading" and "squeezing" phases of the response (Figures 2.4G and 2.5C), indicative of an important role for NMII in IS mechanics. Next, we asked whether synaptic force exertion by NMII modulates cytotoxicity. For these experiments, we utilized shRNA knockdown of the myosin heavy chain MyH9 (shMyH9) to target the NMII complex selectively in CTLs. This strategy yielded only partial suppression of MyH9 (Figure 2.5D), as previously reported[117]. CTLs expressing shMyH9 exhibited a subtle, but consistent killing defect that paralleled the partial knockdown of the protein (Figure 2.4H). Importantly, TCR-induced degranulation was not inhibited in these cells (Figure 2.5E), indicating that TCR activation and signaling remained intact. We conclude that myosin activity, like PI3K signaling, controls both cytotoxicity and synaptic force exertion.

2.2.2. PI3K signaling Accelerates Perforin Pore Formation

Next, we re-examined how PI3K signaling affects cytotoxicity, focusing on events that occur downstream of perforin and granzyme secretion. Perforin initiates killing by forming plasma membrane pores on the target cell[60]. This event can be visualized by imaging CTLs and target cells in the presence of high concentration (100 μM) propidium iodide (PI)[57,59]. Plasma membrane

perforation allows PI to access the cytoplasm, rendering the target cell fluorescent (Figure 2.6A). To quantify the rate of perforin pore formation using this approach, we imaged OVA-loaded RMA-s target cells together with OT-1 CTLs in 50 × 50 μm PDMS microwells, which facilitate extended observation of individual CTL-target cell interactions (Figure 2.6B). These experiments revealed that CTLs expressing shPTEN were significantly more effective at inducing perforin pore formation than shNT expressing controls. The fraction of interactions associated with target cell PI incorporation was higher (93% for shPTEN CTLs versus 71% for shNT CTLs), and among these, the time delay between IS formation and PI fluorescence (influx time) was significantly reduced (Figure 2.6C).

CTLs lacking PTEN exhibited higher total levels of perforin protein (Figure 6D), which could, in principle, explain the enhanced pore formation we observed. This increase in perforin expression could be reversed, however, by removing one copy of the *prf1* gene in the context of PTEN deficiency. Importantly, killing by PTEN-deficient $prf1^{+/-}$ CTLs was essentially equivalent to that of PTEN-deficient $prf1^{+/+}$ CTLs and substantially greater than that of $prf1^{+/+}$ shNT controls (Figure 2.6E). Hence, it is unlikely that the accelerated pore formation seen in the absence of PTEN resulted from changes in perforin expression. Rather, PTEN suppression appeared to boost cytotoxicity by increasing perforin activity on a per molecule basis.

2.2.3. Cell Tension Potentiates Target Cell Lysis

Biophysical studies have shown that increasing the tension of target membranes boosts the activity of pore forming peptides, implying that tangential force can reduce the energetic cost of inserting a hydrophobic

Figure 2.6 PTEN Deficiency Enhances Perforin Pore Formation
(A) Schematic diagram showing perforin pore detection by PI. (B and C) CTLs expressing shNT or shPTEN together with cyan fluorescent protein (CFP) were mixed with carboxyfluorescein succinimidyl ester (CFSE)-labeled, OVA-loaded RMA-s cells and imaged in PDMS microwells in the presence of 100 μM PI. (B) Time-lapse montage of a representative microwell showing conjugate formation (magenta asterisk) and PI influx (purple arrowhead). Time is indicated in H:MM in the bottom left corner of each image. (C) Time between conjugate formation and PI influx (PI influx time) quantified for shNT and shPTEN expressing CTLs. Error bars denote SEM. n ≥ 65 conjugates per sample. P value calculated by two-tailed Mann-Whitney test.(D) Perforin (Prf) expression in the indicated CTLs was analyzed by western blot. Actin served as a loading control. (E) $prf1^{+/+}$ and $prf1^{+/-}$ CTLs expressing the indicated shRNAs were mixed 1:1 with OVA-loaded RMA-s cells. Specific lysis is graphed as a function of OVA concentration. Data are representative of at least two independent experiments. Benjamin Whitlock and Morgan Huse performed these experiments.

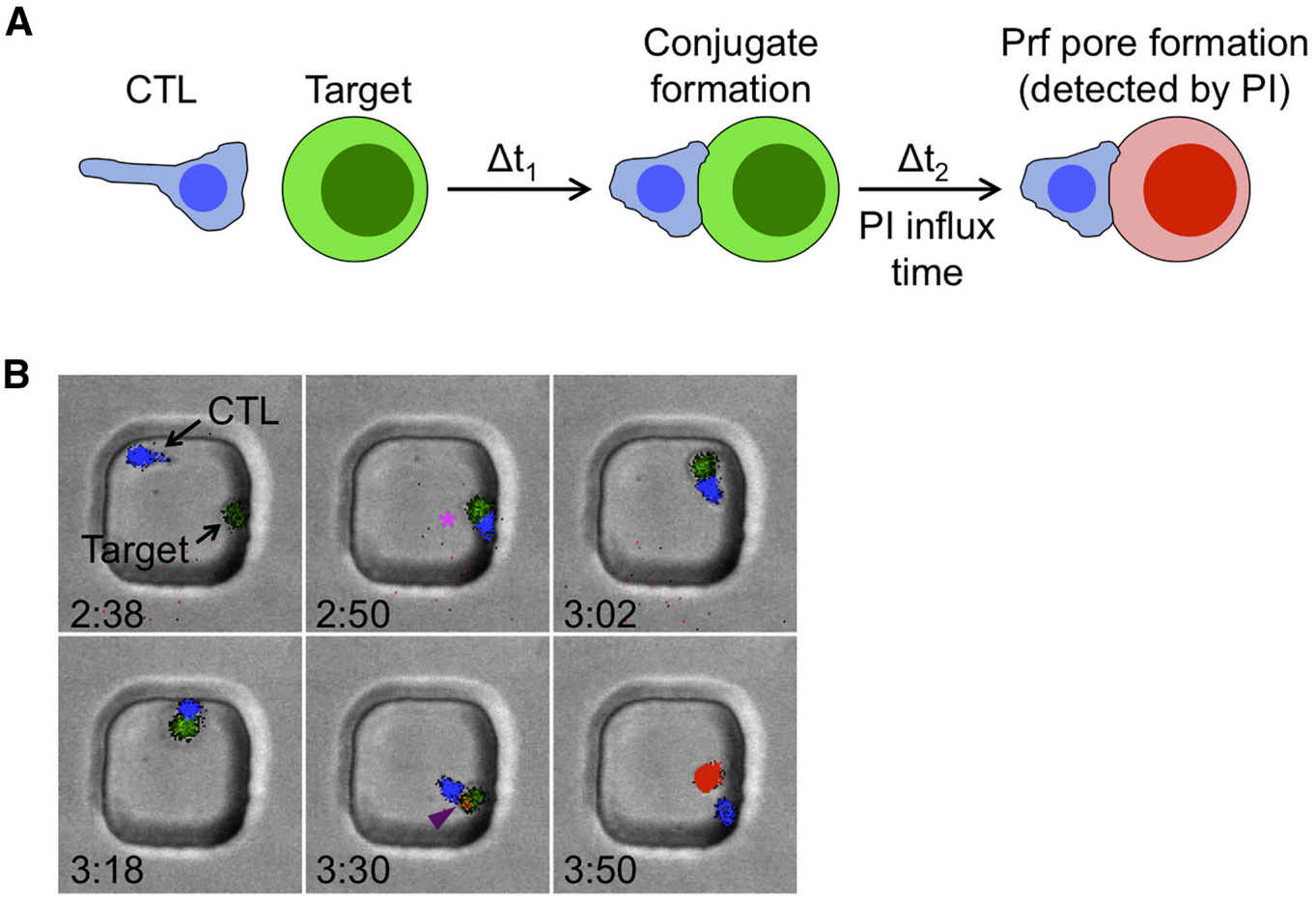
A
CTL
Target
Conjugate formation
Prf pore formation (detected by PI)
Δt1
Δt2
PI influx time
B
CTL
Target
2:38
2:50
3:02
3:18
3:30
3:50

Figure 2.6 (continued)

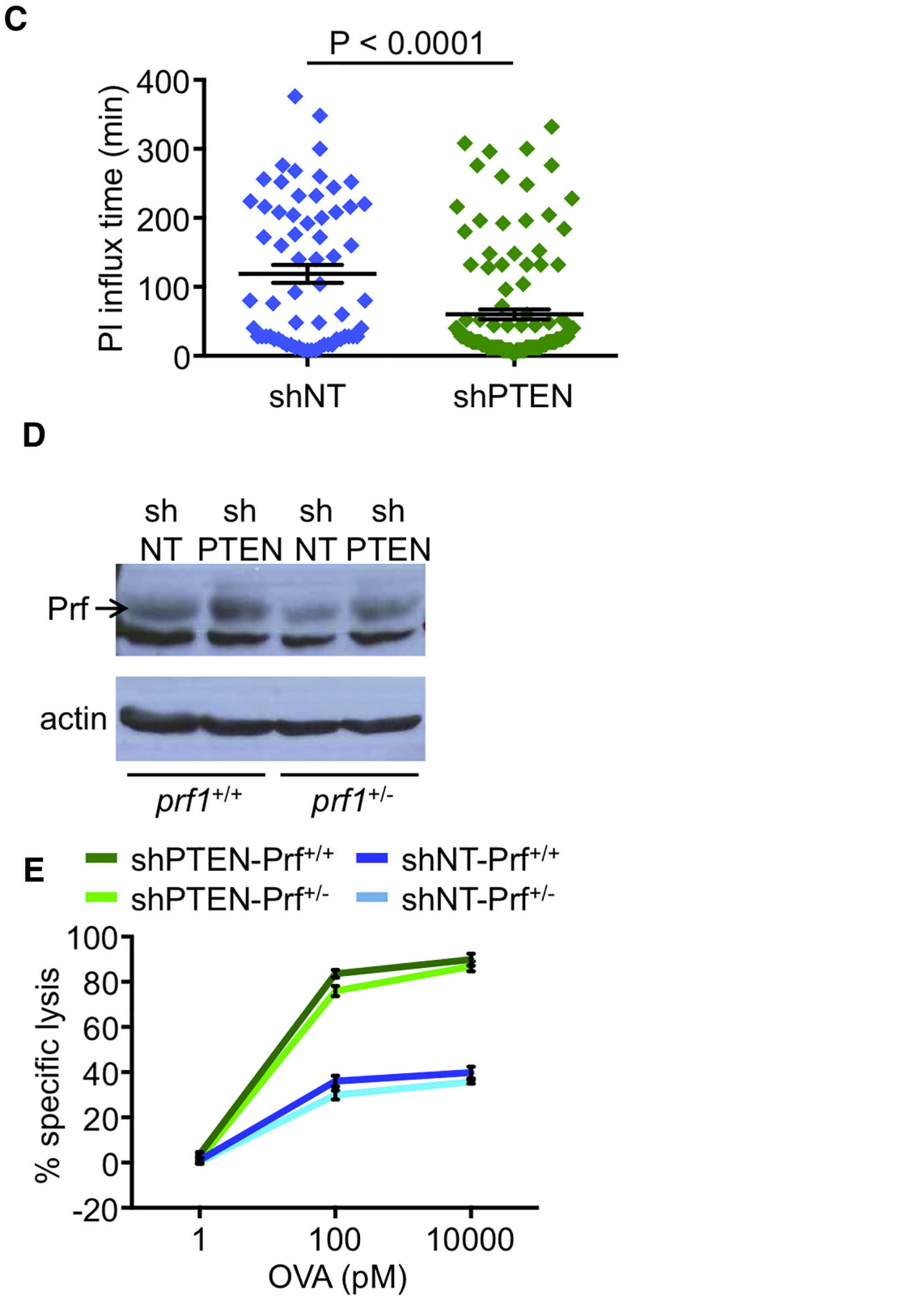

molecule into the bilayer[118–120]. Accordingly, we reasoned that synaptic forces might potentiate perforin pore formation by applying tension to the target cell. To explore the relationship between cell tension and perforin function, we grew adherent cells on polyacrylamide hydrogels of varying elasticity[121]. Cell tension in this culture system mirrors the underlying hydrogel; stiff hydrogels enforce high tension, while soft hydrogels induce the opposite effect[122–125]. Consistent with this principle, we found that B16 melanoma cells adopted a stellate architecture on stiff (E = 50 kPa) hydrogels characteristic of high tension, while on soft (E = 12 kPa) hydrogels they displayed a more collapsed morphology (Figure 2.7). To assess perforin pore formation under each condition, we treated the cells with purified perforin protein (~1 μg/ml) in the presence of 100 μM PI (Figure 2.8A). Although the capacity of perforin to induce PI influx varied from day to day, we consistently observed that cells on 50 kPa substrates were more sensitive to pore formation than those on 12 kPa substrates, implying that increased cell tension potentiates perforin activity (Figures 2.8B, 8C, and 2.9A).

Next, we investigated whether target cell tension similarly modulates CTL-mediated killing. OT-1 CTLs were added to OVA-loaded B16 cells grown on stiff or soft substrates and target cell lysis measured by the release of lactate dehydrogenase (LDH), a cytoplasmic enzyme (Figure 2.8D). Killing was significantly enhanced on 50 kPa hydrogels relative to 12 kPa hydrogels, despite equivalent levels of TCR-induced degranulation (Figures 2.8E and 2.10). Importantly, target cell killing by the small molecule staurosporine, which induces apoptosis in multiple cell types, was unaffected by substrate elasticity (Figures 8F and 8G). B16 cells grown on stiff matrices are therefore

not intrinsically less viable. Rather, they are selectively sensitized to perforin-dependent killing.

Cell tension is imposed both by the cytoskeletal cortex and by the plasma membrane. To determine the relative contributions of membrane and cortical tension to perforin function, we assessed pore formation in the presence of reagents that alter the two parameters differentially (Figure 2.11A). Blebbistatin, by inhibiting myosin II, reduces cortical tension while increasing membrane tension[126,127]. By contrast, the actin depolymerization agent latrunculin A reduces both parameters[128,129]. Treatment of adherent B16 cells with latrunculin A substantially decreased pore formation by purified perforin, while blebbistatin reproducibly enhanced it

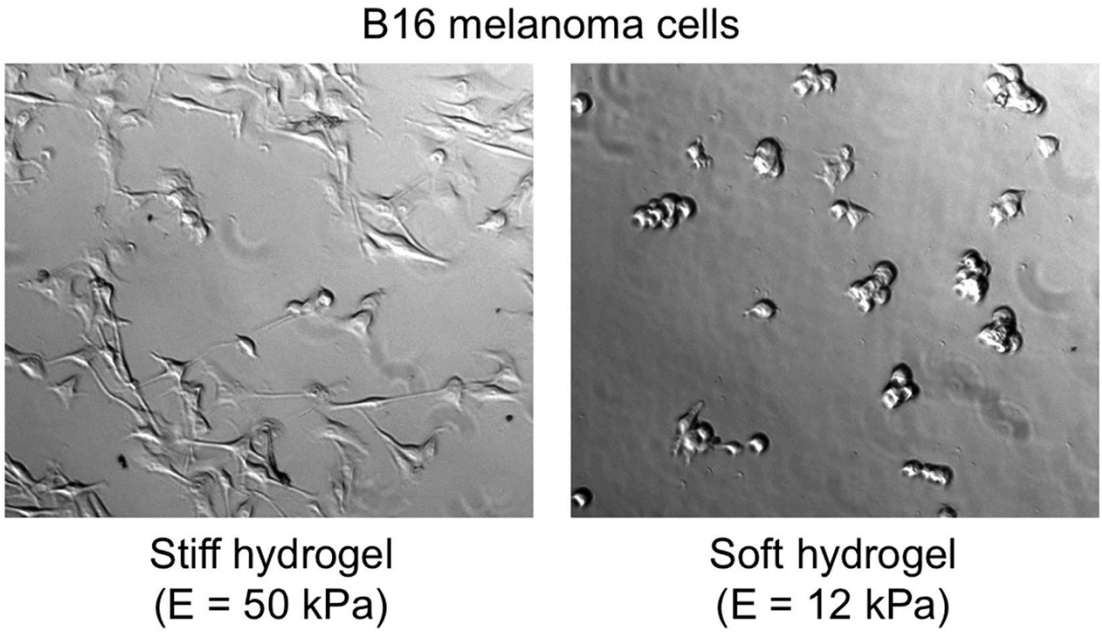

Figure 2.7 Hydrogel Stiffness Controls Cell Morphology
B16 cells were cultured overnight on fibronectin-coated hydrogels of varying elasticity. Representative brightfield images show that cells spread on stiff (E = 50 kPa) substrates and adopt a more collapsed morphology on soft (E = 12 kPa) matrices. Data are representative of five independent experiments. Roshni Basu performed these experiments.

Figure 2.8 Cell Tension Promotes Perforin Pore Formation and CTL-Mediated Killing

(A–C) B16 cells were cultured overnight on stiff (E = 50 kPa) or soft (E = 12 kPa) hydrogels, stained with Hoechst 33342, and treated with the indicated dilutions of perforin (1:1,000 ≈1 μg/ml final concentration) in the presence of 100 μM PI. (A) Schematic diagram of the perforation assay. (B) Representative images before and after perforin treatment on both stiff (top) and soft (bottom) hydrogels. Perforated cells were identified by their PI^+ nuclei. (C) Quantification of a representative perforation experiment on hydrogels. Total cell counts are shown in parentheses above each bar. (D) Schematic diagram of a B16 killing assay on hydrogel substrate. (E) OT1 CTLs were added to OVA-loaded B16 cells grown on stiff or soft hydrogels. Specific lysis was quantified by LDH release at the indicated effector to target (E:T) ratios. (F) Schematic diagram of staurosporine-induced apoptosis on hydrogel substrate. (G) B16 cells grown on stiff or soft hydrogels were exposed to the indicated concentrations of staurosporine. Apoptosis was quantified by LDH release. Error bars denote SEM. Data are representative of at least two independent experiments. Roshni Basu, Benjamin Whitlock, and Morgan Huse performed these experiments.

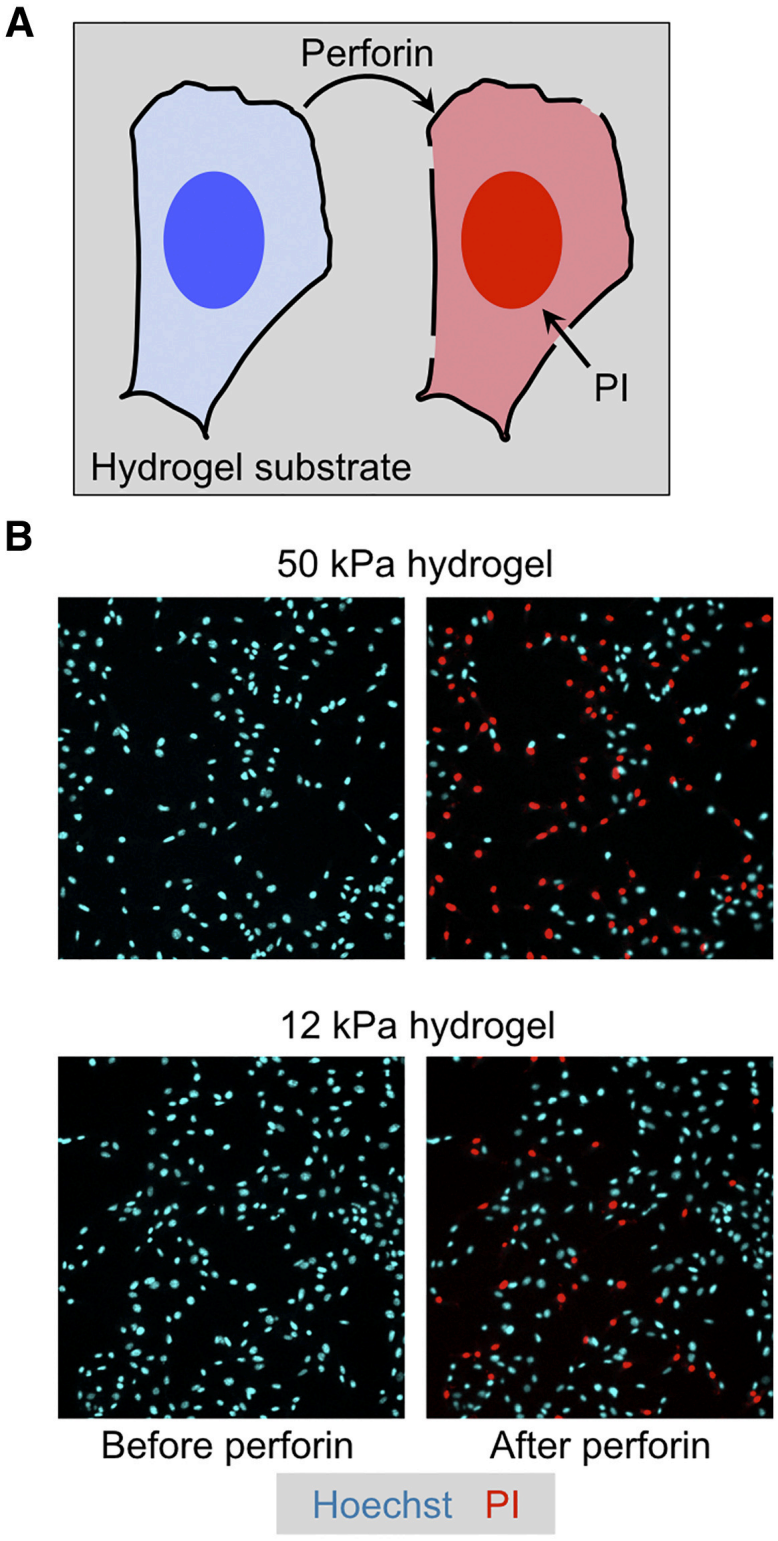
A
Perforin
PI
Hydrogel substrate
B
50 kPa hydrogel
12 kPa hydrogel
Before perforin
After perforin
Hoechst PI

Figure 2.8 (continued)

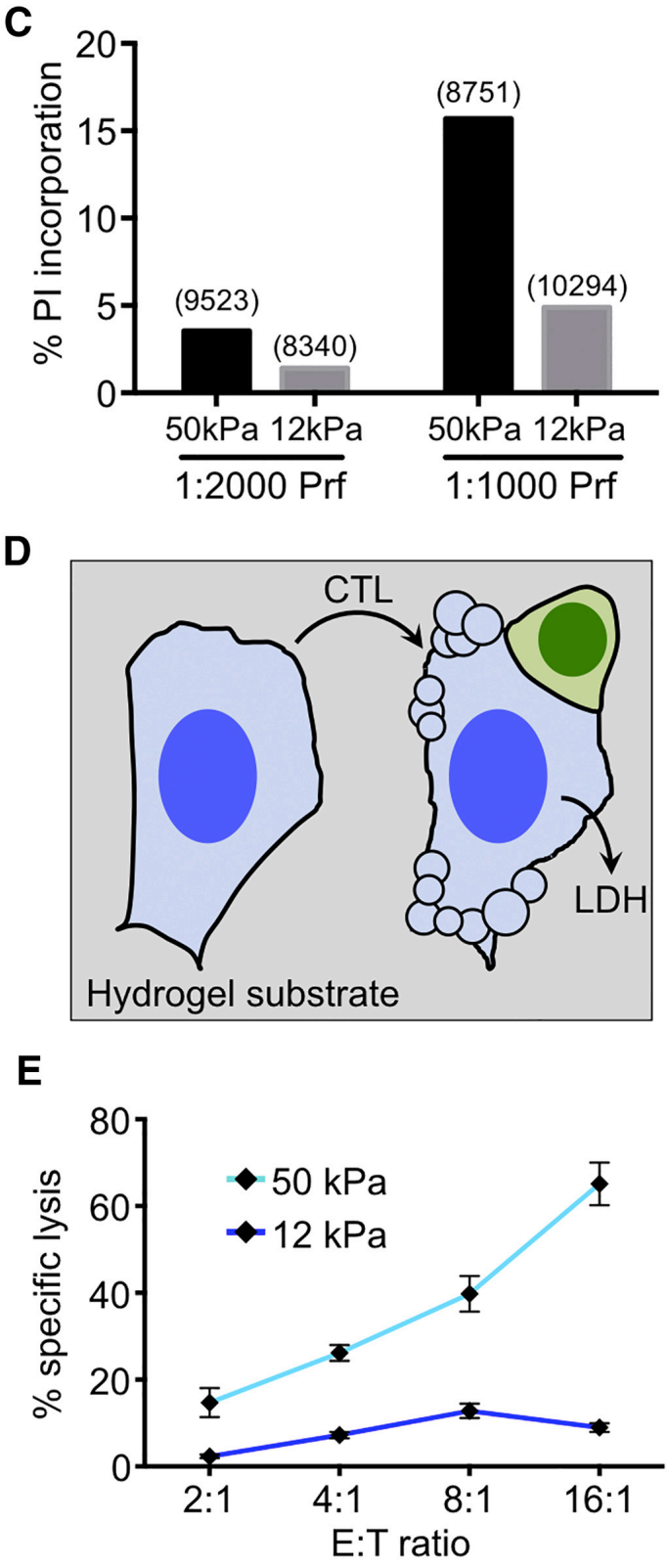

Figure 2.8 (continued)

F

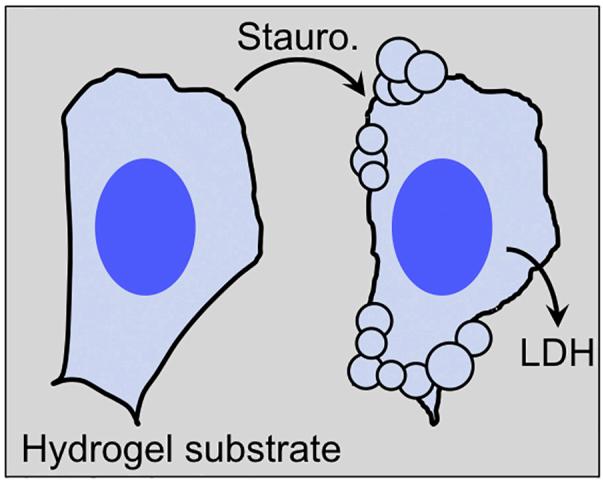

G

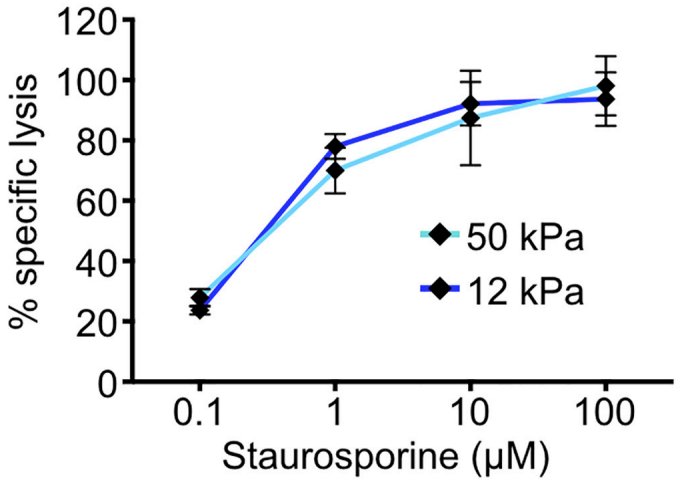

Figure 2.9 Cell Tension Modulates Perforin Pore Formation
Replicate experiments for Figures 2.8C, 11B, and 11D. (A) Quantification of perforin pore formation in B16 cells grown on stiff (E = 50 kPa) or soft (E = 12 kPa) fibronectin-coated hydrogels. (B) Quantification of perforin pore formation in the presence of 7.5 μM latrunculin A (Lat A) or vehicle control (Veh). (C) Quantification of perforin pore formation in the presence of the indicated concentrations of blebbistatin (Bleb) or Veh. (D) Quantification of perforin pore formation in hypertonic (Hyper), hypotonic (Hypo), and isotonic (Iso) medium. A 1:1000 dilution of perforin was used in all experiments except the left graph in (A), which was performed using a 1:25 dilution of a low concentration prep. In all graphs, total cell counts are shown in parentheses above each bar. Roshni Basu, Benjamin Whitlock, and Morgan Huse performed these experiments.

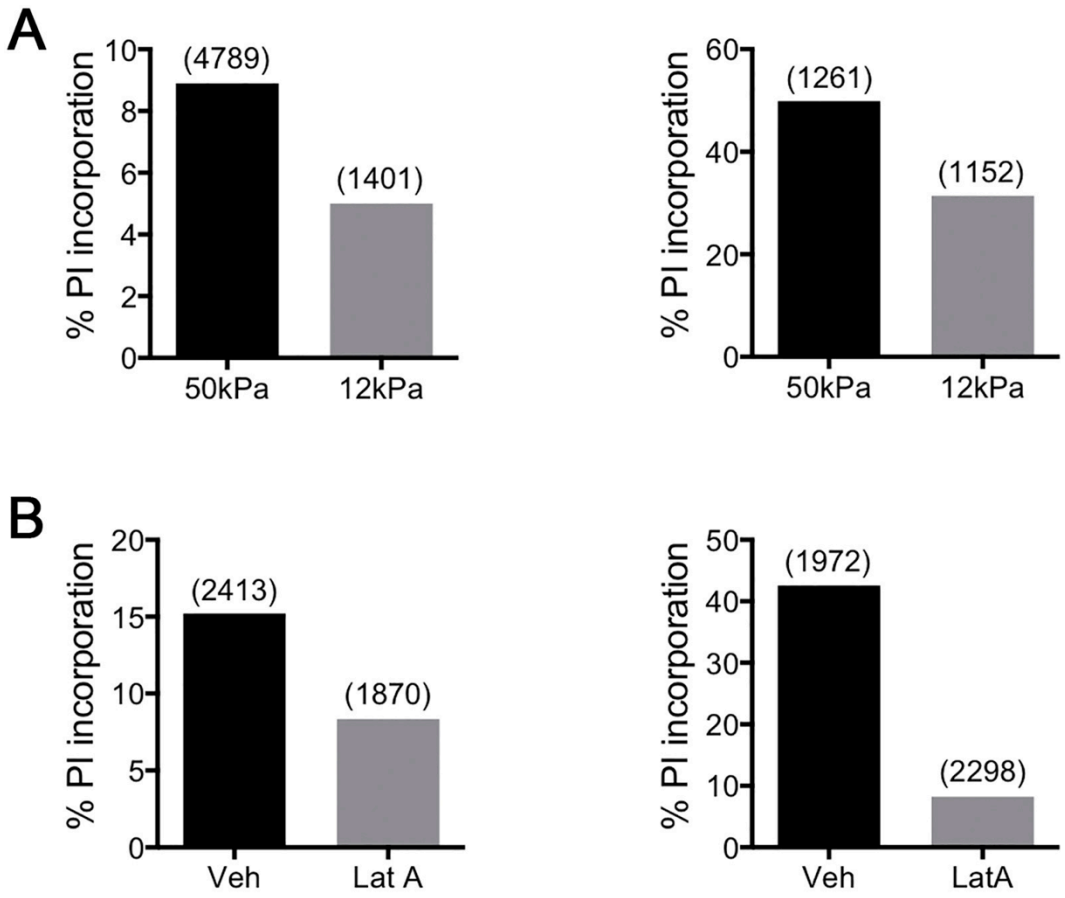

Hydrogels

Latrunculin A

Figure 2.9 (continued)

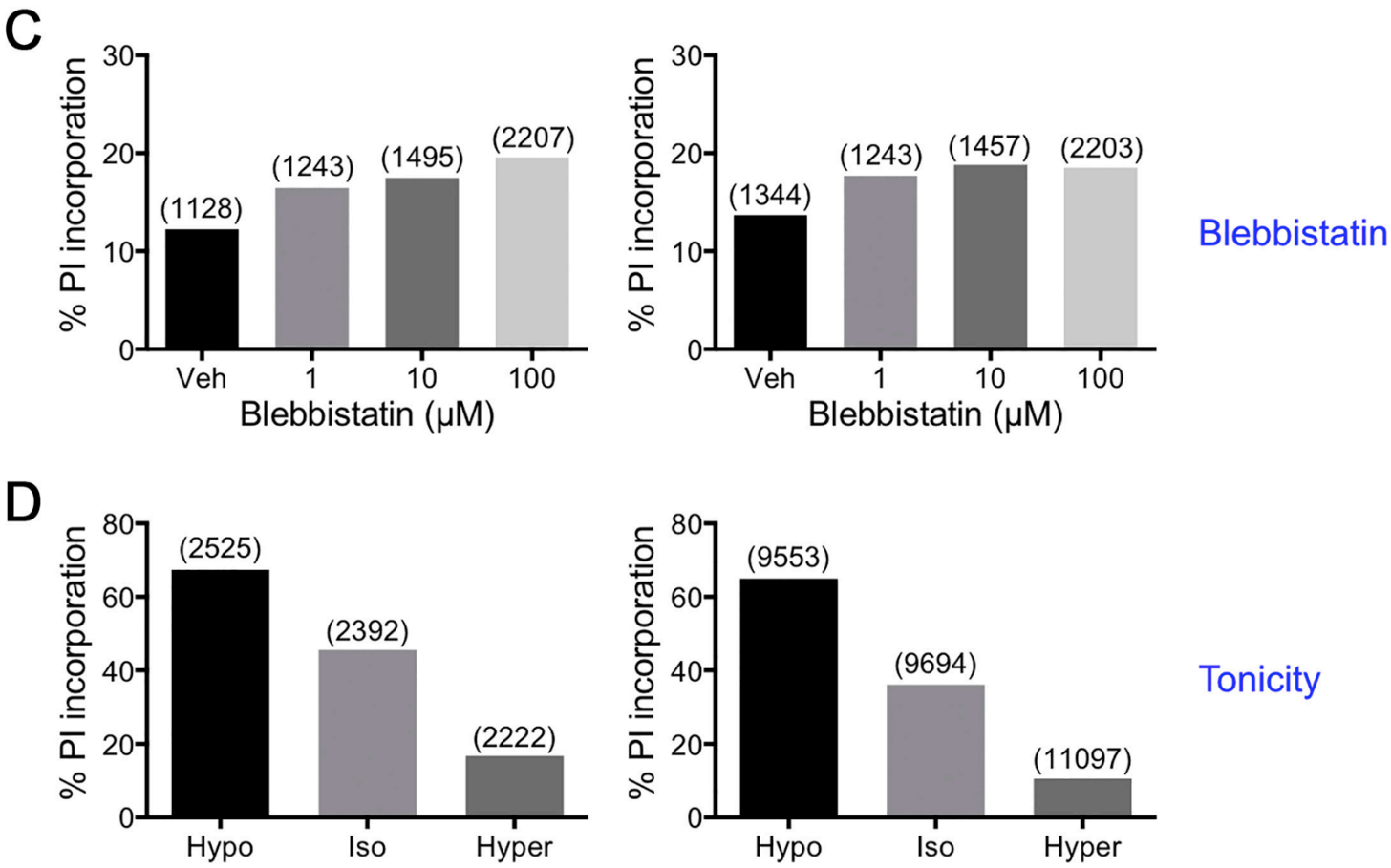

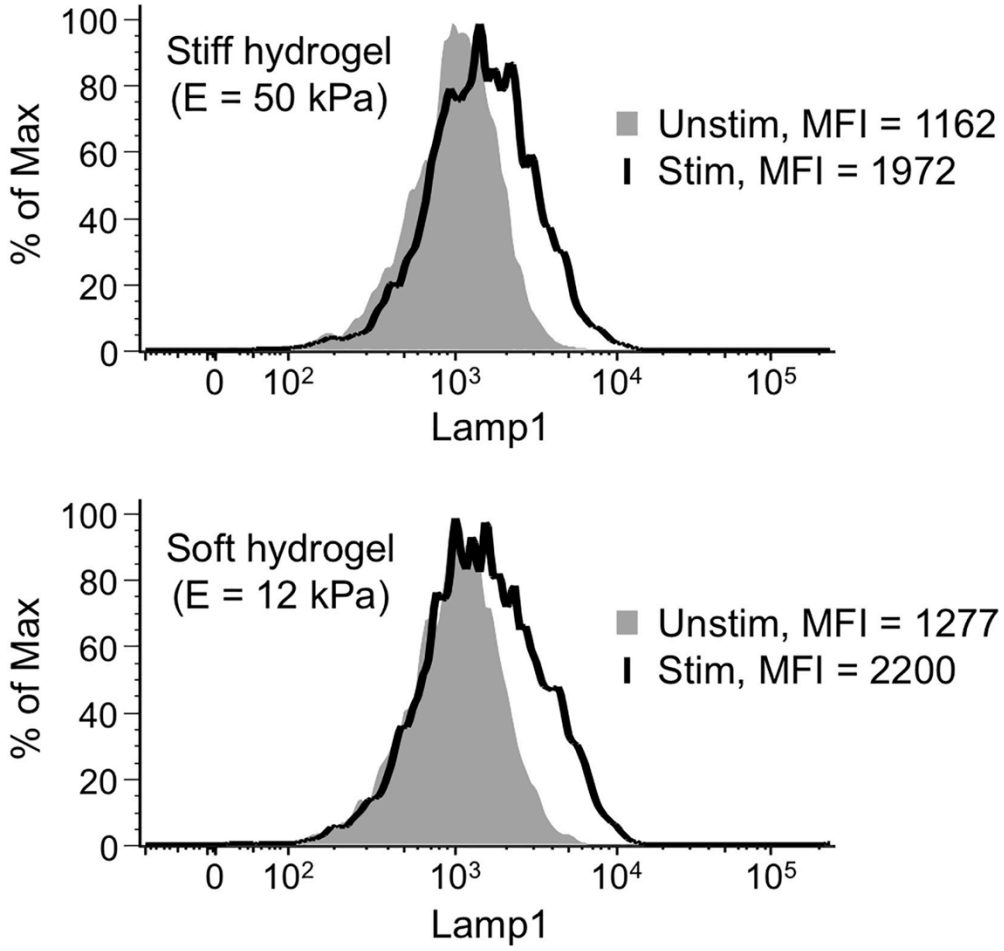

Figure 2.10 Matrix Stiffness Does Not Alter TCR-Induced Degranulation
B16 cells were cultured overnight on fibronectin-coated hydrogels, loaded with OVA as necessary, and then mixed with OT1 CTLs. Representative histogram plots show T cell degranulation on stiff (50 kPa, above) or soft (12 kPa, below) matrices, as assessed by Lamp1 staining. Unstimulated samples (Unstim, no OVA) are shown in solid gray, and stimulated samples (Stim, OVA) in black outline. Mean Fluorescence Intensity (MFI) is indicated for each curve. Data are representative of two independent experiments. Roshni Basu performed these experiments.

(Figures 2.11B, 2.9B, and 9C). These results suggested that membrane tension, rather than cortical tension, controls perforin activity. To further test this idea, we treated cells with hypotonic and hypertonic buffers, which increase and decrease, respectively, membrane tension (Figure 2.11C)[126]. Pore formation was enhanced by hypotonic buffer and suppressed by hypertonicity (Figures 2.11D and 2.9D), further supporting the idea that perforin and membrane tension function synergistically.

2.2.4. Synaptic Force Exertion is Coordinated with Degranulation

Finally, we examined whether perforin release is spatiotemporally correlated with the application of force at the IS, using a degranulation probe containing a pH-sensitive GFP (pHluorin) attached to the C-terminal domain of Lamp1[130]. pHluorin-Lamp1 is sorted into lytic granules, where its fluorescence is quenched by the acidic environment. Granule fusion with the plasma membrane, however, neutralizes the pH around the pHluorin, allowing it to fluoresce. When CTLs expressing pHluorin-Lamp1 were imaged on PDMS micropillars coated with H2-K^b-OVA and ICAM-1, degranulation events appeared as abrupt increases in green fluorescence within the interface between the CTL and the array (Figures 2.12A and 12B). Most events occurred within 5 min of initial contact (Figure 2.12C) and many seemed to be closely associated with hotspots of strong force exertion (Figure 2.12D).

To quantify the relationship between degranulation and force, we computed the distance between each granule fusion event and the closest pillar experiencing strong deflections during that time (called the distance to displaced pillar [DDP]. We then compared each value to a null distribution

Figure 2.11 ***Membrane Tension Potentiates Perforin Pore Formation***
(A) Diagram schematizing the effects of blebbistatin (Bleb) and latrunculin A (Lat A) on cortical (C) and membrane (M) tension. Lamellipodial F-actin and stress fibers are indicated in orange. (B) B16 cells cultured on plastic were treated with perforin (1:1,000 dilution) in the presence of 100 μM PI and either 100 μM Bleb, 7.5 μM Lat A, or vehicle control (Veh) as indicated. Perforation was quantified by PI incorporation. (C) Diagram schematizing the effects of hypotonic (Hypo) or hypertonic (Hyper) medium on membrane tension. (D) B16 cells cultured on plastic were treated with perforin (1:1,000 dilution) in the presence of 100 μM PI either in isotonic (Iso), hypotonic, or hypertonic medium as indicated. Perforation was quantified by PI incorporation. In (B) and (D), total cell counts are shown in parentheses above each bar. Data are representative of three independent experiments. Roshni Basu performed these experiments.

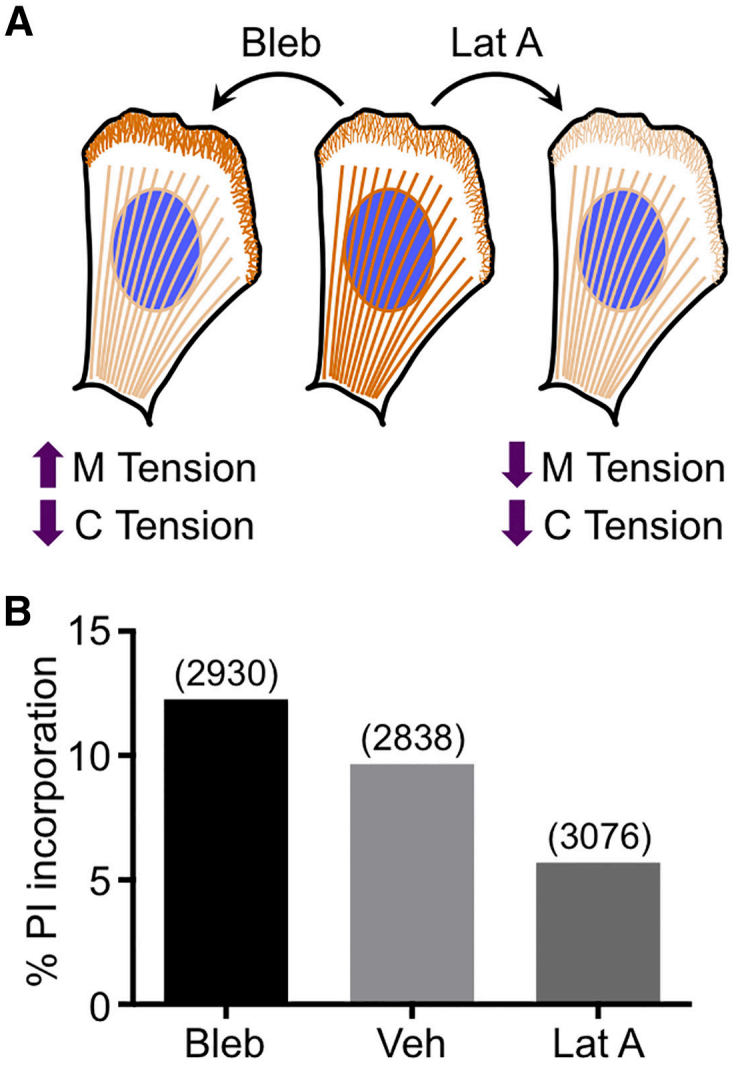
A
Bleb
Lat A
M Tension
C Tension
M Tension
C Tension
B
% PI incorporation
15
10
5
0
(2930)
(2838)
(3076)
Bleb
Veh
Lat A

Figure 2.11 (continued)

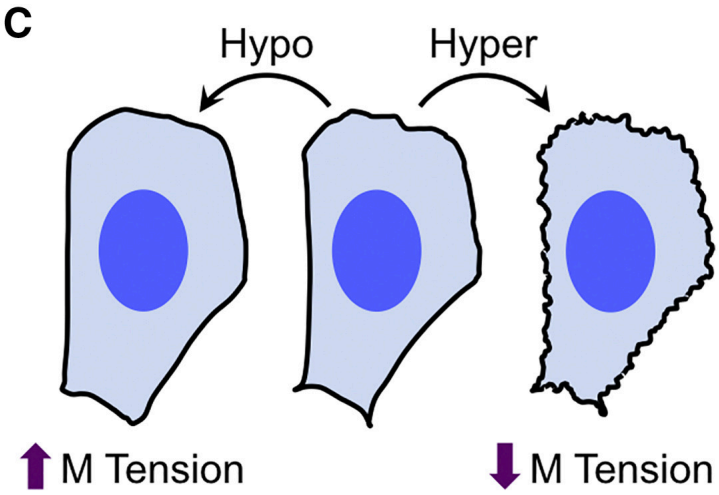

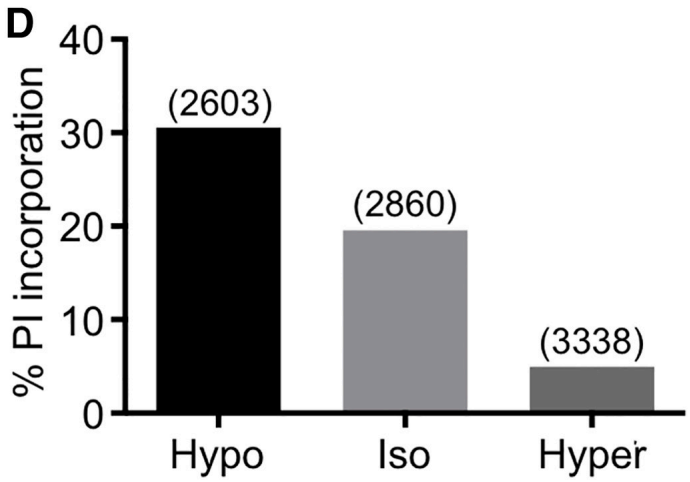

Figure 2.12 Degranulation Is Spatiotemporally Correlated with Force Exertion at the IS

(A) Diagram schematizing fluorescent detection of degranulation during a micropillar experiment. (B–I) CTLs expressing pHluorin-Lamp1 were imaged on stimulatory micropillar arrays. (B) Representative time-lapse montage showing pillar deflections during a degranulation event (indicated by the yellow arrowhead). Time is indicated in M:SS in the top right corner of each image. (C) Graph of the offset time between contact formation and degranulation (degranulation time). (D) Graphical representation of the pillar array in (B), with the degranulation position depicted as a green circle and the cell envelope at the moment of degranulation shown in black. Pillars are color-coded based on their average deflection during the degranulation. Warmer colors (e.g., orange, red) denote stronger deflections. The DDP for this degranulation is indicated by the double-headed white arrow. (E) Histogram plot derived from the experiment in (B) showing the DDP for each position in the CTL interface. The mean value for the distribution is denoted by the vertical cyan line. The vertical green line indicates the DDP for the degranulation itself. (F) DDPs of degranulation (Degran) were compared to the mean values of their paired null distributions. $^{***}p < 0.001$*, calculated by two-tailed paired t test. (G) Schematic diagram of the CTL-array interface showing the radial shells used for spatial analysis. (H and I) The radial distribution of total force exertion (H) and degranulation position (I) in degranulating cells. Color-coding of the bars corresponds to the shells shown in (G). Gray bars indicate the spatial distribution that would be expected by chance (outer shells are larger than inner ones). All error bars denote SEM. For (C), (F), and (I),* $n = 49$ *degranulation events pooled from three independent experiments. Benjamin Whitlock, Weiyang Jin, and Morgan Huse performed these experiments.*

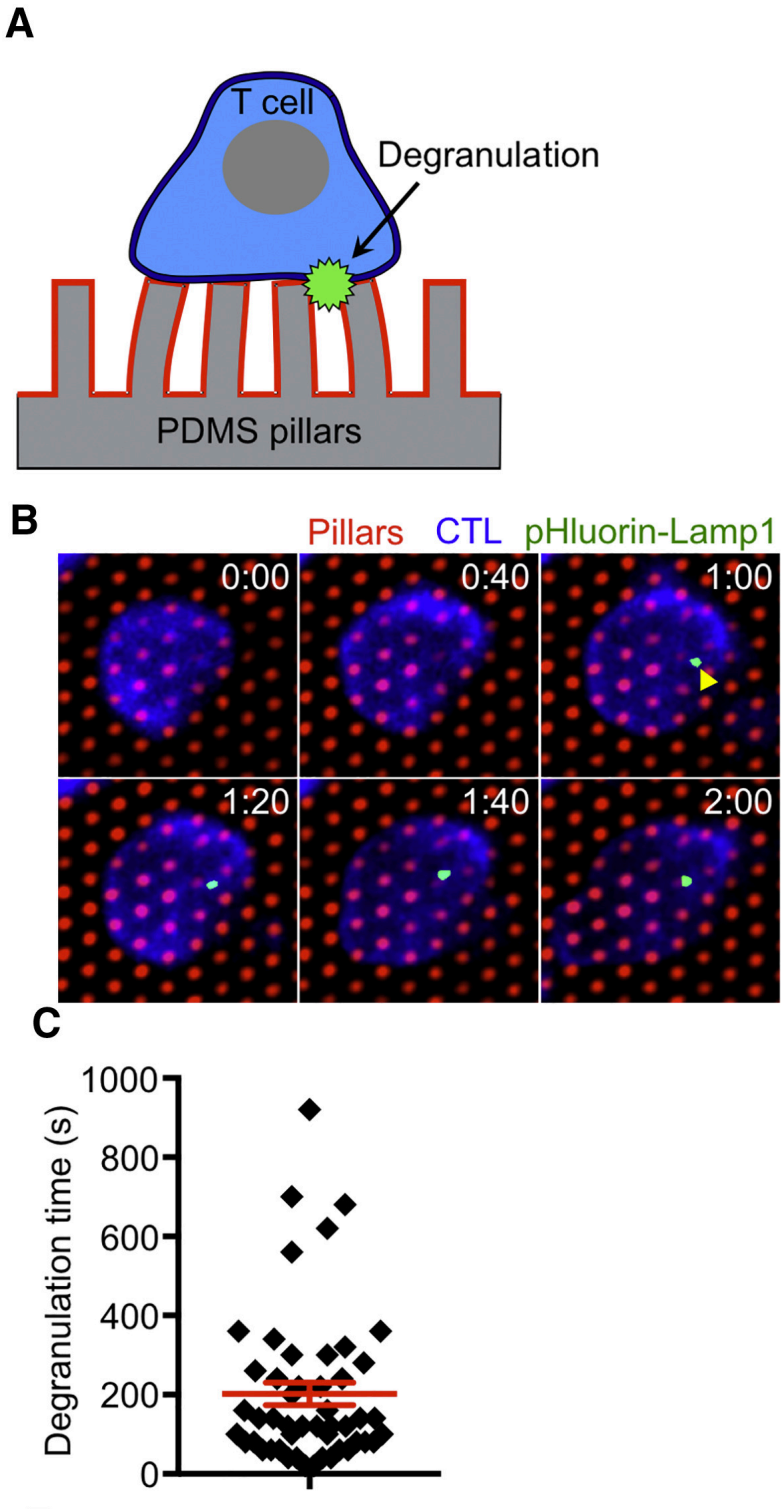
A
T cell
Degranulation
PDMS pillars
B
Pillars CTL pHluorin-Lamp1
0:00
0:40
1:00
1:20
1:40
2:00
C
Degranulation time (s)
1000
800
600
400
200
0

Figure 12 (continued)

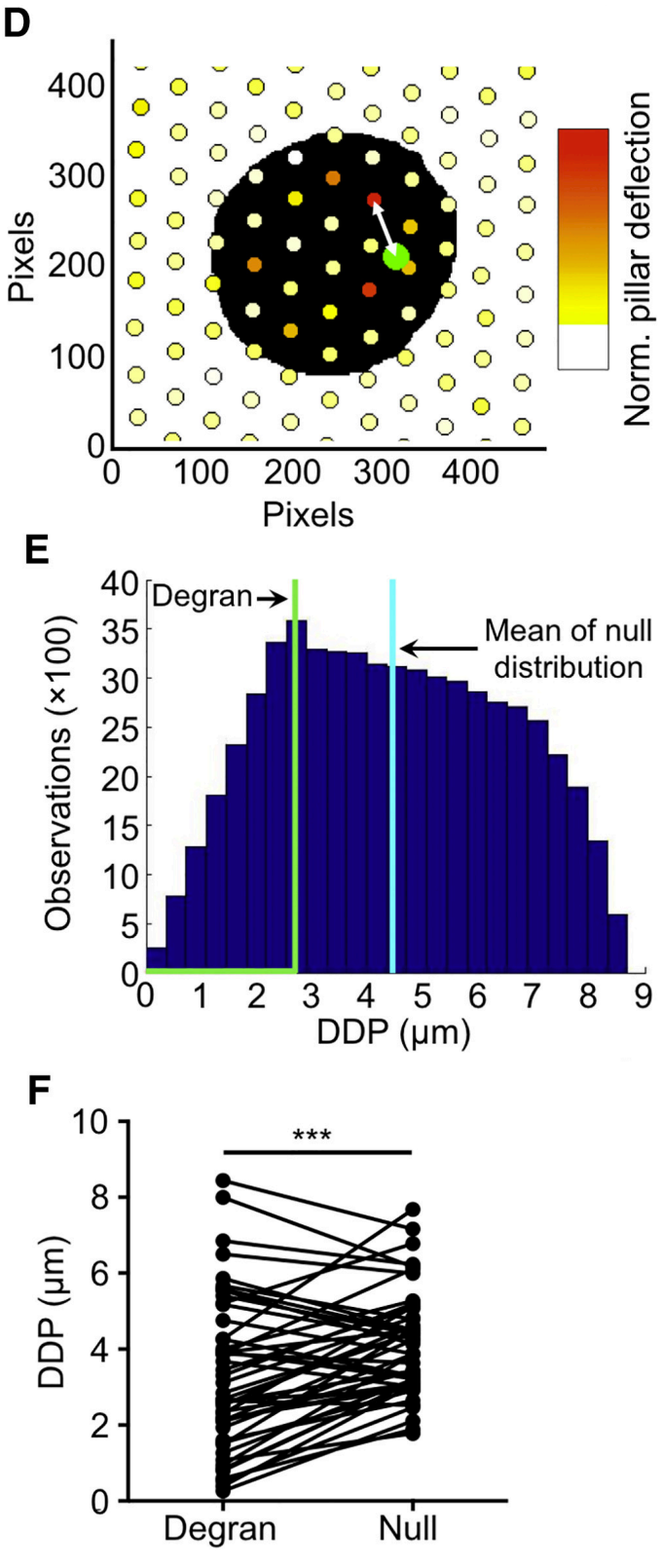

Figure 12 (continued)

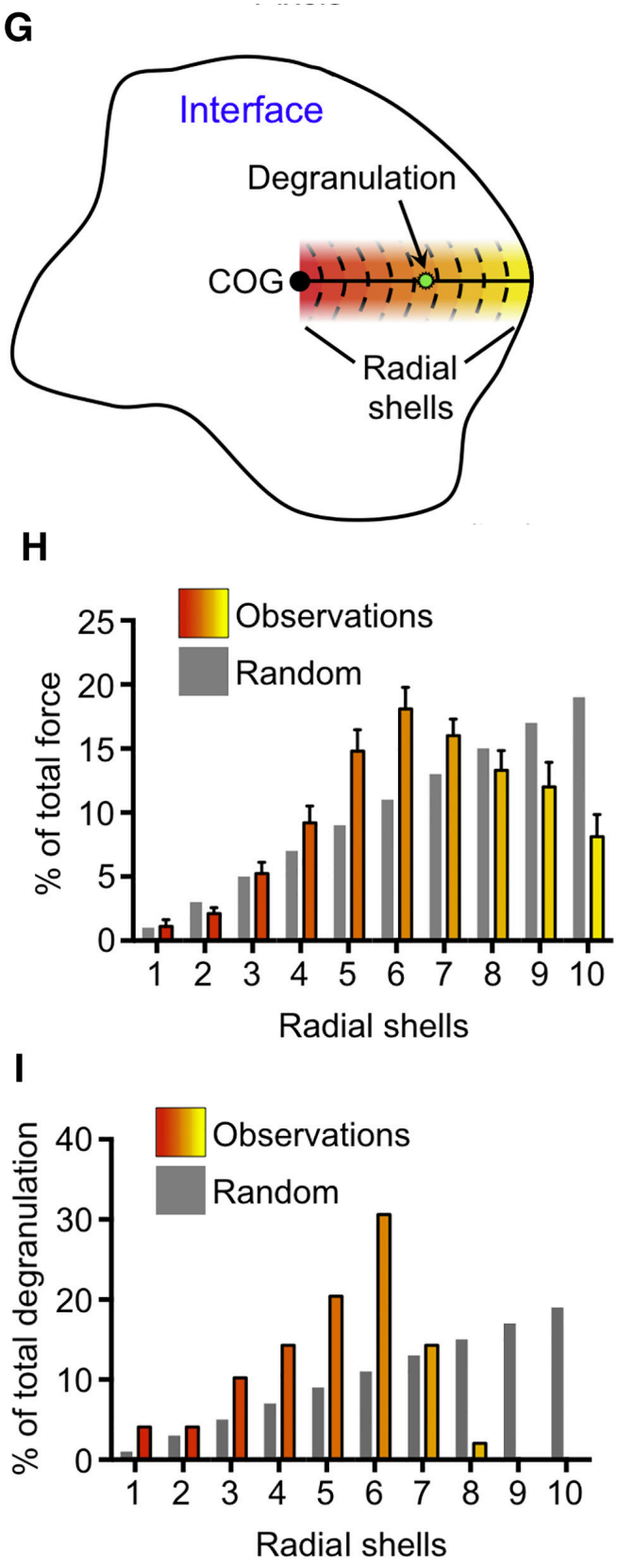

generated by performing the DDP calculation for every x-y position within the interface between the CTL and the array (Figure 2.12E). DDP values associated with degranulation events were significantly lower than the mean values of their paired null distributions, indicating that the observed coupling between granule release and pillar deflection did not occur by chance (Figure 2.12F). We also quantified the radial distribution of degranulation and force exertion within the IS (Figure 2.12G) and found that both parameters were enriched within an annular region slightly more than halfway between the center of the IS and its outer edge (Figures 2.12H and 12I). Taken together, these results suggest that CTLs spatiotemporally coordinate cytolytic secretion with the local application of force, and they also identify a domain within the IS in which these interactions occur.

Could forces within this degranulation zone apply enough membrane tension to potentiate perforin pore formation? To address this question, we first determined the membrane tension change necessary to sensitize a cell to perforin. Using an established approach in which an optical trap is used to pull a thin tether of membrane from the cell surface (Figures 2.13A and 13B), we calculated the membrane tension of adherent B16 cells to be 100 μN/m[131]. In the presence of latrunculin A, which protects cells from perforin pore formation (Figures 2.11B and 2.9B), membrane tension decreased to 15 μN/m. These data suggest that an ~85 μN/m difference in membrane tension (equivalent to 85×10^{-18} J/μm^2) is sufficient to make perforin pore formation more energetically favorable (Figure 2.13C). Assuming a pore size of 15 nm, this tensional difference implies a free energy change of 1.5×10^{-20} J per pore. In micropillar experiments, we routinely observed pillar deflections of >1 μm

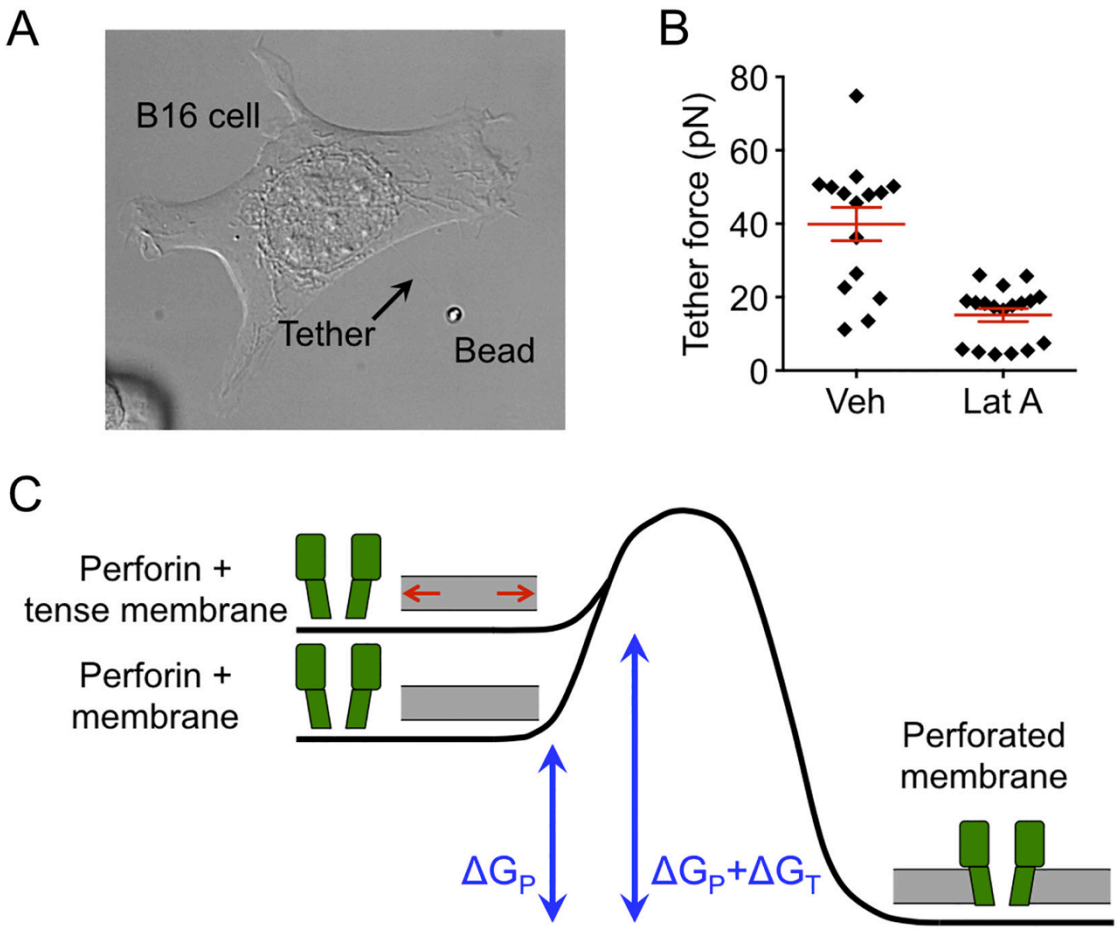

Figure 2.13 Membrane Tension of B16 Target Cells
(A) DIC image showing a membrane tether connecting a B16 cell to a 2 μm diameter polystyrene bead, which is held in an optical trap. (B) Membrane tethers were generated from B16 cells treated with 5 μM Latrunculin A (Lat A) or vehicle control (Veh) as indicated. Tether forces were determined from the displacement of the bead within the optical trap (n ≥ 15 for each sample). (C) Schematic diagram of the reaction coordinate for perforin pore formation in a membrane, illustrating how increased membrane tension can effectively reduce the activation barrier of the process. ΔGP = free energy of pore formation, ΔGT = free energy of tension release. Roshni Basu performed these experiments.

within force exertion hotspots. Each of these strong deflections required >340 pN of force (Figure 2.4D), implying the transfer of >170 × 10^{-18} J of mechanical energy within an ~1 μm^2 region of the array. This degree of energy transmission (170 × 10^{-18} J/μm^2) compares favorably with the tensional change (85 × 10^{-18} J/μm^2) demonstrated by the tether experiments to modulate perforin activity, and it would be sufficient, in principle, to mechanically potentiate a large number of pores. Hence, under conditions of close synaptic contact, CTLs should be capable of locally sensitizing the target cell membrane to perforin.

2.3. Discussion

Communication between immune cells is generally presented as a chemical process based on ligand recognition by receptors. It is becoming increasingly clear, however, that mechanical forces at cell-cell interfaces are necessary both to enable and to regulate communicative chemical interactions. Recent studies have documented the importance of cytoskeletally driven pulling for receptor activation and antigen uptake, which are both processes that mediate information flow into the lymphocyte[69,132,133]. Our results demonstrate that physical forces can also modulate information flow out of the cell, in this case by potentiating the activity of a secreted protein, perforin. This synergy between applied force and outgoing chemical signals, which we term mechanopotentiation, conceptually expands the purview of cellular mechanics as an active mediator of not only afferent but also efferent intercellular communication.

It has been proposed that the IS enhances the intensity and specificity of intercellular communication by restricting the diffusion of secreted

factors[13,134,135]. Studies of cytokine-mediated communication, however, indicate that soluble proteins escape the T cell-target cell interface very quickly[136–138]. An alternative strategy for boosting selectivity and efficiency would involve locally increasing the specific activity of secreted molecules. Synaptic mechanopotentiation of perforin pore formation falls into this second class of mechanisms. Synergy between force exertion and perforin activity would reduce the amount of degranulation required for each killing event and thereby limit bystander damage resulting from excessive cytolytic secretion. It would also facilitate serial killing by enabling CTLs to reserve perforin and granzyme for other targets. We expect that other cytotoxic lymphocytes will also employ this strategy.

Our results demonstrate that NMII is critical for force exertion at the IS. This is surprising given that myosin activity is dispensable for IS formation and only modestly affects synaptic architecture[113–115]. We also found that depletion of NMII reduced CTL-mediated cytotoxicity, implying that myosin-dependent forces contribute to mechanopotentiation during target cell killing. Although we favor this interpretation, it must be noted that CTLs lacking NMII also exhibit delayed centrosome polarization[117]. A partial polarity defect could affect cytotoxicity by altering the directionality of cytolytic secretion. Hence, at this stage we cannot attribute the killing phenotype of NMII-deficient cells solely to a defect in force exertion.

Perforin pores drive target cell killing by inducing a membrane repair response that stimulates the uptake of additional perforin and granzymes[57,58]. Although the methods used in this study assessed the effects of cellular mechanics on initial pore formation, they did not address whether force might

also modulate membrane repair downstream. Membrane tension has been implicated in the regulation of both exo- and endocytosis in multiple cell types[139]. It is therefore quite plausible that CTL-induced distortions within the IS could influence membrane repair and in this manner control not only the initiation but also the progression of cytotoxicity.

F-actin accumulates in the periphery of the IS and is depleted from the center, forming a stereotyped annular pattern[107]. Lytic granules cluster beneath the center of the F-actin ring, and it has been proposed that they release their contents primarily by fusing with the actin-free plasma membrane in this region[14,134]. Using a fluorescent probe for degranulation, we found that cytolytic secretory events are not enriched in the very center of the IS, but rather in an intermediate domain that overlaps with the region of strongest force exertion. In the canonical IS, this intermediate zone is occupied by the inner aspect of the F-actin ring and clusters of integrin; it therefore contains the adhesive and cytoskeletal machinery required to transmit force[140]. Super-resolution imaging studies have demonstrated that this zone can also accommodate the formation of actin hypodense regions of plasma membrane suitable for vesicle fusion[130,141]. Accordingly, we favor a model in which degranulation occurs at the border between the central F-actin-depleted area and the peripheral F-actin ring. This would enable the CTL to balance the physical requirements of exocytosis with the benefits of synaptic mechanopotentiation.

The striking spatiotemporal correlation we observed between lytic granule release and force exertion suggests that CTLs create local mechanical hotspots on the target cell surface that are particularly sensitive to perforin.

Although the fluid nature of lipid bilayers generally promotes rapid equilibration of applied force, local interactions with the cytoskeleton have been shown to generate inhomogeneities in tension[139]. The idea that physical inhomogeneities of this kind could be established within dynamic and strongly adhesive interfaces, such as the IS, is quite intriguing, and represents an interesting topic for future studies.

The mechanical component of cytotoxicity could be particularly important in the context of anti-cancer immunity. Within solid tumors, cells tend to be stiffer because of enhanced cytoskeletal contractility and extracellular matrix rigidity[142]. Although increased stiffness would be expected to promote CTL-mediated killing, any advantage gained by the immune system would likely be overwhelmed by the tolerogenic signals that prevail within the tumor microenvironment[143]. During metastatic dissemination, however, cells from the tumor move away from this immunosuppressive milieu. In that regard, it is interesting to note that isolated cancer cells tend to be softer than their non-transformed counterparts[144–146]. This deformability could enable them to resist immune-mediated attack when outside of the tumor microenvironment.

The intricate cytoskeletal dynamics of lymphocyte synapses include both actin flows that propagate in the plane of the interface and filopodial protrusions that can deform the surface of the target cell[70,108,109,147,148]. As we work to define the functional relevance of these and other structures, it will be important to consider their capacity to transmit information physically during the effector phase of lymphocyte responses. Mechanical forces are well suited for rapid and highly compartmentalized signaling within cell-cell interfaces and

as such, they represent a valuable mode of intercellular communication in complex environments.

2.4. Materials and Methods

2.4.1. Mice

The animal protocols used for this study were approved by the Institutional Animal Care and Use Committee of Memorial Sloan-Kettering Cancer Center.

2.4.2. Cell culture and transductions

CTLs were prepared by mixing T cells from OT-1 αβTCR transgenic mice (Taconic) with irradiated congenic splenocytes pulsed with 100 nM OVA and cultured in RPMI medium containing 10 % (vol/vol) FCS. Cells were supplemented with interleukin 2 (IL2, 30 IU/ml) after 24 h and were split as needed in RPMI containing IL-2. B16-F10 cells were maintained in DMEM containing 10 % (vol/vol) FCS, while RMA-s and EL4 cells were grown in RPMI containing 10 % (vol/vol) FCS.

Expression constructs for shNT, shDock2, shPTEN, shMyH9, and pHluorinLamp1 have been described[8,117,130]. To prepare retrovirus, Phoenix E cells were transfected with expression vectors together with packaging plasmids using the calcium phosphate method. Ecotropic viral supernatants were collected after 48 hr at 37°C and added to OT-1 blasts 2 days after primary peptide stimulation. Mixtures were centrifuged at 1400 × g in the presence of polybrene (4 μg/ml) at 35°C. T cells were then split 1:3 in medium containing IL-2.

2.4.3. Pillar studies

Micropillar coating and data acquisition. For coating, arrays were washed with ethanol and phosphate buffered saline (PBS) and then incubated in Alexa568-labeled streptavidin (20 μg/ml in PBS) at room temperature for at least two hours. After further washing in PBS, the arrays were incubated with biotinylated H2-Kb -OVA and ICAM-1 (each 20 μg/ml in PBS) for 2 hours at room temperature. The pillars were then washed into colorless RPMI containing 5% FCS (Imaging medium). Data acquisition was implemented using Metamorph software. For standard force quantification experiments (Figure 2.4), brightfield, Alexa488 (CTL), and Alexa568 (pillars) images were collected every 15 s. For degranulation experiments (Figure 2.12), brightfield, Alexa488 (degranulation), Alexa647 (CTL), and Alexa568 (pillars) images were collected every 20 s. Images were exported as tif files and aligned using a custom Matlab script.

2.4.4. Micropillar deflection analysis

Center of gravity (COG) projections of pillar deflections were determined by calculating the projection of each deflection along a line connecting the pillar to the COG of the CTL footprint. Degranulation events were identified as an abrupt increase in GFP fluorescence. To determine the DDP (Distance to Displaced Pillar) parameter for a degranulation event, average deflections were 2 determined for the time period beginning 40 s before degranulation and extending 120 s after. “Strongly deflected” pillars were then identified as pillars with mean deflections ≥ 0.75 × the mean deflection of the most strongly deflected pillar during this time frame. The distance between the degranulation position and the closest “strongly

deflected" pillar was defined as the DDP. DDP values for degranulation events were compared to null distributions generated by performing the DDP calculation for every position in the CTLarray interface at the time of degranulation. Paired analysis of degranulation DDPs and mean DDPs from null distributions was carried out using Prism (GraphPad). Radial shell analysis was performed by determining the position of relevant pillars and degranulation events along a segment beginning at the COG of the interface (assigned a value of 0) and ending at the edge of the interface (assigned a value of 10). The mechanical energy required for pillar deflections was calculated using the following expression (E = Fd/2), where E is the energy, F is the force, and d is the length of the deflection.

2.4.5. Cytotoxicity assays

RMA-s cells labeled with the membrane dye PKH26 (Sigma-Aldrich) were pulsed with varying concentrations of OVA and mixed 1:1 in 96-well plates with OT-1 CTLs. After 6 hr at 37° C, samples were treated with 2.5 mM EDTA to disrupt conjugate formation and specific lysis of PKH26+ target cells was assessed by flow cytometry as described[149].

B16-F10 cells were cultured overnight on fibronectin-coated hydrogels in the presence of 20 ng/ml IFNγ, which was included to induce upregulation of class I MHC. They were then loaded with 100 nM OVA for 1 hour and washed three times in lactate dehydrogenase (LDH) release assay medium (RPMI with 5% vol/vol FCS). OT-1 CTLs were added at various effector to target (E:T) ratios and incubated for 5 hr at 37° C in LDH medium. Target cell death was quantified with an LDH cytotoxicity assay kit (Clontech) using the manufacturer's recommended protocol. All measurements were performed in

triplicate. To assess degranulation responses, CTLs were added to B16-F10 cells at a 1:1 E:T ratio and incubated for 2 hr at 37° C in the presence of eFluor660 conjugated anti-Lamp1 antibody (1 μg/ml, Clone 1D4B, eBiosciences). Staining was quantified by flow cytometry. In staurosporine-induced apoptosis assays, B16 cells cultured on fibronectin-coated hydrogels were treated with varying concentrations of 3 staurosporine, and lysis was quantified by LDH release after 17 h at 37 C.

2.4.6. Perforin pore formation in microwells

PDMS grids containing 50 × 50 × 50 μm wells were submerged in imaging medium and seeded with CFSE-labeled RMA-s cells that had been pulsed with 1 μM OVA. In general, individual wells contained one to three RMA-s cells; 100 μM PI (Life Technologies) was added to the medium to enable real-time visualization of perforated cells. Then, CTLs expressing shNT or shPTEN together with CFP were added and the cells imaged using a 20× objective lens (Olympus) at 6-min intervals for 8 hr. Brightfield, GFP, CFP, and PI images were collected at each time point. Quantification was restricted to target cells forming synapses with only one T cell during the first 6 hr of the imaging experiment. All cells in this category were scored for the time of initial IS formation and also for the first appearance of PI signal above background.

2.4.7. Micropipette preparation and calibration

Tapered micropipettes were prepared by pulling borosilicate glass capillaries (1 mm OD, 0.78 mm ID, Harvard Apparatus) with a P-97 device (Sutter Instruments). A microforge (MF-200, WPI) was used to cut the bead micropipette and the rigid CTL micropipette at the desired diameters (typically 1 μm and 3 μm, respectively). Another microforge (MF-900, Narishige) was

then used to introduce a 90° bend at the end of the bead micropipette. 45° angles were also introduced into the bodies of both pipettes to position their extremities orthogonal to the imaging plane during experiments. The bending stiffness k of the bead micropipette was measured by pushing its tip against the tip of a thicker micropipette of known stiffness. A single-axis piezo translation stage (Thorlabs) was used to move the bead micropipette in a sinusoidal fashion and the position of each tip was detected at 30Hz using a homemade Labview program (National Instruments). The observed ratio of pipette deflections was then used to deduce the stiffness of the bead micropipette (typically k = 0.1 nN/μm).

2.4.8. Micropipette-Based Force Measurements

Stimulatory beads were prepared by coating 6-μm diameter streptavidin-coated polystyrene particles (Spherotech) with biotinylated H2-K^b-OVA and ICAM-1 (1 μg/ml each) for 2 hr in 20 mM HEPES pH 7.5, 150 mM NaCl, 2% w/v BSA. Micropipettes for stimulatory beads and CTLs were prepared from borosilicate glass capillaries (1 mm OD, 0.78 mm ID, Harvard Apparatus). Imaging was carried out in an open top, environmentally controlled chamber mounted on an inverted microscope (Nikon TE300) equipped with a 100× objective lens. The rigid CTL micropipette was attached to a motorized micromanipulator (MP285, Sutter Instruments) and the bead micropipette to manual micrometers (Thorlabs). Beads were aspirated into the tip of the calibrated micropipette by applying ~6 kPa aspiration pressure using a syringe (typically 1 ml air volume depression). Two hundred pascals of pressure (applied using a water reservoir) was used to aspirate a CTL into the tip of the rigid pipette. Time-lapse recordings were started just before the CTL

was gently brought into contact with the bead. In general, 50 ms brightfield exposures were taken at 2-s intervals for 3–5 min using Micromanager software. The deflection of the flexible micropipette was determined by tracking the position of the bead using a customized ImageJ macro[110]. Bead position was determined with a precision of <60 nm, corresponding to a precision in force better than 6 pN for probe bending stiffness k = 0.1 nN/μm.

2.4.9. Cellular perforation assay

Twenty-four hours prior to imaging, B16-F10 cells were plated at 10^4cells/100 μl/well in either fibronectin-coated 96-well plates (Costar) or in 96-well flat-bottom plates coated with polyacrylamide hydrogels (Matrigen) and fibronectin. One hour prior to imaging, cells were transferred into C^+ buffer HBSS (Hank's balanced salt solution) with 10 mM HEPES pH 7.2, 4 mM $CaCl_2$, 2 mM $MgCl_2$, 0.4% BSA) containing Hoechst 33342 stain (1:2,000, Invitrogen). PI (100 μM final concentration) was added along with Blebbistatin (Sigma) or Latrunculin A (Sigma) as necessary. After 5 min, Hoechst and PI images were collected at 2-min intervals for 30 min using an inverted wide-field microscope (Zeiss Axiovert 200M, Metamorph acquisition software) fitted with a 5× objective lens (Zeiss). Dilutions of purified perforin in 50 μl C^- buffer (HBSS, 10 mM HEPES pH 7.2, 1 mM EGTA, 0.4% BSA) were added 4 min into the imaging run. To vary tonicity, hypertonic (+150 mM sucrose) or hypotonic (H_2O instead of HBSS) C^+ and C^- buffers were used instead of isotonic C^+ and C^-.

2.4.10. Perforin purification and fibronectin coating for perforation assay

Human perforin was purified from YT-Indy cells as described[150], but using the following modified relaxation buffer: 100 mM KCl, 3.5 mM MgCl2, 10 mM PIPES pH 6.8, 1.25 mM EGTA, and 1 mM ATP. Perforin is a metastable, hydrophobic molecule with a tendency to aggregate. The overall activity of each preparation varied considerably, and the activity of any one preparation changed over the course of a few hours. To circumvent this issue, we collected each experimental condition either right before or right after its associated control, and switched the order of data collection in repeat experiments. This enabled us to observe robust relative changes, despite the day-to-day variation in overall perforin activity. For coating, plastic wells were incubated with 10 µg/ml fibronectin (Calbiochem) for 1 hr at 37° C, and polyacrylamide hydrogels (Matrigen) were incubated with 10 µg/ml fibronectin for 30 min at room temperature.

2.4.11. Lytic granule polarization

OT-1 CTLs expressing shNT, shDock2, or shPTEN together with GFP were mixed 1:1 with EL4 thymoma cells that had been loaded with 1 µM OVA. After 10 min, cells were transferred into warm HBSS, attached to poly-D-lysine-coated coverslips, and fixed with 4% paraformaldehyde. After washing with PBS and permeabilization with 0.2% Triton X-100 in PBS, cells were blocked with PBS + 10% normal goat serum and then incubated in blocking buffer containing antibodies against Lamp1 (eBioscience, clone 1D4B, 1:200 dilution) and pericentrin (Abcam, rabbit polyclonal, 1:200 dilution) overnight at 4° C. Cells were then washed in PBS and incubated in blocking buffer

containing Alexa594 labeled anti-Rat antibodies and Alexa647 labeled anti-Rabbit antibodies (both 1:1000 dilution) for 2 hr at 4° C. After a final wash in PBS, Cells were mounted on glass slides and sealed. CTL-target cell conjugates were imaged using an inverted fluorescence microscope (Olympus IX-81) fitted with a 65× objective lens (Olympus). In addition to a brightfield image, z-stacks (1 μm increments, 20 μm total) of Alexa594, Alexa647, and GFP were collected for each field of view. Lytic granule polarization was quantified using projection images derived from the z-stack data. For each CTL, intensity thresholding was used to establish a mask encompassing the lytic granule compartment. Polarization of this mask toward the IS was then quantified by calculating a polarization index = (Distance between the IS and the center of gravity of the granule mask)/(Distance between the IS and the opposite side of the CTL). T-test analysis of the resulting distributions was performed in Prism.

2.4.12. Immunoblot

0.2-1 × 106 CTLs were lysed in ice cold buffer containing 10 mM TrisHCl, 5 mM EDTA, 1% NP-40, 0.5% sodium deoxycholate, and 0.15 M NaCl. Perforin expression was assessed using a rabbit polyclonal antibody (Cell Signaling). Actin served as a loading control (clone AC-15, Sigma).

2.4.13. Ca^{2+} imaging

CTLs were loaded with 5 μg/ml Fura-2AM and then added to glass or PDMS surfaces that had been coated with H2-Kb -OVA and ICAM-1. Stimulatory PDMS was prepared as described above and glass surfaces were coated using an established protocol[149]. Fura2 images using 340 nm and 380 nm excitation were acquired every 30 seconds for 20–30 min with a 20×

objective lens (Olympus). Single cell Ca^{2+} responses were quantified by normalizing the Fura2 ratio of each cell using the last image before the initial rise in Ca^{2+}.

CHAPTER 3: INSIGHTS INTO ADOPTIVE CELL THERAPIES FROM MODULATING PI3K IN A TRANSPLANTABLE MELANOMA MODEL

3.1. Introduction

For decades, there has been great interest in using the immune system to treat cancer. Recently, several pioneering strategies have emerged that have reinvigorated the field, especially with respect to the idea of ACTs as a way to treat cancer[96,98]. These treatments involve isolating a patient's cells from peripheral blood and expanding them *ex vivo*. When the cells are being cultured *ex vivo*, they can be treated with various cytokine cocktails or transfected with various plasmids. Constructs of interest include ones to drive expression of an engineered receptor such as a CAR, which targets the T cell to attack cells expressing tumor antigens like CD19. These expanded cells are then transferred back into the patient where they attack the patient's cancer.

We wondered whether the shRNA targeting PTEN we had identified and characterized previously would be a viable way to increase the killing capacity of T cells *in vivo* and to improve ACTs. We hypothesized that increasing the cytotoxic potential of T cells used in ACT would increase the efficiency of ACT. We chose to examine ACT using a mouse melanoma model[151,152]. Surprisingly, we found that T cells expressing the shRNA targeting PTEN performed worse than control cells despite exhibiting increased cytotoxicity *in vitro*. We discovered that shPTEN T cells experienced reduced persistence *in vivo* that diminished their ability to form an anti-tumor

response and to control tumor growth. This provided us with an opportunity to examine how migration, survival, and proliferation contribute to persistence. We discovered that shPTEN CTLs have defects in migration and homeostatic proliferation, which contribute to reduced persistence relative to control CTLs.

3.2. Results

3.2.1. PTEN depletion increases cytotoxicity

Even though PTEN depletion has been previously shown to enhance T cell cytotoxicity *in vitro*[8,153], we wanted to demonstrate that the increase in cytotoxicity we observe with shPTEN CTLs was not due to an off-target effect of the shRNA. To do this, we isolated OT-1 T cells from a mouse expressing Cas9 in the Rosa26 locus and transduced them with a retroviral construct to express a gRNA targeting PTEN[154]. Complete deletion of PTEN was confirmed by Western Blot (Figure 3.1A). Next, we assessed the cytotoxic capacity of PTEN depleted cells, comparing cells that were treated with the shRNA and the gRNA. We found that both methods of deleting PTEN result in increased cytotoxicity relative to nontargeting control constructs (Figure 3.1B). This shows that the increase in cytotoxicity we observe is due to PTEN depletion and not off target effects of an shRNA.

3.2.2. PTEN depletion reduces anti-tumor effect

We next assessed the effect shPTEN CTLs had on tumor rejection using a transplantable B16-OVA melanoma model to evaluate ACT[151,152]. A schematic of the experimental outline is shown in 3.2A. Mice were implanted with $2x10^5$ B16-OVA cells subcutaneously (s.c.) and small tumors were allowed to develop. After 7-9 days, the mice were sublethally irradiated with 600cGy to establish a lymphopenic environment. The following day, $1x10^6$ CTLs

transduced with either a control shNT or shPTEN vector were transferred to the mice by i.v. injection. The tumors were then monitored over the next few weeks and measured with calipers. We observed an impaired anti-tumor response in mice that received shPTEN CTLs relative to control mice (Figure 3.2B). This was unexpected as we thought the mice receiving shPTEN CTLs would experience an enhanced anti-tumor effect given their increased cytotoxicity *in vitro* (Figure 3.1B). This provided us with an intriguing opportunity to study the components of ACT necessary for anti-tumor effects that are independent of cytotoxicity.

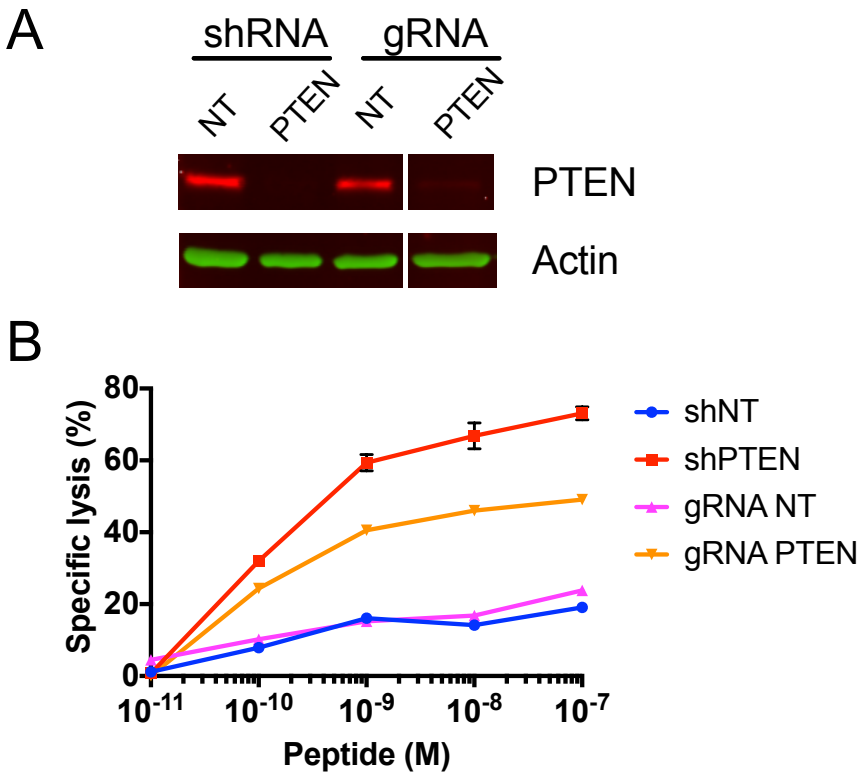

Figure 3.1 PTEN depletion enhancing cytotoxicity
(A) PTEN was depleted using CRISPR/Cas9 and knockout was confirmed by Western Blot.(B) We observed a similar increase in cytotoxicity when we deleted PTEN using CRISPR/Cas9 as shRNA. The provided Western Blot was cropped from a single membrane to display the relevant bands. Error bars denote SEM.

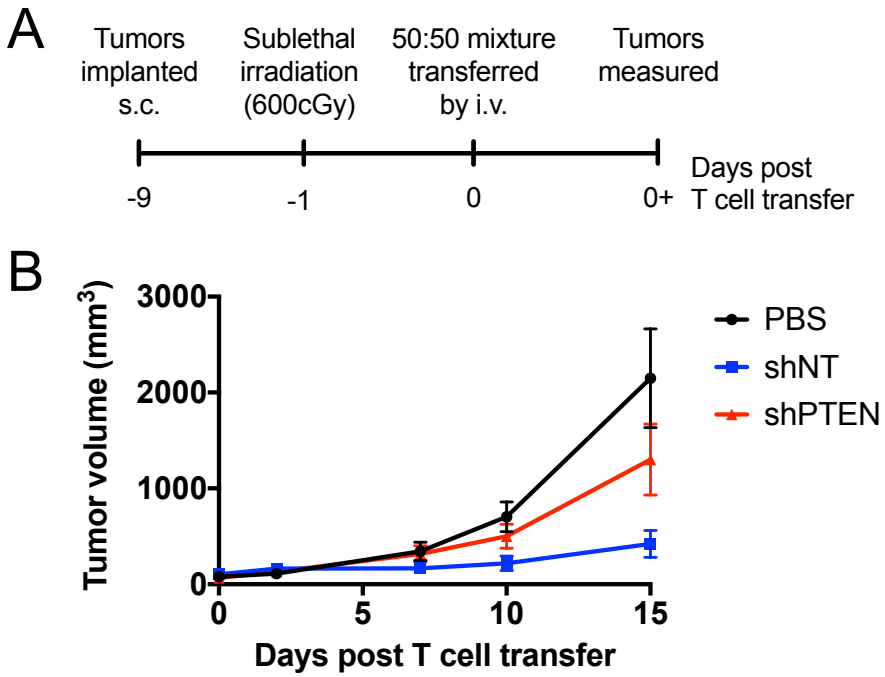

Figure 3.2 PTEN deletion results in reduced anti-tumor effect in vivo
(A) Schematic showing experimental procedure where B16-OVA cells were implanted and OT-I cells were transferred after 9 days. (B) Tumor growth was measured over 15 days post transfer of T cells transduced to express the indicated shRNA. Error bars denote SEM.

3.2.3. PTEN deficient T cells fail to persist *in vivo*

To understand the diminished anti-tumor effect observed for mice receiving shPTEN CTLs, we conducted experiments to monitor persistence of the cells. We adapted our experimental setup to utilize congenic recipients. This provided us with a way to differentiate host cells from transferred cells. We transferred a 50:50 mixture of congenically marked CD45.1/2 CTLs expressing shPTEN and shNT into a tumor bearing recipient mice expressing CD45.2 (Figure 3.3A). We distinguished shPTEN and shNT cells by marking them with different fluorescent reporters.

Figure 3.3 PTEN depleted T cells have reduced persistence in vivo
(A) Schematic showing the experimental procedure where a mixture of CD45.1/2 expressing T cells were transferred into a tumor bearing CD45.2 recipient. (B) Organs were harvested at the indicated times and analyzed for the presence of transferred cells. The draining lymph node (dLN), non-draining lymph node (ndLN), and mesenteric lymph node (mLN) were also analyzed. (C) Additional organs were analyzed for the presence of shPTEN T cells after 3 days. Error bars denote SEM.

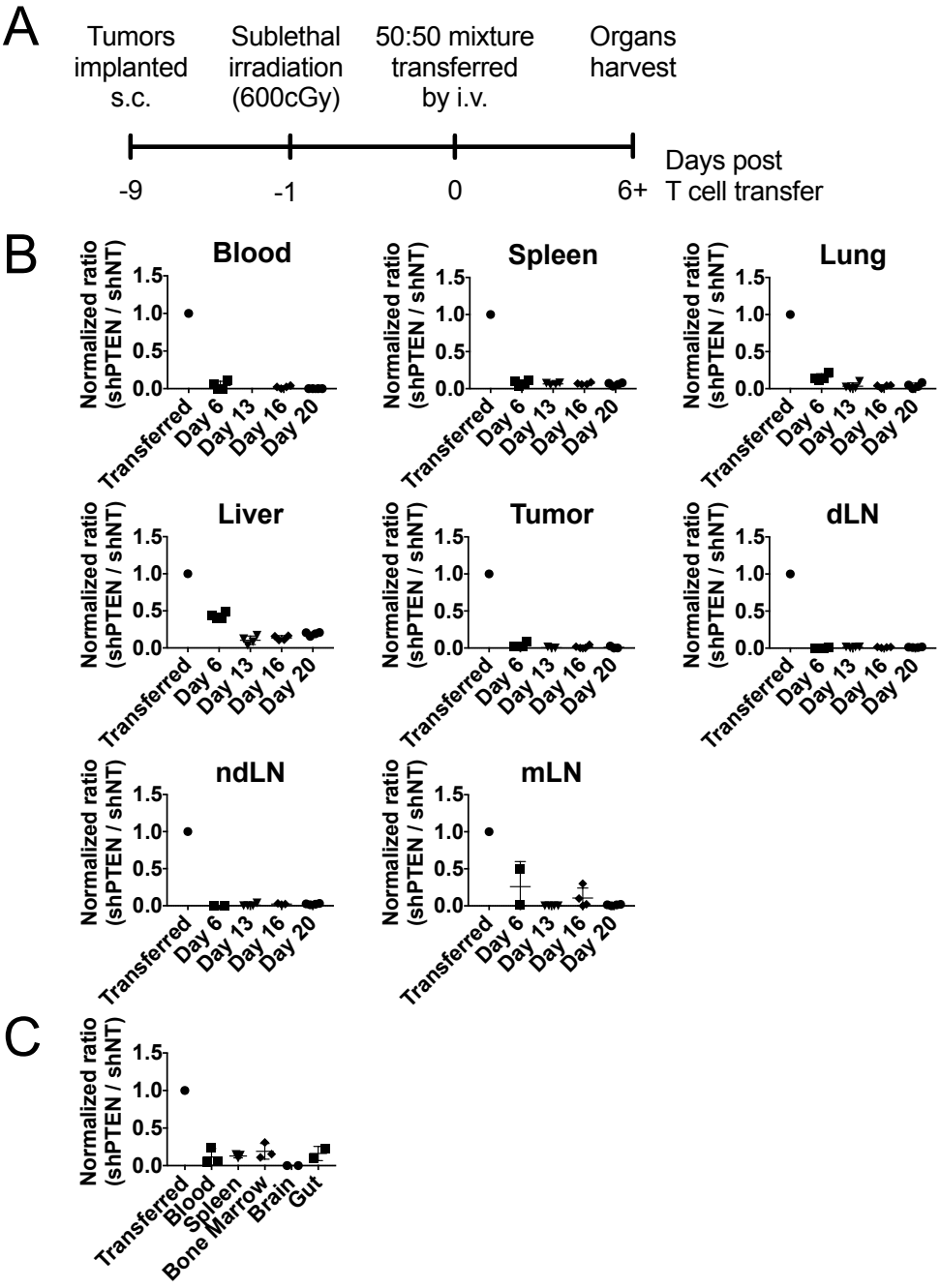
A
Tumors implanted s.c.
Sublethal irradiation (600cGy)
50:50 mixture transferred by i.v.
Organs harvest
-9
-1
0
6+
Days post T cell transfer
B
Blood
Spleen
Lung
Liver
Tumor
dLN
ndLN
mLN
Normalized ratio (shPTEN / shNT)
1.5
1.0
0.5
0.0
Transferred
Day 6
Day 13
Day 16
Day 20
C
Transferred
Blood
Spleen
Bone Marrow
Brain
Gut

We found that that within 6 days after transfer there was a reduced ratio of shPTEN cells to shNT control cells in all organs (Figure 3.3B). PTEN depleted T cells seemed to stay in the lungs and liver temporarily. However, the shPTEN cells were not present in the secondary lymphoid organs including the spleen and various lymph nodes (Figure 3.3B). We assessed whether the shPTEN cells could be homing to other tissues and examined the gut, bone marrow, and brain (Figure 3.3C). The shPTEN cells found in these tissues were at similar ratios to control cells as previously found (Figure 3.3B). Hence, depletion of PTEN induced a persistence defect after adoptive transfer into lymphopenic recipients.

3.2.4. Persistence defect not due to shRNA specificity

We wanted to test whether the persistence phenotype we observed for CTLs expressing shPTEN could be an off-target effect of the shRNA. To address this, we conducted co-transfer experiments using multiple methods of depleting PTEN. We depleted PTEN using the CRISPR/Cas9 system and performed a co-transfer experiment with a nontargeting gRNA. We also examined whether the phenomenon we had only observed in $CD8^+$ T cells could also occur in $CD4^+$ T cells by transducing polyclonal T cells isolated from a mouse expressing the $PTEN^{fl/fl}$ allele with a retroviral Cre[155]. We observed the same loss of CTLs in mice that received Cas9/gRNA and shRNA treated cells (Figure 3.4A). Furthermore, we observed the same effect when we adoptively transferred polyclonal T cells isolated from $PTEN^{fl/fl}$ mice and transduced with Cre or an empty vector control into a lymphopenic recipient mouse (Figure 3.4B). Interestingly, we found that $CD4^+$ T cells seemed to also be affected but to a lesser degree than $CD8^+$ T cells. This suggested to us that

the loss of PTEN deficient cells we were observing was the direct result of PTEN loss and not an off-target effect.

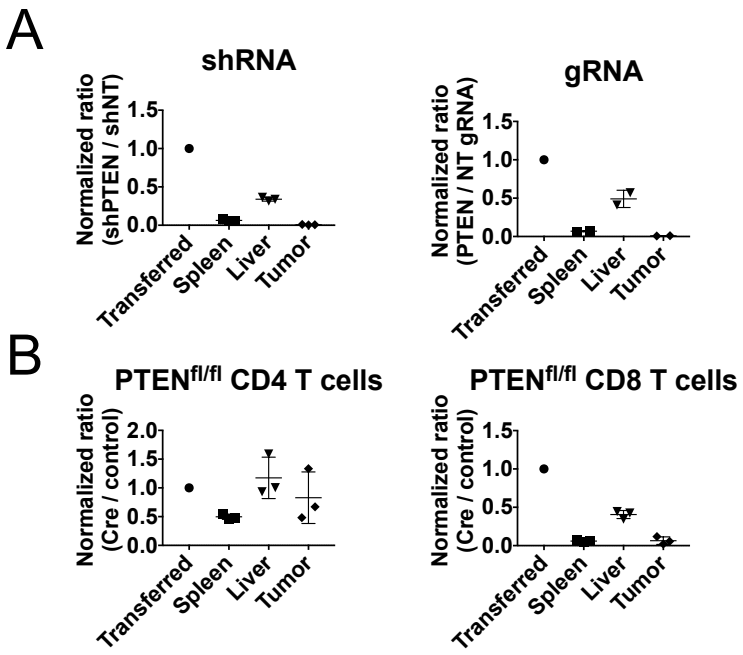

Figure 3.4 Loss of PTEN depleted cells is not due to shRNA
Co-transfer experiments confirmed that depleting PTEN by CRISPR/Cas9 (A) and by transducing PTEN$^{fl/fl}$ cells with Cre (B) phenocopy loss of shPTEN cells(A). Error bars denote SEM.

These observations agree with previous work demonstrating that T cells with a constitutively active AKT had a defect in persistence following LCMV infection[156]. This is also consistent with work showing that enhancing PI3K signaling in thymocytes isolated from Lck-Cre PTEN$^{fl/fl}$ mice reduces their persistence in a PDK1 dependent manner[157]. Together, these results demonstrate that modulating PI3K signaling has detrimental effects on T cell persistence *in vivo*.

Persistence of shPTEN cells *in vivo* is reflective of several factors including survival, migration, and proliferation. As adoptively transferred cells

migrate through secondary lymphoid organs, they are exposed to survival signals[158]. If transfer occurs into a lymphopenic host, the lymphocytes will undergo homeostatic expansion, which can further obfuscate persistence. In order to properly understand the persistence defect of shPTEN T cells, we sought to disentangle these components and evaluate them separately.

3.2.5. PTEN deficient T cells have a defect in migration

We wanted to assess whether the defect in persistence we observed could be the result of a trafficking defect. We designed a series of short-term migration experiments to assess the ability of shPTEN CTLs to migrate *in vivo*. We transferred a 50:50 mixture of shPTEN and shNT cells as before (Figure 3.3A). Tissues were processed and analyzed 2 hours post transfer. At this time point, most of the shNT and shPTEN cells were isolated from the lungs and liver. An appreciable number of cells could also be found in the blood, spleen, lymph nodes, and tumor, however, enabling comparative analysis. The ratio of shPTEN to shNT cells was reduced within two hours after transfer (Figure 3.5A). The shPTEN T cells were unable to migrate to secondary lymphoid organs (Figure 3.5A-D). shPTEN T cells were mainly found in the liver and lungs, but did not persist in these tissues long enough and were not present after 6 days (Figure 3.3B). Between the 2 hour and 22 hour time point, there was a significant loss of shPTEN cells in the blood and an increase in the number of cells in the liver (Figure 3.5A-D). There was also an increase in the number of shPTEN cells in the spleen at 22 hours even though the ratio is unchanged. These data suggest that PTEN deficient cells have a defect in migration *in vivo*.

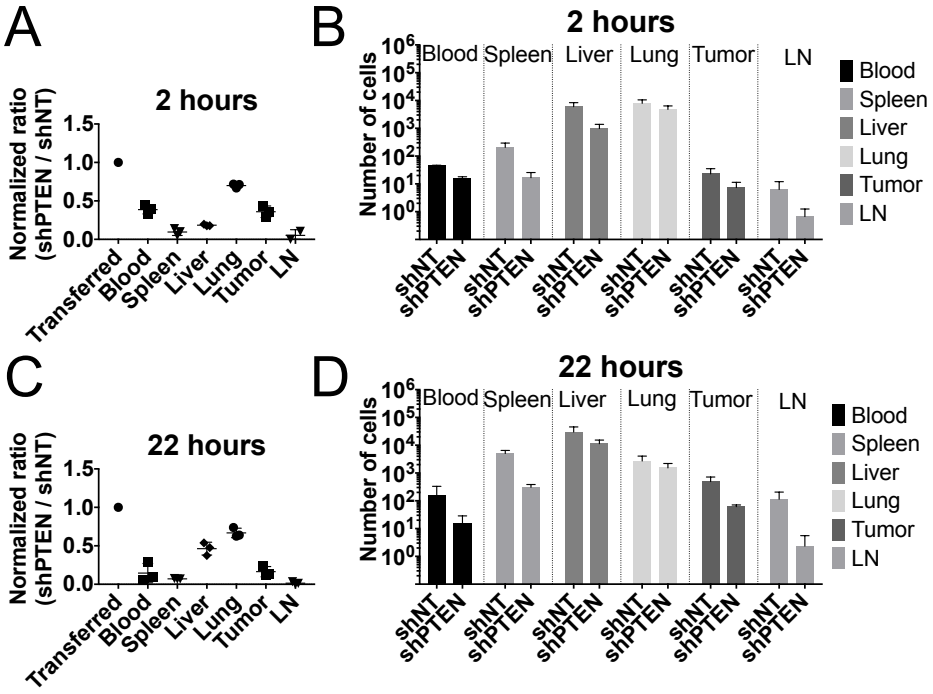

Figure 3.5 PTEN deficient cells have migration defect
(A-B) A short term migration experiment was conducted and organs were harvested and processed 2 hours after T cell transfer. The normalized ratio for shPTEN to shNT cells is given (A) and the number of cells collectd from each organ (B). Mice were also analyzed 22 hours after transfer (C-D). Lymph nodes (LN) were pooled and analyzed. Error bars denote SEM.

3.2.6. PTEN deficient T cells have reduced expression of trafficking receptors

We examined the PI3K/AKT signaling pathway to identify proteins that might be differentially expressed in PTEN deficient T cells. We identified the transcription factor KLF2, downstream of mTORC1 and FOXO1, as a protein that could contribute to a migration defect (Figure 3.6A). KLF2 plays an important role in regulating expression of CCR7, S1PR1, and CD62L[29]. We found that shPTEN CTLs expressed reduced levels of CD62L (Figure 3.6B-C). We also found that shPTEN CTLs expressed reduced levels of IL-7Rα (Figure

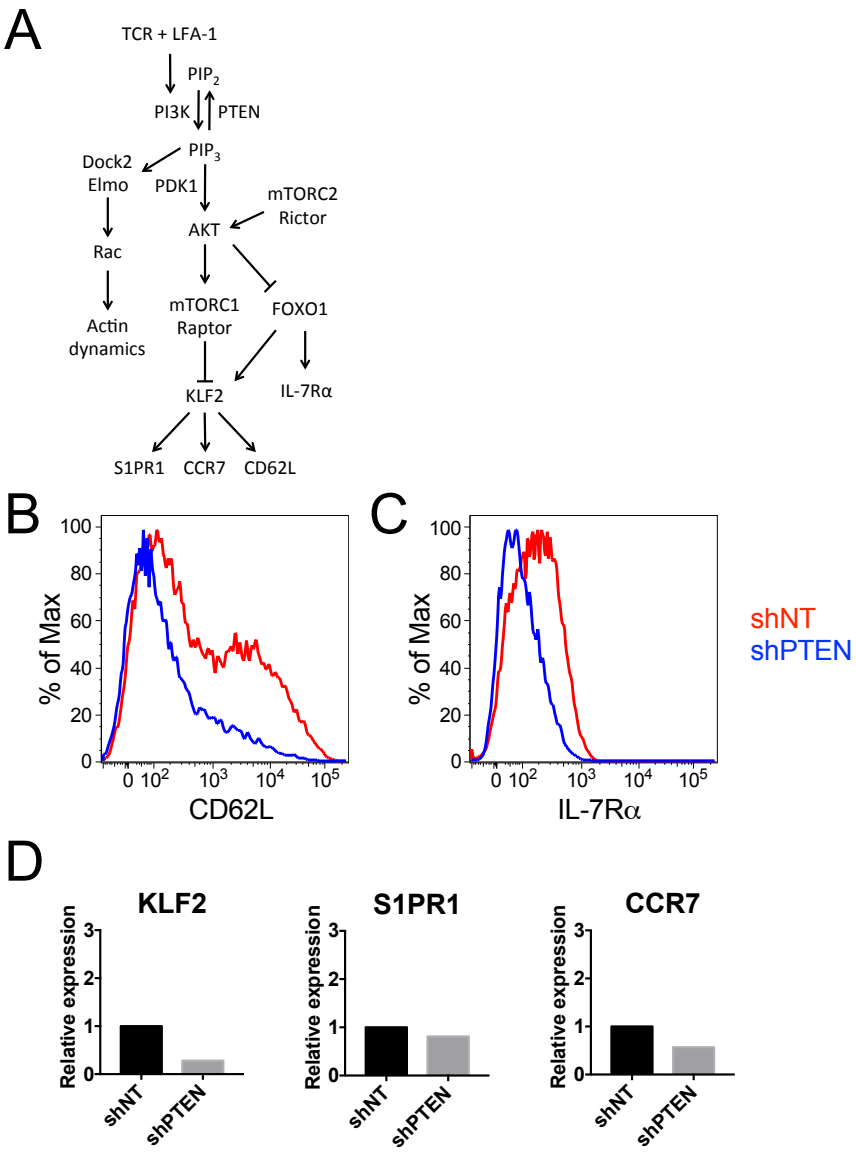

Figure 3.6 Enhancing PI3K signaling disrupts expression of key receptors

(A) Diagram of PI3K signaling showing the proteins that are disrupted by depleting PTEN. (B) CD62L expression was reduced on shPTEN T cells. (C) CD62L and IL-7Rα was increased by treating cells with 2ng/mL IL-15 and 2nM rapamycin (R). (D) Expression of KLF2, S1PR1, and CCR7 was assessed by qPCR and found to be reduced in shPTEN CTLs.

3.6C). Furthermore, we found that the expression of KLF2 was reduced by qPCR. We also observed reduced expression of CCR7 and S1PR1 in shPTEN CTLs by real time polymerase chain reaction (RT-PCR) (Figure 3.6D). These results agree with previous data implicating PI3K signaling in T cell migration[9,157]. However, the observation that shPTEN cells have a defect in migration does not rule out other defects that might contribute to defective persistence.

3.2.7. PTEN deficient T cells have increased cell survival *in vitro*

Previous research has identified PTEN as a tumor suppressor as its loss promotes increased cell growth and proliferation[159,160]. We hypothesized that PTEN deficiency in T cells would drive a similar increase in cell survival and proliferation through PI3K and AKT signaling. However, T cell survival *in vivo* and homeostatic proliferation are driven by IL-7 and IL-15[161]. We found that IL-7Rα was downregulated on shPTEN CTLs (Figure 3.6C). We wondered whether this would effect the survival of shPTEN T cells *in vivo* where they depend on IL-7. We also wondered whether the increase in cell survival and proliferation associated with PTEN loss would occur in T cells moving from a high nutrient environment *in vitro* to a low nutrient environment *in vivo*. To assess these possibilities, we designed a survival assay to monitor T cell survival in low nutrient conditions. To understand how cytokine signaling could impact cell survival in low nutrient conditions, we incorporated a variety of cytokine conditions into the assay. We monitored survival after 1 and 2 days in the presence of 30 IU/mL IL-2, 1ng/mL IL-7, and 10ng/mL IL-7. As a control, we also monitored survival in the absence of cytokines (Figure 3.7A-D). PTEN

Figure 3.7 PTEN Deficient cells have similar or increased survival relative to control T cells

(A-D) CTLs transduced with shPTEN or shNT shRNAs were incubated for 1 or 2 days with the media with the indicated nutrients removed or present. Error bars denote SEM.

A

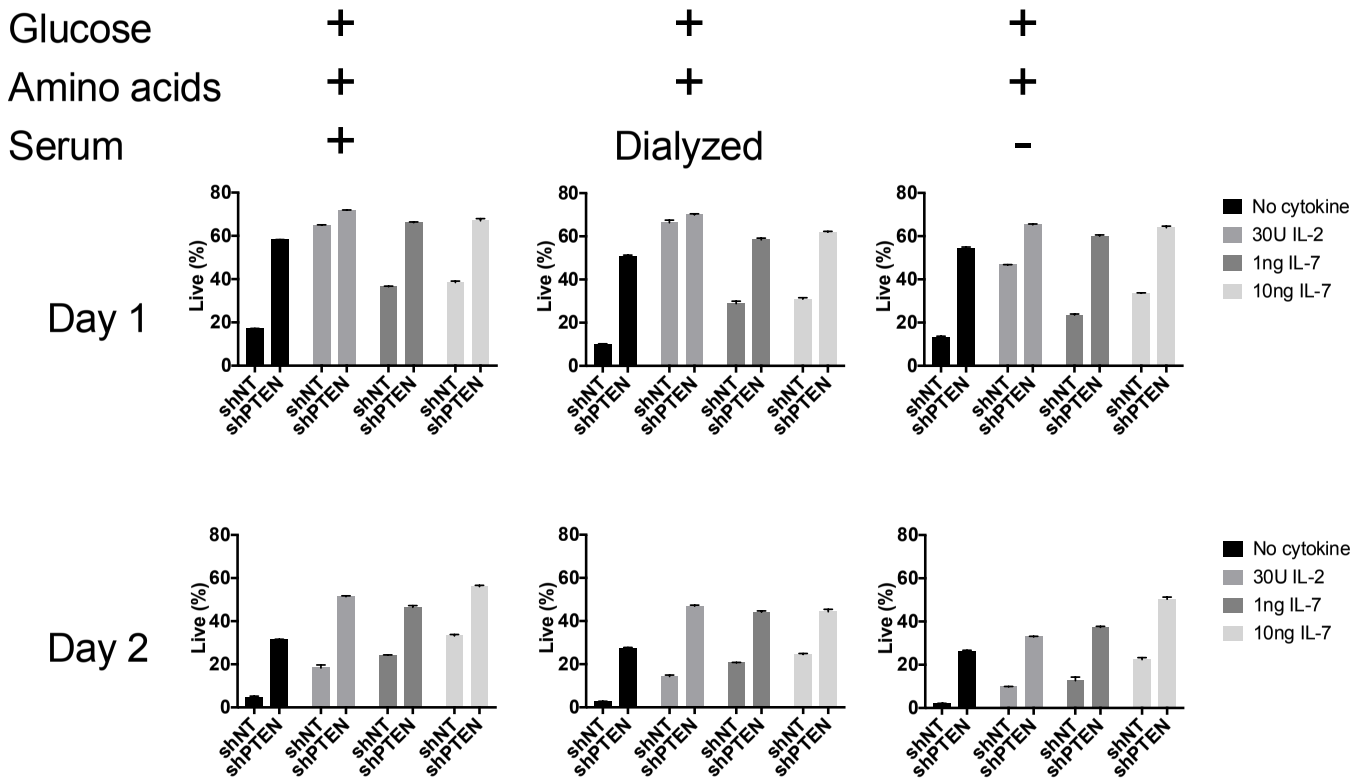
Glucose + + +
Amino acids + + +
Serum + Dialyzed -
Day 1
Day 2
Live (%)
0
20
40
60
80
shNT
shPTEN
No cytokine
30U IL-2
1ng IL-7
10ng IL-7

Figiure 3.7 (continued)

B

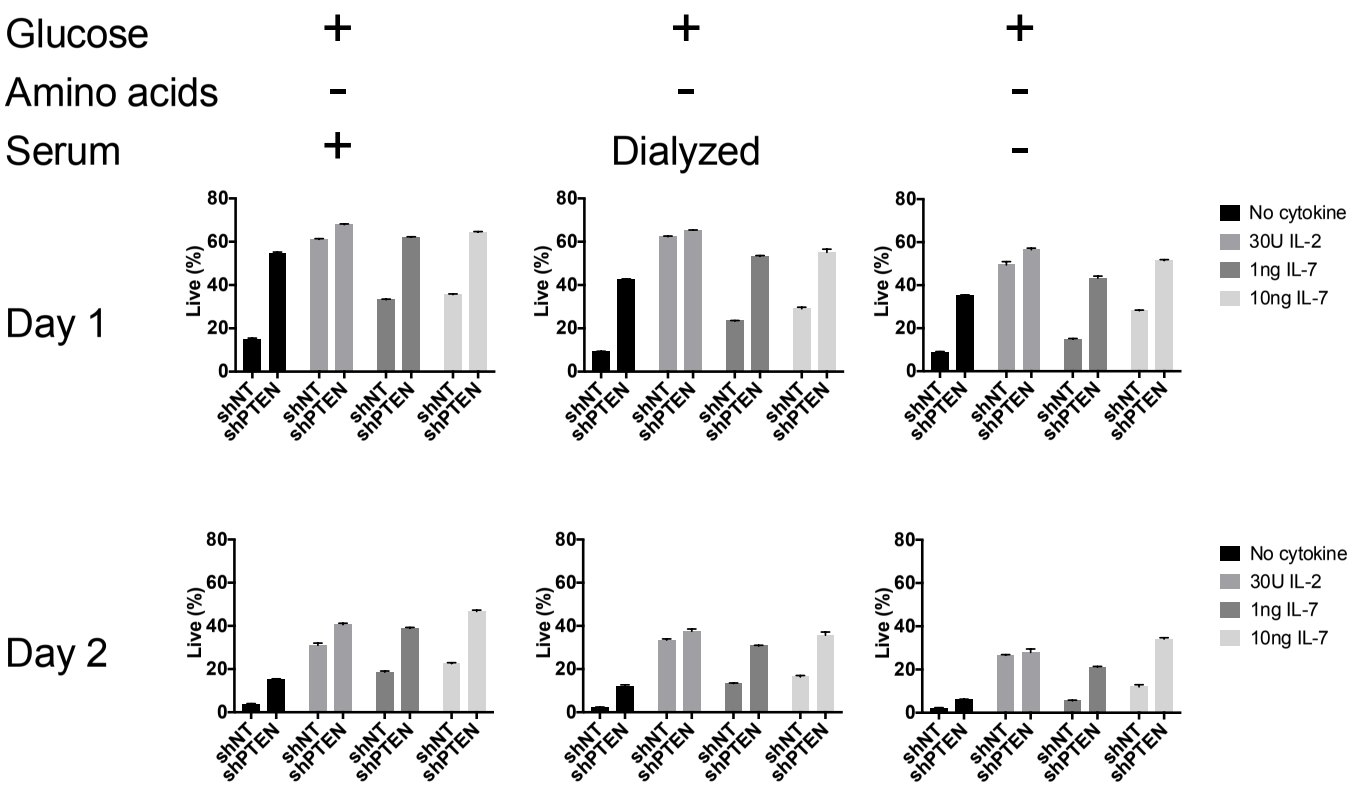

Figiure 3.7 (continued)

C

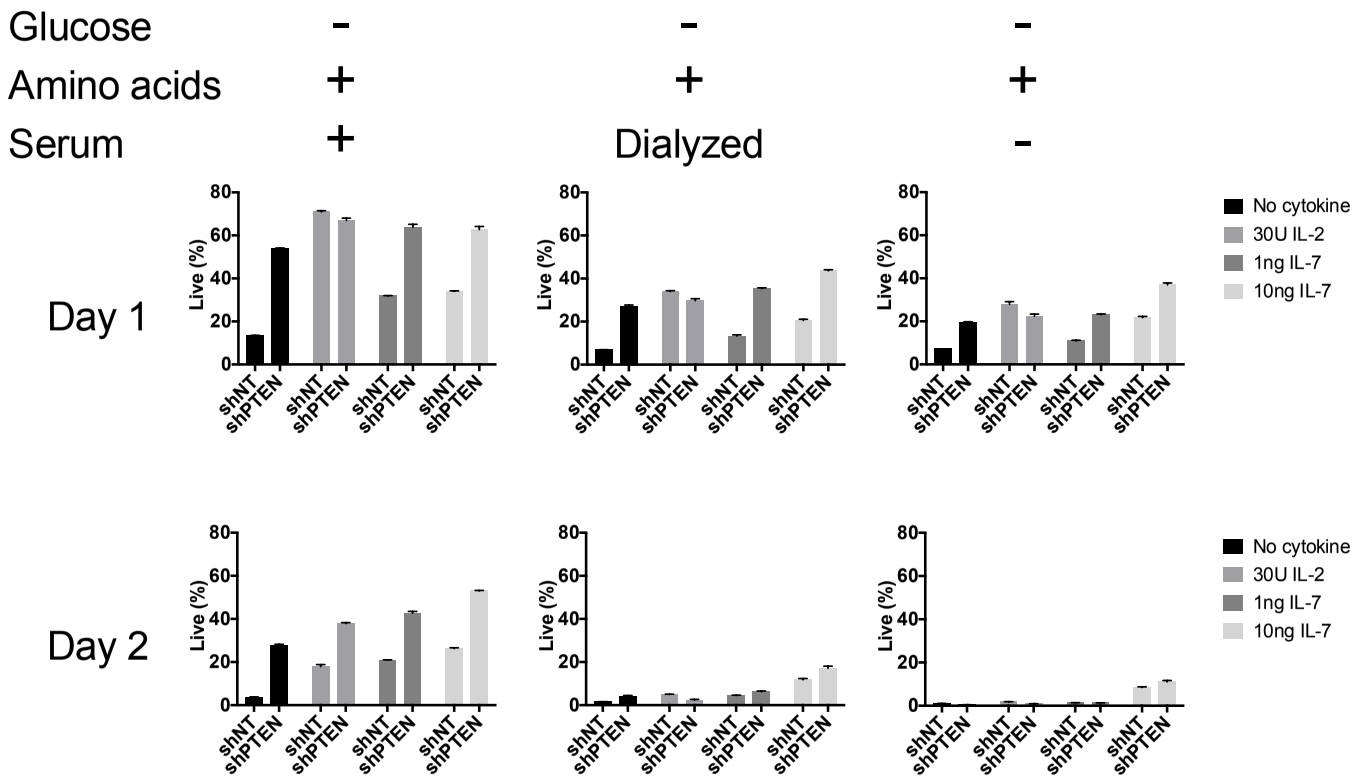

Figiure 3.7 (continued)

D

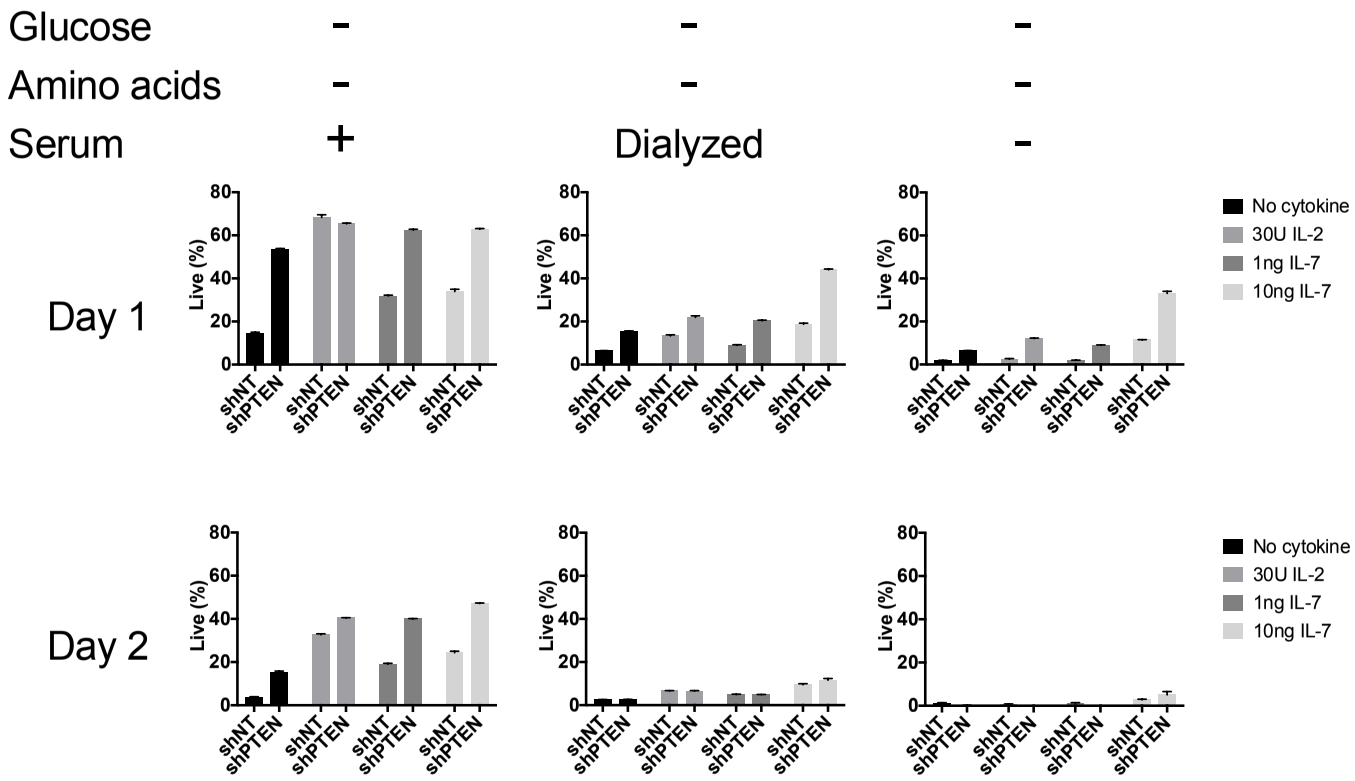

deficient cells were found to have the same or increased survival in every condition measured. Thus, even though shPTEN T cells have reduced expression of IL-7Rα, there is sufficient expression for an IL-7 dependent increase survival relative to the no cytokine condition. However, the lack of evidence supporting a cell survival defect *in vitro* does not rule out the possibility that PTEN deficient T cells have a survival defect *in vivo*.

3.2.8. Enhancing survival of PTEN deficient T cells does not rescue persistence *in vivo*

To investigate the relationship between T cell survival and *in vivo* persistence, we attempted to perturb cell survival *in vivo.* We chose to do this by designing a construct to over express Bcl-2 together with the mApple fluorescent reporter (Figure 3.8A). Over expression of this construct significantly increased survival of T cells cultured without cytokines for 3 days *in vitro* (Figure 3.8B). Expression of Bcl-2 was also confirmed by Western Blot (Figure 3.8C).

We designed an experiment to test the effect of increased survival on T cell persistence *in vivo*. The previous co-transfer experimental protocol (Figure 3.2A) was adapted to form three groups of mice. Group A was to measure the effect that increased survival had on persistence (Figure 3.8D). Group B was a control showing that PTEN deficiency results in a persistence defect. Group C assessed whether increasing survival was able to rescue persistence in PTEN deficient T cells (Figure 3.8D). We found that Bcl-2 overexpression resulted in a marginal improvement to persistence in the blood, liver, and lung (Figure 3.8E-G). However, it did not boost persistence in the tumor, which confirms the existence of the migration defect previously identified (Figure 3.8H, also

Figure 3.8 Increasing survival of PTEN deficient cells has modest effect on persistence

(A) Schematic for the BCL-2 over expression construct that was used in these experiments. (B) BCL-2 over expression enhanced the survival of T cells transduced with the indicated constructs. Survival was evaluated after 3 days without cytokines. (C) BCL-2 over expression was confirmed by Western Blot. (D) Schematic showing the three groups A, B, and C that were transferred into tumor bearing CD45.2 mice. (E-H) Normalized ratios of each group after 6 days.

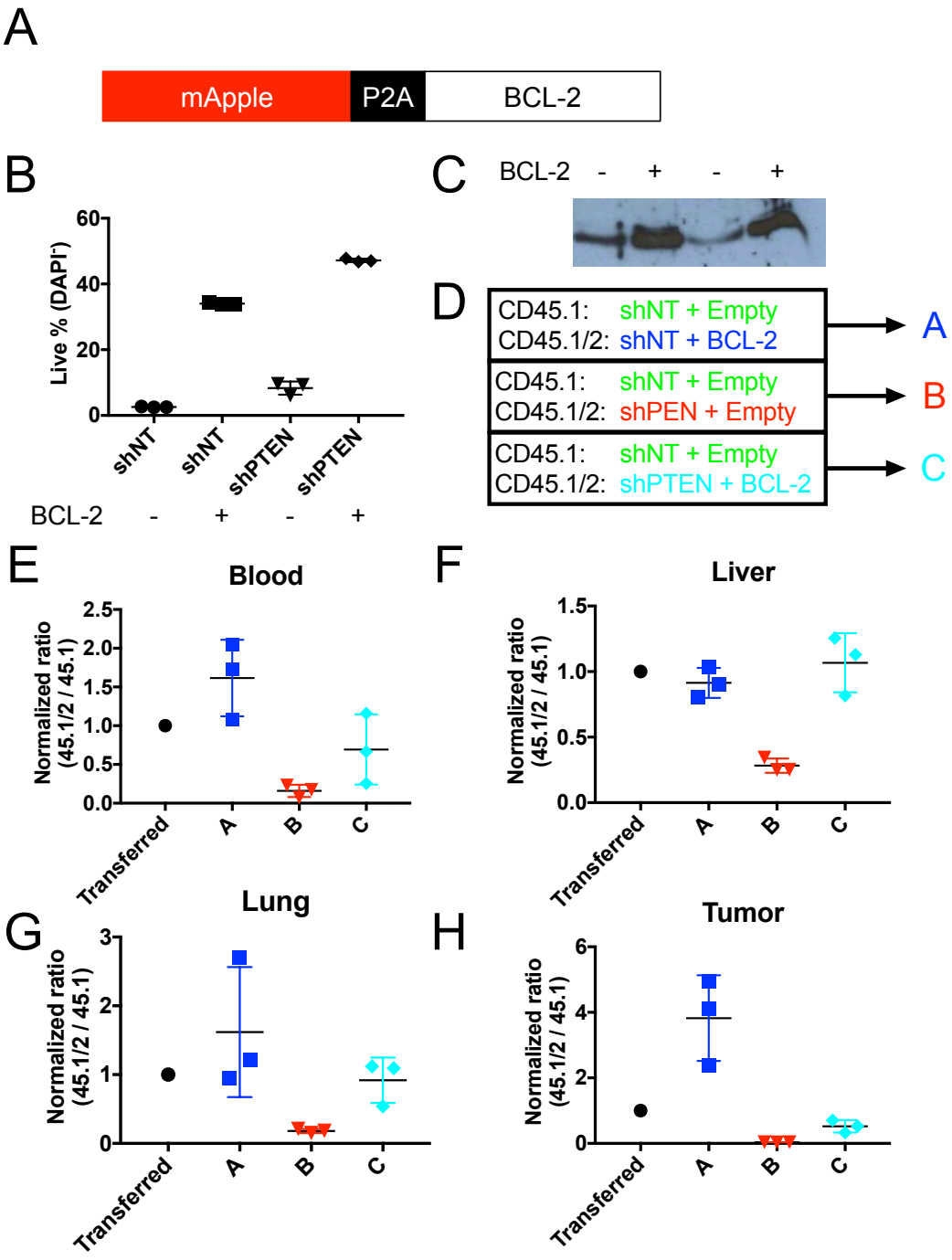
A
mApple
P2A
BCL-2
B
Live % (DAPI-)
60
40
20
0
shNT
shNT
shPTEN
shPTEN
BCL-2 - + - +
C
BCL-2 - + - +
D
CD45.1: shNT + Empty
CD45.1/2: shNT + BCL-2
A
CD45.1: shNT + Empty
CD45.1/2: shPEN + Empty
B
CD45.1: shNT + Empty
CD45.1/2: shPTEN + BCL-2
C
E
Blood
Normalized ratio (45.1/2 / 45.1)
2.5
2.0
1.5
1.0
0.5
0.0
Transferred
A
B
C
F
Liver
Normalized ratio (45.1/2 / 45.1)
1.5
1.0
0.5
0.0
Transferred
A
B
C
G
Lung
Normalized ratio (45.1/2 / 45.1)
3
2
1
0
Transferred
A
B
C
H
Tumor
Normalized ratio (45.1/2 / 45.1)
6
4
2
0
Transferred
A
B
C

Figure 3.5A-D). There was a boost in the number of transferred cells circulating in the blood, but this did not quite match the boost in circulating cells observed for the control cells overexpressing Bcl-2 (Figure 3.8E). This suggests that any survival defect in shPTEN T cells is likely minor and not playing a predominant role in their persistence defect.

3.2.9. PTEN deficient T cells have defect in homeostatic proliferation

The transplantable model of melanoma used throughout this work relies on a 600 cGy dose of radiation to create a lymphopenic environment for the transferred cells to proliferate. Homeostatic proliferation is driven by IL-7 and IL-15[161], and PTEN deficient CTLs have reduced levels of IL-7Rα. Accordingly, we hypothesized that PTEN depletion impairs homeostatic proliferation, leading to defective persistence. To examine the role of proliferation on persistence, we compared sublethally irradiated mice with wild-type (WT) mice. We also examined mice that were double knockouts for recombination-activating gene (RAG) and the common gamma chain receptor ($RAG^{-/-}$ $\gamma_C^{-/-}$) mice, which are very lymphopenic and lack B, T, and NK cells[162]. We adapted our previous experimental setup to examine the role of proliferation by harvesting organs after 4 days. We found that WT mice had similar levels of transferred cells in the spleen and lungs after 4 days (Figure 3.9A). The ratio of shPTEN to shNT cells in the blood was reduced in both sublethally irradiated mice and $RAG^{-/-}$ $\gamma_C^{-/-}$ mice relative to WT mice (Figure 3.9A). There was also a dramatic reduction in the ratio of shPTEN to shNT cells in the spleen and lung of the lymphopenic mice compared with WT mice. We observed an increase in the ratio of shPTEN to shNT cells in the liver in

Figure 3.9 PTEN deficient CTLs have defect in proliferation
(A) T cells expressing either shNT or shPTEN shRNAs were transferred into WT, sublethally irradiated (600 cGy), or RAG$^{-/-}$ $\gamma_C^{-/-}$ double knokckout tumor bearing mice. After 4 days, the normalized ratio was calculated for the cells present in the indicated organs. (B) Proliferation was assessed by dilution of CellTrace Violet on day 4 post transfer. Error bars denote SEM.

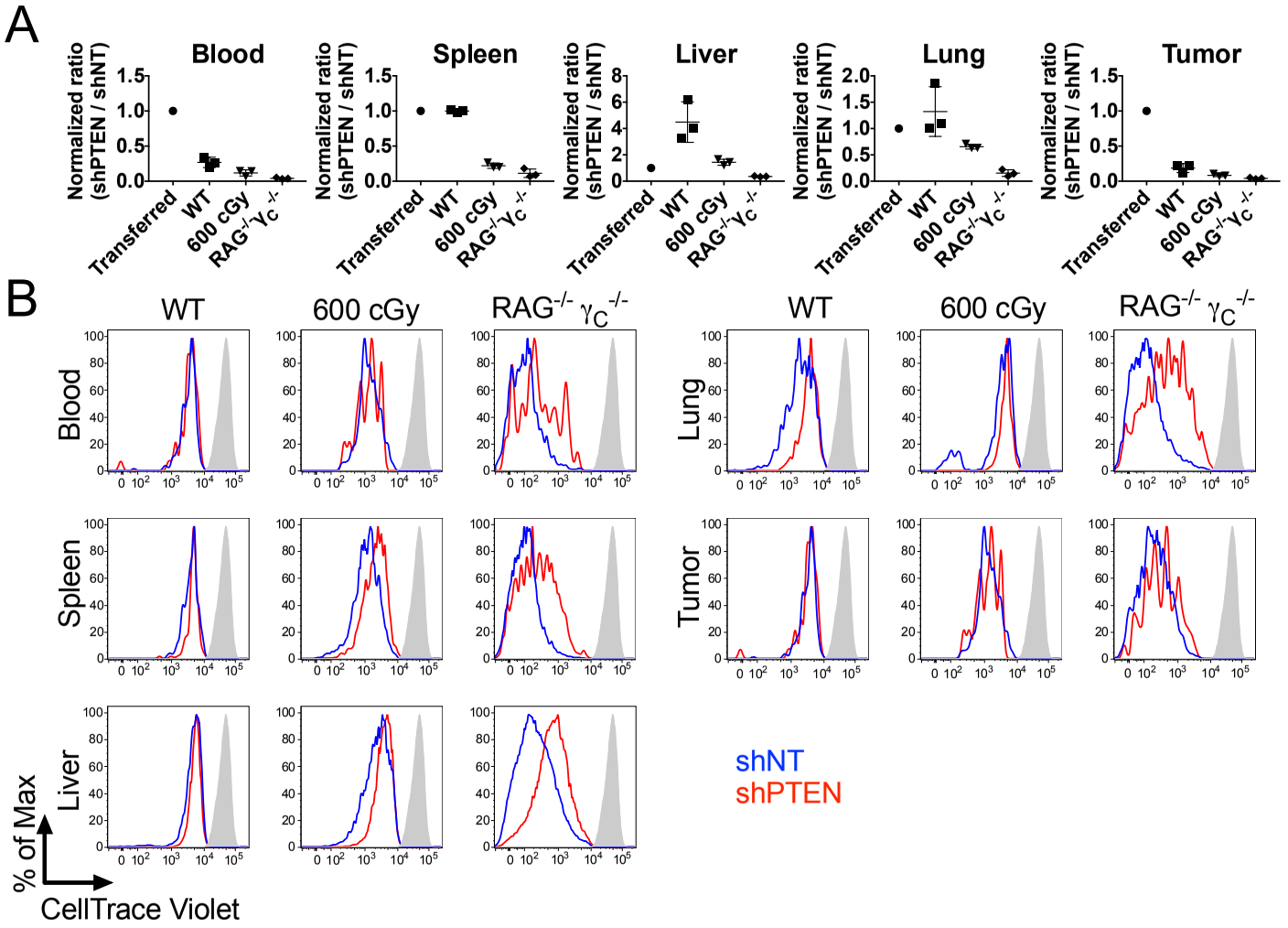
A
Blood
Spleen
Liver
Lung
Tumor
Normalized ratio (shPTEN / shNT)
Transferred
WT
600 cGy
RAG-/-γc-/-
B
WT
600 cGy
RAG-/- γc-/-
Blood
Spleen
Liver
Lung
Tumor
% of Max
CellTrace Violet
shNT
shPTEN

non-lymphopenic mice (Figure 3.9A). This was not surprising as we have already shown that PTEN depletion results a migration defect that enhances T cells 'propensity to traffic to the liver over secondary lymphoid organs. However, all groups of mice had reduced ratios of shPTEN cells to shNT cells in the tumor (Figure 3.9A). This further reinforces our previous observation that shPTEN cells are unable to properly migrate *in vivo*. In the absence of proliferation, there are reduced numbers of shPTEN cells in the tumor relative to shNT control cells. These results indicate that by removing the homeostatic proliferation component of persistence we rescued the persistence of shPTEN cells in a subset of organs (lung, liver, and spleen). This demonstrates that part of the problem shPTEN T cells have persisting *in vivo* results from a defect in homeostatic proliferation.

To assess whether PTEN depleted cells undergo reduced levels of proliferation, we stained a mixture of shPTEN and shNT T cells with a fluorescent dye and monitored dilution of the dye after 4 days *in vivo*. We found that the cells transferred into WT mice underwent almost no proliferation *in vivo* as expected (Figure 3.9B). We saw that shPTEN T cells transferred into mice treated with 600 cGy of radiation underwent reduced proliferation in the spleen, liver, and lung. Control T cells transferred into $RAG^{-/-}$ $\gamma_C^{-/-}$ mice underwent robust homeostatic proliferation but the shPTEN T cells had reduced levels of proliferation in the blood, spleen, liver, and lung. This suggests that PTEN deficient cells have a reduced ability to undergo homeostatic proliferation, which could be due to decreased expression of IL-7Rα.

It is important to note that there are similar levels of proliferation for shPTEN and shNT cells in the tumor of WT as in the spleen (Figure 3.9B). This is interesting because the cells in the tumor are exposed to antigen, which promotes antigen driven proliferation. T cells in the spleen are not exposed to antigen and thus are only undergoing homeostatic proliferation. Cells isolated from the tumors of lymphopenic mice were found to have undergone proliferation (Figure 3.9B). This demonstrates that homeostatic proliferation plays an important role in ACT and suggests that tumor-infiltrating lymphocytes may undergo homeostatic proliferation before entering the tumor. This suggests that while antigen driven proliferation is important in the tumor and likely driving the anti-tumor response, homeostatic proliferation may play a critical role prior to antigen driven proliferation. This is an interesting observation and supports the idea that creating a lymphopenic environment is crucial component for ACT.

3.2.10. PTEN deficient T cells experience mild proliferation defect *in vitro*

In order to establish the role of reduced IL-7Rα expression in the homeostatic proliferation defect, we attempted to recapitulate the proliferation phenotype *in vitro* using recombinant cytokines. We cultured a mixture of shPTEN and shNT transduced T cells under a variety of conditions and monitored proliferation. We found that activating T cells with CD3/CD28 dynabeads induced robust proliferation, but there was no difference between shPTEN and shNT cells (Figure 3.10). This is consistent with our hypothesis that the defect in proliferation observed *in vivo* stems from reduced level of IL-7Rα effecting IL-7 signaling and homeostatic proliferation. Interestingly, PTEN

Figure 3.10 PTEN deficient CTLs have proliferation defect in vitro
T cells transduced to express shNT or shPTEN were stained with CellTrace Violet and proliferation was assessed after the indicated number of days. CD3/CD28 stimulation was performed with dynabeads. IL-2 was used at 30IU/mL. IL-7 and IL-15 were used at 5ng/mL. The mixture of IL-7 and IL-15 contained 5ng/mL of each cytokine.

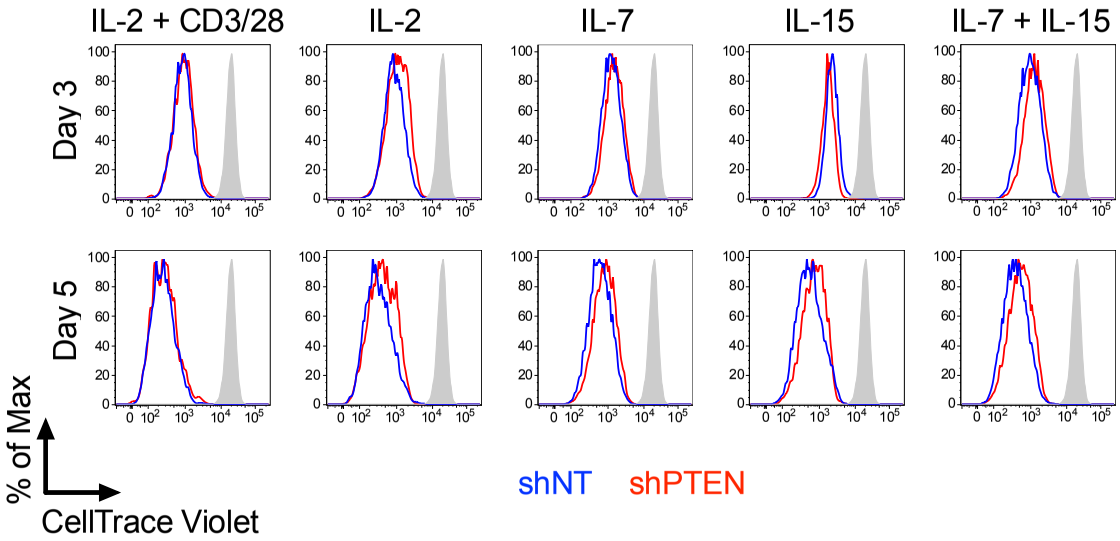
IL-2 + CD3/28
IL-2
IL-7
IL-15
IL-7 + IL-15
Day 3
Day 5
% of Max
CellTrace Violet
shNT
shPTEN

deficient T cells exhibited a modest proliferation defect with IL-2, IL-7, IL-15 and a mixture of IL-7 and IL-15 (Figure 3.10). These defects in proliferation were milder that the defects observed *in vivo*. This suggests that the environment for promoting homeostatic proliferation *in vivo* is more complex than our *in vitro* environment and that we were not able to fully reconstitute it. Hence, more research is needed to fully implicate decreased expression of IL-7Rα as the cause for reduced homeostatic expansion of shPTEN CTLs.

3.3. Discussion

The goal of this work was to examine whether we could apply our knowledge of cytotoxicity to improve ACTs. While we have not identified a way to harness the increased cytotoxicity of shPTEN CTLs, we have learned a significant amount about the necessary components of successful ACTs. We have shown that PTEN depletion reduces T cell anti-tumor effects in a transplantable model (Figure 3.2B). Furthermore, we showed that this is due to a loss of shPTEN T cells relative to control cells (Figure 3.3B). We examined the possible causes for this loss of shPTEN cells and discovered these cells display multiple defects that limit their utility in vivo.

First, shPTEN T cells have a defect in migration that is associated with reduced expression of KLF2, which likely stems from increased PI3K/AKT signaling (Figure 3.6A). We believe that this results in reduced levels of CD62L, CCR7, and S1PR1 (Figure 3.6C-D), which causes the migration defect experienced by PTEN deficient cells.

In addition, shPTEN T cells have a defect in homeostatic proliferation (Figure 9B). We suspect this stems from reduced expression of IL-7Rα due to

increased AKT signaling, which increases the pool of phospho-FOXO1 (Figure 3.6A). This reduction in IL-7Rα expression does not impair IL-7 dependent survival of T cells *in vitro*, but seems to be sufficient to result in a significant defect in homeostatic proliferation *in vivo*. To confirm that the defect in homeostatic proliferation results from decreased levels of IL-7Rα, future work will investigate whether T cells lacking IL-7Rα phenocopy the PTEN deficiency.

Over expression of Bcl-2 robustly blocks cell death *in vitro* (Figure 3.8C), but only provides a slight improvement to the number of shPTEN cells migrating to the tumor. Furthermore, there is only a slight improvement in the number of cells in the blood, suggesting that something other than cell death is driving the apparent loss of shPTEN cells. These observations suggest that any defect in the survival of shPTEN T cells *in vivo* appears to be secondary to the defects in trafficking and proliferation.

Subcutaneous tumor models require lymphocytes to undergo extensive migration to travel from the circulatory system to the secondary lymphoid organs and to the tumor. We found that CTLs expressing shPTEN had defects in migration that resulted in reduced ability of the cells to migrate to the tumor. This limited our ability to assess whether PTEN deficiency increases cytotoxicity *in vivo*. In order to demonstrate this, it may be necessary to examine shPTEN CTLs in a different tumor model. A model of lung or liver cancer may be better suited for evaluating the cytotoxicity of shPTEN T cells since they are capable of migrating to and surviving in the lung and liver. Another possible way to avoid the trafficking defects of shPTEN T cells is to perform on an intratumoral injection of T cells. While this is a technically

difficult procedure, it would circumvent the trafficking issues observed in the melanoma model. These avenues are worth considering as we examine ways to improve ACT using PTEN deficiency.

The other issue with the model we used is that it relies on homeostatic proliferation to expand the adoptively transferred cells in order to generate an anti-tumor effect. When shPTEN cells were transferred into non-lymphopenic mice, they were able to persist at the same level as control cells in the spleen, liver, and lung even though they had reduced levels in the blood. It is worth considering whether shPTEN cells could provide increased survival in a tumor model that did not rely on homeostatic proliferation.

In order to mitigate some of the negative side effects of PTEN deficiency, we examined whether we could reduce PI3K signaling with an inhibitor. We chose to use the AKT inhibitor A-443654 because previous work had demonstrated its ability to alter AKT signaling *in vivo*[156]. We pretreated mice with A-443654 before adoptively transferring T cells. However, treatment with A-443654 was unable to rescue the persistence of the transferred cells (data not shown). We also tried treating T cells *in vitro* prior to transfer with the AKT inhibitor ab142088. T cells were highly sensitive to this inhibitor and it was quite toxic (data not shown). The cells that survived the treatment had increased expression of CD62L but it is unclear how long this expression would have remained after transfer into mice. Nonetheless, it may be possible to boost the duration of effect by treating mice with different AKT inhibitors or by combining it with preconditioning the CTLs.

Another possible way to mitigate the negative side effects of enhanced PI3K/AKT signaling is by treating mice with rapamycin. Rapamycin is highly specific inhibitor for mTOR[159]. Pretreating mice with rapamycin might be able to reduce mTOR signaling enough to restore KLF2 and FOXO1 expression in the transferred cells. Rapamycin has been shown to enhance the formation of memory $CD8^+$ T cells in response to an LCMV infection[163]. Modulating mTOR signaling with rapamycin may be a better way forward than treating mice with AKT inhibitors. It is also worth considering a combination approach whereby CTLs are pretreated with IL-15 and rapamycin and transferred into mice that are subsequently treated with rapamycin. Accordingly, we wondered whether we could apply combined rapamycin-IL15 treatment to increase the level of trafficking proteins to resolve the migration defect caused by enhanced PI3K signaling. Treating shPTEN and shNT CTLs with IL-15 and rapamycin increased the level of CD62L and IL-7Rα (data not shown). However, pretreating shPTEN CTLs with rapamycin and IL-15 was unable to improve persistence after 6 days (data not shown). The mice were not treated with rapamycin and IL-15 after ACT, however, and it is possible that levels of CD62L And IL7R reverted during this time. Hence, more research is needed to fully examine this strategy as a way to fix the persistence defect.

Another possible way to mitigate the effects of enhanced PI3K/AKT signaling is by increasing IL-7 or IL-15 signaling to improve homeostatic proliferation. This could be achieved by treating mice with lipopolysaccharides (LPS) or polyinosinic:polycytidylic acid (poly(I:C)). LPS and poly(I:C) stimulate IL-15 production by APCs through toll-like receptor 3 (TLR3)[161,164]. Treating with poly(I:C) may be more impactful as it has been shown to stimulate

hepatocytes to produce IL-7[165]. Enhancing production of IL-7 by hepatocytes could boost IL-7 signaling in PTEN deficient T cells, which we have shown have a tendency to reside in the liver. However, it is conceivable that the expression of IL-7Rα is sufficiently low to make it the limiting factor in IL-7 signaling. In this case increasing the levels of IL-7 will be unable to restore IL-7 signaling.

Another way to enhance IL-7 signaling is to over express of IL-7Rα. This could rescue enough IL-7 signaling to restore homeostatic proliferation. It is also worth considering over expression of FOXO1 or a constitutively active FOXO1 to achieve this. This is more complicated, however, than over expressing IL-7Rα as FOXO1 signaling is important for many cellular process and could generate unanticipated consequences. FOXO1 is downstream of AKT and mTOR, but it also regulates genes that modulate the activity of AKT and mTOR[166]. This makes understanding the consequences of increased PI3K/AKT coupled with increased FOXO1 activity hard to predict. Furthermore, expression of a constitutively active mutant of FOXO1 in T cells has been shown to decrease tumor infiltration, which is already a problem for shPTEN CTLs[167].

Our studies of shPTEN T cells have highlighted the importance of T cell trafficking and homeostatic proliferation in the B16-OVA melanoma model of ACT. This work also suggests that while examining cytotoxicity *in vitro* can provide mechanistic insight, it may not be the best way to improve ACTs. Improving ACT with T cell screens assessing tumor infiltration, migration, and tumor growth may be more impactful than studies optimizing for cytotoxicity *in vitro*.

3.4. Materials and methods

3.4.1. Mice

The animal protocols used for this study were approved by the Institutional Animal Care and Use Committee of Memorial Sloan-Kettering Cancer Center. For *in vivo* experiments, C57BL/6J mice were purchased from Jackson Laboratories (stock #000664) at 6-8 weeks old. For experiments requiring congenic mice, B6.SJL-Ptprc^{a}Pepc^{b}/BoyJ mice were purchased from Jackson Laboratory (stock #002014). For experiments utilizing gRNAs, OT-1 mice (Taconic) were crossed to Rosa26-Cas9 knockin mice (Gt(ROSA)26Sor$^{tm1.1(CAG-cas9*,-EGFP)Fezh/J}$, stock #024858)[154]. PTEN$^{fl/fl}$ mice were purchased from Jackson Laboratories (stock #006440)[155]. RAG$^{-/-}$ $\gamma_C^{-/-}$ mice were purchased from Taconic Farms (stock #: 4111).

3.4.2. *In vivo* tumor experiments

B16-OVA cells were a gift from Jedd Wolchok. The cells were grown for at least 2 passages before they were counted, washed into PBS, and transferred s.c. to mice. The tumors were allowed to grow for 7-9 days before the mice were exposed to a sublethal dose of irradiation (600cGy). The following day, CTLs were transferred into the mice i.v. by retro-orbital injection. The tumor volume was calculated as $V = \frac{LW^2}{6\pi}$. Measurements were performed with a caliper.

3.4.3. Lymphocyte isolation from tissues

Lung, liver, tumor, gut, and brain tissues were prepared by mechanical disruption followed by 40 min treatment with collagenase (Sigma, C5138) at 1mg/mL in Hanks Buffered Salt Solution with calcium and magnesium. The tissues were washed filtered through 70 μm filters and subsequently layered in

a 44% and 66% percoll gradient (Sigma). The percoll gradient was performed by centrifuging at 3000 rpm for 30 minutes without the brake. The cells were collected from the interface and analyzed by flow cytometry.

3.4.4. Flow cytometry and staining

All flow cytometry was performed on a BD LSR II (Becton Dickinson). Antibodies used were purchased from Tonbo Biosciences, Biolgend, eBiosciences, and BD. The gating strategy used to detect cells that were transferred *in vivo* consisted of gating on single lymphocytes, $CD3^+$ $CD8^+$ double positive cells, and then the appropriate congenic marker. In experiments utilizing only one congenic in a co-transfer, GFP was used with either cyan fluorescent protein or mApple to distinguish the populations of cells. The ratio of shPTEN to shNT cells was calculated and then normalized by the ratio of the cells that were transferred into mice.

The clones for antibodies used are as follows: CD127/IL-7Rα (A7R34), CD62L (MEL-14), CD3ε (145-2C11), CD8α (53-6.7), CD4 (RM4-5), CD45.1 (A20), and CD45.2 (104). Cells were stained at room temperature for at least 15 minutes in FACs buffer. Cells were stained with CellTrace Violet (Life Technologies) according to the manufacturers directions.

3.4.5. Cloning

The Bcl-2 over expression construct was generated from mouse cDNA was generated by PCR using the primers P2A-BCL2-fw (5'-AGAACCCAGGCCCTATGGCGCAAGCC -3') and BglII-BCL2-rev (5'-AAAAAAGATCTTCACTTGTGGCCCAGGTATGCACC -3'). A P2A site was added to mApple-N1 by PCR with the oligos: NotI-mApple-fw (5'-

TTTTTGCGGCCGCATGGTGAGC -3'), P2A-rev (5'-GGCTTGCGCCATAGGGCCTGGGTTCT -3'), and the P2A fragment (5'-GGAAGTGGTGCAACAAATTTCAGCCTTCTCAAACAAGCAGGTGATGTCGAGGAGAACCCAGGCCCT -3'). mApple-N1 was a gift from Michael Davidson (Addgene plasmid # 54567).[168] The final product was cloned into an empty MSCV vector containing a Zeocin resistance cassette using NotI and BglII. A control was also generated of mApple in the same vector. The PCR was performed using Phusion (NEB) and according to the manufacturers protocol. The constructs were confirmed by sequencing (Genewiz).

Expression constructs for shNT and shPTEN that were previously described were moved the LEPG vector with a miR30E backbone[8,117,169]. The miR30E vector was a gift from Scott Lowe. The primers to move the hairpins from their original vector to the miR30E vector were miRE-Xho-fw (5'-TGAACTCGAGAAGGTATAT TGCTGTTGACAGTGAGCG -3') and miRE-EcoOligo-rev (5'-TCTCGAATTCT AGCCCCTTGAAGTCCGAGGCAGTAGGC -3')[169]. The mApple fluorescent protein as cloned into the miR30E vector by performing PCR to assemble an IRES-mApple fragment with PacI and ApaI cut sites. The mApple fragment was generated using primers IRES-mApple-F (5'- TGGCCACAACCATGGTGAGCAAG -3') and (5'-ATAATTCTTAATTAATTCACTTGTACAGCTCGTCCATG -3'). The IRES fragment was generated using ApaI-IRES-F (5'-AATGTGAGGGCCCGGAAACC -3') and IRES-mApple-R (5' CCATGGTTGTGGCCATATTATCATCG -3'). PCR was performed to combine these two fragments and the product was cloned into the miR30E vector using

the PacI and ApaI cutsites (NEB). Proper insertion of mApple was confirmed by sequencing (Genewiz).

gRNAs to knokckout PTEN were generated using previously published methods[170]. The selected gRNA was made by annealing oligo-1 (5'-CACCGaacttgtcctcccgccgcgt -3') and (5'- AAACacgcggcgggaggacaagttC -3') and cloned into the lenti-Guide-Puro vector according to published protocols[171,172]. The portion of the construct containing the gRNA was then amplified by PCR using LMP BamHI F2 (5'-TTTTTGGATCCTAGTAGGAGGCTTGGTAG -3') and LMP EcoRI R2 (5'-TTTTTGAATTCTGTCTACTATTCTTTCCC -3'). This fragment was digested with BamHI and EcoRI (NEB) and ligated into the miR30E vector digested with EcoRI and BglII (NEB). The presence of the gRNA was confirmed by sequencing (Genewiz).

3.4.6. Cell culture and transductions

CTLs were prepared by mixing T cells from OT-1 αβTCR transgenic mice (Taconic) with irradiated congenic splenocytes pulsed with 100nM OVA and cultured in RPMI medium containing 10 % (vol/vol) FCS. Polyclonal T cells were activated using CD3/CD28 Dynabeads (Life Technologies). Lymphocytes were isolated from the spleen, counted, and incubated with dynabeads at a 1:1 ratio. Cells were supplemented with interleukin 2 (IL2, 30 IU/ml) after 24 h and were split as needed in RPMI containing IL-2. B16-OVA cells were maintained in RPMI containing 10 % (vol/vol) FCS with 50ug/mL G418, while RMA-s cells were grown in RPMI containing 10 % (vol/vol) FCS.

To prepare retrovirus, Phoenix E cells were transfected with expression vectors together with packaging plasmids using the calcium phosphate method. Ecotropic viral supernatants were collected after 48 hr at 37°C and added to OT-1 blasts 2 days after primary peptide stimulation. Mixtures were centrifuged at 1400 × g in the presence of polybrene (4 μg/ml) at 35°C. T cells were then split 1:3 in medium containing IL-2. Selection was added 24 hours after transduction. Puromycin was used at 5-10ug/mL and Zeocin was used at 100ug/mL (Life Technologies).

Restimulation experiments were conducted with CD3/CD28 dynabeads (Life Technologies) at a 1:1 ratio. For other experiments, cells were treated in 2ng/mL mouse IL-15 (eBioscience), 5ng/mL mouse IL-7 (eBioscience), and 2nM rapamycin (EMD Millipore) overnight at 37°C.

For *in vitro* experiments involving AKT inhibitors, we used The AKT1/2 inhibitor ab142088 (Abcam). For the AKT inhibitor A-443654 (Abovchem), we injected mice s.c. twice per day as previously described[156].

3.4.7. Immunoblot

0.2-1 × 10^6 CTLs were lysed in ice cold buffer containing 10 mM TrisHCl, 5 mM EDTA, 1% NP-40, 0.5% sodium deoxycholate, and 0.15 M NaCl. PTEN expression was assessed using a rabbit monoclonal antibody (clone: D4.3, Cell Signaling). Actin served as a loading control (clone: AC-15, Sigma). Images were collected on film or with the LICOR.

3.4.8. Nutrient depletion survival experiments

For all experiments, media was obtained form the Memorial Sloan Kettering Cancer Center Media Preparation core facility. For the nutrient depletion experiments, RPMI was purchased without glucose, amino acids, or both. Fetal bovine serum (Sigma) or dialyzed fetal bovine serum (Sigma) was added to 10% (v/v). Human IL-2 was used at 30IU/mL. Mouse IL-7 (Life Technologies) was used at 1ng/mL and 10ng/mL. Cells were incubated in flat bottom 96 well plates at 37°C for 1 or 2 days. The samples were then washed into FACS buffer, stained with DAPI, and analyzed by flow cytometry.

3.4.9. *In vitro* killing assays

Cytotoxicity assays were performed using RMA-s cells that were stained with CellTrace Violet (Life Technologies) and then pulsed with varying concentrations of the SIINFEKL peptide for 1 hour. The cells were washed, counted and mixed with OT-1 CTLs at a 1:2 (effector:target) ratio in V bottom 96 well plates in triplicate and incubated at 37°C for 3-4 hours. The cells were washed into FACS buffer and cell death was measured by flow cytometry.

3.4.10. RNA isolation and RT-PCR

RNA was generated from CTLs by performing a Trizol (Life Technologies) extraction with chloroform following standard protocols (Sigma). RNA was used to generate cDNA using qScript cDNA Supermix (Quanta Biosciences). For all reactions, GAPDH was used as a control. RT-PCR was performed using the primers: GAPDH-fw (5'-CTTTGTCAAGCTCATTTCCTGG -3'), GAPDH-rev (5'-TCTTGCTCAGTGTCCTTGC -3'), KLF2-fw (5'-GGCTAGATGCCTTGTGAGAAA -3'), KLF2-rev (5'-

TGCCATCGTCTCCCTTATAGA -3'), S1P1R-fw (5'-GGAGTATGTTTGTGGCTCTCTC -3'), S1PR1-rev (5'-TGCTCCCGTTGTGTAGTTTC -3'), CCR7-fw (5'-GGTTCCTGCCTCTCATGTATT -3'), and CCR7-rev (5'-GTAGGTATCCGTCATGGTCTTG -3').

CHAPTER 4: CONCLUDING REMARKS

In the present study, we examined T cell cytotoxicity and discovered an association between mechanical force and target cell killing. We examined force generation by T cells both in the plane of the IS and orthogonal to the IS. We found that shPTEN CTLs exerted larger pulling and pushing forces in both dimensions. We showed that these forces correlate with the increased cytotoxicity observed in PTEN deficient cells. We demonstrated a relationship between increased membrane tension on target cells and increased susceptibility to perforin. We proposed a model in which CTLs use the mechanical properties of the IS to increase membrane tension of target cells, thereby increasing the potency of LGs. We propose that the increased plasma membrane tension destabilizes the membrane by increasing the space between the phospholipids. Although our data supports this model, there are additional hypotheses for the mechanism of increased cytotoxicity, and some key questions related to our study remain unanswered.

There are several alternative hypotheses for how force could contribute to perforin function that we did not address in our study. Force could increase the membrane susceptibility to perforin pore formation directly or it could alter the lipid composition of membrane, thereby enhancing its affinity for perforin. It is also possible that increased membrane tension could alter the topology of the membrane (e.g. by enforcing either convex or concave curvature), which could alter its susceptibility to perforin. Another possibility is that CTL-derived forces could physically damage target cells and that the target cell's response to this damage might increase its susceptibility to perforin. These hypotheses

are not mutually exclusive with our other hypotheses and additional research is needed to address them.

Although our studies implied that T cells alter target cell tension by exerting synaptic forces, we did not show this definitively. Technical limitations prevented us from examining plasma membrane tension in CTL-target cell conjugates. Current approaches to measure membrane tension rely on atomic force microscopy (AFM) or an optical trap. Unfortunately, the cantilever tip of an AFM is unable to access the target cell plasma membrane within the IS. The same is true for the optical trap approach. One way to circumvent these limitations, in principle, is by using genetically encoded tension sensors. There are fluorescent reporters that measure cortical membrane tension[173], but these do not report the tension of the plasma membrane.

Another way to measure membrane tension could be to use various tension sensitive ion channels, such as Piezo1 and Piezo2[174]. These ion channels have been shown to permit the flow of calcium ions in response to increased membrane tension[174]. We could over express these proteins on target cells and use intracellular calcium as a readout for membrane tension using a small molecule dye. We would then be able to monitor membrane tension during a CTL-target cell conjugate. This approach is intriguing but it would be unable to distinguish between alterations in global membrane tension versus localized membrane tension within the IS. Membrane tension has been shown to modify the activity of other pore forming proteins such as alamethicin[175], but these proteins would have the same issues. Furthermore, it is conceivable that T cells could disrupt the integrity of the target cell membrane in a perforin independent manner within a conjugate. T cells

perform trogocytosis while in T cell-target cell conjugates so it is possible that T cells could disrupt the integrity of the plasma membrane. This could make changes in ion concentration an inaccurate readout for membrane tension.

We would like to monitor membrane tension of T cells during the formation of conjugates and visualize it with degranulation using the pHluorin-Lamp1 reporter. If this could be done at high resolution, it might be possible to examine whether a T cell releases lytic granules near regions of enhanced target cell membrane tension. It would also be interesting to measure membrane tension of the CTL plasma membrane to see whether it could play a role in protecting CTLs from perforin and granzyme. The precise mechanism of how CTLs protect themselves is unknown and membrane tension could play a role. Unfortunately, monitoring T cell membrane tension has the same associated challenges as monitoring it in target cells.

Out efforts to apply PTEN deficiency to ACT have generated a number of interesting observations. We have demonstrated that modulating PI3K signaling by depleting PTEN does not improve tumor rejection in a transplantable melanoma model. In fact, we observed the opposite effect, and our subsequent studies highlighted the importance of trafficking and homeostatic proliferation for productive anti-tumor responses.

In T cells, PI3K signaling drives cytoskeletal remodeling through Dock2/Rac and transcriptional and metabolic responses through AKT. We believe that this branched pathway structure explains why enhanced PI3K signaling leads to an increase in cytotoxicity (via Dock2/Rac) at the cost of reduced homeostatic proliferation and defects in migration (downstream of

AKT). By properly separating the two arms of the pathway, we might be able to increase cytotoxicity without diminishing homeostatic proliferation and migratory potential of the T cells. One way to do this is to only deplete PTEN upon TCR activation. Then the T cell will migrate properly to the tumor and, upon engagement of the TCR with pMHC, it will turn on expression of the shRNA to deplete PTEN. We previously tried expressing the PTEN shRNA under control of early T cell signaling promoters including nerve growth factor IB (Nur77), IL-2, and NFAT. These constructs resulted in leaky expression of the shRNA and depletion of PTEN in the absence of TCR signaling. Hence, we were not able to fully explore the potential of this idea.

Relying on homeostatic proliferation to generate anti-tumor responses might be a better approach than transferring more cells into a patient. Expanding CTLs *in vitro* over many generations can cause the cells to become dysfunctional and express exhaustion markers[176]. Dysfunctional CTLs respond poorly to antigen and produce reduced levels of cytokines upon restimulation. These cells also upregulate various inhibitory molecules including PD-1, VISTA, and others[41,42,93]. That being said, homeostatically expanded T cells are also known to express exhaustion markers and to exhibit some signs of dynsfunction[177]. These factors make the idea of using homeostatic expansion as an alternative to in vitro expansion less appealing. However, our work suggests that homeostatic proliferation as part of ACT is important and that it increases the anti-tumor response.

Future studies will seek to find the optimal balance between CTL cytotoxicity, migration, and homeostatic proliferation when mounting an anti-tumor immune response. In an anti-tumor response, cytotoxicity is obviously

important as it allows T cells to kill, but it seems unlikely that maximizing cytotoxicity will be an effective approach if it comes at the expense of homeostatic proliferation and migration. Indeed, our data imply that the opposite strategy may even be more fruitful. If, for example, a T cell could be modified to significantly enhance homeostatic proliferation and tumor infiltration by a factor of 10 while reducing *in vitro* cytotoxicity by half, these cells might provide an enhanced anti-tumor effect while performing worse in cytotoxicity assays *in vitro*. Ideally, T cell proliferation and migration could be improved without altering cytotoxicity but reduced cytotoxicity *in vitro* could still lead to an improvement in ACT *in vivo* if other alterations compensated for this deficiency.

BIBLIOGRAPHY

1. Cox MA, Harrington LE, Zajac AJ. Cytokines and the inception of CD8 T cell responses. Trends Immunol [Internet]. 2011;32(4):180–6. Available from: http://dx.doi.org/10.1016/j.it.2011.01.004

2. Carpenter AC, Bosselut R. Decision checkpoints in the thymus. Nat Immunol. 2010;11(8):666–73.

3. Lee HM, Bautista JL, Hsieh CS. Thymic and Peripheral Differentiation of Regulatory T Cells [Internet]. 1st ed. Vol. 112, Advances in Immunology. Elsevier Inc.; 2011. 25-71 p. Available from: http://dx.doi.org/10.1016/B978-0-12-387827-4.00002-4

4. Huse M. The T-cell-receptor signaling network. J Cell Sci [Internet]. 2009;122(9):1269–73. Available from: http://jcs.biologists.org/cgi/doi/10.1242/jcs.042762

5. Kane LP, Lin J, Weiss A. Signal transduction by the TCR for antigen. Curr Opin Immunol. 2000;12(3):242–9.

6. Lin X, Mahony AO, Mu Y, Geleziunas R, Greene WC. Protein Kinase C-θ Participates in NF- κ B Activation Induced by CD3-CD28 Costimulation through Selective Activation of I κ B Kinase β Protein Kinase C- Participates in NF- B Activation Induced by CD3-CD28 Costimulation through Selective Activation o. Society. 2000;20(5):1–9.

7. Martini M, De Santis MC, Braccini L, Gulluni F, Hirsch E. PI3K/AKT signaling pathway and cancer: An updated review. Ann Med. 2014;46(6):372–83.

8. Le Floc'h A, Tanaka Y, Bantilan NS, Voisinne G, Altan-Bonnet G, Fukui Y, et al. Annular PIP3 accumulation controls actin architecture and modulates cytotoxicity at the immunological synapse. J Exp Med [Internet]. 2013 Nov 18 [cited 2013 Nov 7];210(12):2721–37. Available from: http://www.ncbi.nlm.nih.gov/pubmed/24190432

9. Sinclair L V, Finlay D, Feijoo C, Cornish GH, Gray A, Ager A, et al. Phosphatidylinositol-3-OH kinase and nutrient-sensing mTOR pathways control T lymphocyte trafficking. Nat Immunol [Internet]. 2008;9(5):513–21. Available from: http://www.nature.com/doifinder/10.1038/ni.1603

10. Ouyang W, Beckett O, Flavell RA, Li MO. An Essential Role of the Forkhead-Box Transcription Factor Foxo1 in Control of T Cell Homeostasis and Tolerance. Immunity [Internet]. 2009;30(3):358–71. Available from: http://dx.doi.org/10.1016/j.immuni.2009.02.003

11. Kerdiles YM, Beisner DR, Tinoco R, Dejean AS, Castrillon DH, DePinho

RA, et al. Foxo1 links homing and survival of naive T cells by regulating L-selectin, CCR7 and interleukin 7 receptor. Nat Immunol [Internet]. 2009;10(2):176–84. Available from: http://www.nature.com/doifinder/10.1038/ni.1689

12. Yu Y, Smoligovets AA, Groves JT. Modulation of T cell signaling by the actin cytoskeleton. J Cell Sci [Internet]. 2013 Mar 1;126(5):1049–58. Available from: http://jcs.biologists.org/cgi/doi/10.1242/jcs.098210

13. Huse M, Lillemeier BF, Kuhns MS, Chen DS, Davis MM. T cells use two directionally distinct pathways for cytokine secretion. Nat Immunol [Internet]. 2006 Mar [cited 2012 May 9];7(3):247–55. Available from: http://www.ncbi.nlm.nih.gov/pubmed/16444260

14. Stinchcombe JC, Majorovits E, Bossi G, Fuller S, Griffiths GM. Centrosome polarization delivers secretory granules to the immunological synapse. Nature [Internet]. 2006 Sep 28 [cited 2015 Jan 4];443(7110):462–5. Available from: http://www.ncbi.nlm.nih.gov/pubmed/17006514

15. Derivery E, Gautreau A. Generation of branched actin networks: Assembly and regulation of the N-WASP and WAVE molecular machines. BioEssays. 2010;32(2):119–31.

16. Goley ED, Welch MD. The ARP2/3 complex: An actin nucleator comes of age. Nat Rev Mol Cell Biol. 2006;7(10):713–26.

17. Mullins RD, Heuser JA, Pollard TD. The interaction of Arp2/3 complex with actin: Nucleation, high affinity pointed end capping, and formation of branching networks of filaments. Proc Natl Acad Sci [Internet]. 1998;95(11):6181–6. Available from: http://www.pnas.org/cgi/doi/10.1073/pnas.95.11.6181

18. Monks CRF, Freiberg B a, Kupfer H, Sciaky N, Kupfer A. Three-dimensional segregationofsupramolecular activation clustersinTcells. Nature [Internet]. 1998;395(6697):82–6. Available from: http://www.nature.com/doifinder/10.1038/25764

19. Tseng S-Y, Waite JC, Liu M, Vardhana S, Dustin ML. T Cell-Dendritic Cell Immunological Synapses Contain TCR-dependent CD28-CD80 Clusters That Recruit Protein Kinase C . J Immunol [Internet]. 2008;181(7):4852–63. Available from: http://www.jimmunol.org/cgi/doi/10.4049/jimmunol.181.7.4852

20. Freiberg BA, Kupfer H, Maslanik W, Delli J, Kappler J, Zaller DM, et al. Staging and resetting T cell activation in SMACs. Nat Immunol. 2002;3(10):911–7.

21. Delon J, Kaibuchi K, Germain RN. Exclusion of CD43 from the immunological synapce is mediated by phosphorylation-regulated

relocation of the cytoskeletal adaptor Moesin. Immunity. 2001;15(5):691–701.

22. Brossard C, Feuillet V, Schmitt A, Randriamampita C, Romao M, Raposo G, et al. Multifocal structure of the T cell - dendritic cell synapse. Eur J Immunol [Internet]. 2005 Jun [cited 2013 Aug 26];35(6):1741–53. Available from: http://www.ncbi.nlm.nih.gov/pubmed/15909310

23. Dupré L, Houmadi R, Tang C, Rey-Barroso J. T lymphocyte migration: An action movie starring the actin and associated actors. Front Immunol. 2015;6(NOV).

24. Negulescu PA, Krasieva TB, Khan A, Kerschbaum HH, Cahalan MD. Polarity of T cell shape, motility, and sensitivity to antigen. Immunity [Internet]. 1996 May;4(5):421–30. Available from: http://www.ncbi.nlm.nih.gov/pubmed/8630728

25. Hunter MC, Teijeira A, Halin C. T cell trafficking through lymphatic vessels. Front Immunol. 2016;7(DEC).

26. Preece G, Murphyt G, Ager A. Metalloproteinase-mediated regulation of L-selectin levels on leucocytes. J Biol Chem. 1996;271(20):11634–40.

27. Lewis M, Tarlton JF, Cose S. Memory versus naive T-cell migration. Immunol Cell Biol [Internet]. 2008 Mar;86(3):226–31. Available from: http://doi.wiley.com/10.1038/sj.icb.7100132

28. Girard JP, Moussion C, Förster R. HEVs, lymphatics and homeostatic immune cell trafficking in lymph nodes. Nat Rev Immunol [Internet]. 2012;12(11):762–73. Available from: http://dx.doi.org/10.1038/nri3298

29. Sackstein R, Schatton T, Barthel SR. T-lymphocyte homing: an underappreciated yet critical hurdle for successful cancer immunotherapy. Lab Investig [Internet]. 2017;97(6):669–97. Available from: http://www.nature.com/doifinder/10.1038/labinvest.2017.25

30. Tomura M, Yoshida N, Tanaka J, Karasawa S, Miwa Y, Miyawaki A, et al. Monitoring cellular movement in vivo with photoconvertible fluorescence protein “Kaede” transgenic mice. Proc Natl Acad Sci [Internet]. 2008;105(31):10871–6. Available from: http://www.pnas.org/cgi/doi/10.1073/pnas.0802278105

31. Kastenmüller W, Brandes M, Wang Z, Herz J, Egen JG, Germain RN. Peripheral Prepositioning and Local CXCL9 Chemokine-Mediated Guidance Orchestrate Rapid Memory CD8+T Cell Responses in the Lymph Node. Immunity. 2013;38(3):502–13.

32. Chaffin KE, Perlmutter RM. A pertussis toxin-sensitive process controls thymocyte emigration. Eur J Immunol [Internet]. 1991 Oct;21(10):2565–73. Available from: http://doi.wiley.com/10.1002/eji.1830211038

33. Sharma S, Mathur A, Pradhan S, Singh D, Gupta S. Fingolimod (FTY720): First approved oral therapy for multiple sclerosis. J Pharmacol Pharmacother [Internet]. 2011;2(1):49. Available from: http://www.jpharmacol.com/text.asp?2011/2/1/49/77118

34. Bousso P, Robey E. Dynamics of CD8+ T cell priming by dendritic cells in intact lymph nodes. Nat Immunol [Internet]. 2003 Jun;4(6):579–85. Available from: http://www.ncbi.nlm.nih.gov/pubmed/12730692

35. Krummel MF, Bartumeus F, Gérard A. T cell migration, search strategies and mechanisms. Nat Rev Immunol [Internet]. 2016;16(3):193–201. Available from: http://dx.doi.org/10.1038/nri.2015.16

36. Huang J, Brameshuber M, Zeng X, Xie J, Li Q jing, Chien Y hsiu, et al. A Single peptide-major histocompatibility complex ligand triggers digital cytokine secretion in CD4+ T Cells. Immunity [Internet]. 2013;39(5):846–57. Available from: http://dx.doi.org/10.1016/j.immuni.2013.08.036

37. Altan-Bonnet G, Germain RN. Modeling T cell antigen discrimination based on feedback control of digital ERK responses. PLoS Biol. 2005;3(11):1925–38.

38. Miller MJ, Wei SH, Cahalan MD, Parker I. Autonomous T cell trafficking examined in vivo with intravital two-photon microscopy. Proc Natl Acad Sci U S A. 2003;100(5):2604–9.

39. Weninger W, Crowley MA, Manjunath N, von Andrian UH. Migratory properties of naive, effector, and memory CD8(+) T cells. J Exp Med [Internet]. 2001 Oct 1;194(7):953–66. Available from: http://www.pubmedcentral.nih.gov/articlerender.fcgi?artid=2193483&tool=pmcentrez&rendertype=abstract

40. Bellone M, Calcinotto A. Ways to Enhance Lymphocyte Trafficking into Tumors and Fitness of Tumor Infiltrating Lymphocytes. Front Oncol [Internet]. 2013;3(September):1–15. Available from: http://journal.frontiersin.org/article/10.3389/fonc.2013.00231/abstract

41. Pauken KE, Wherry EJ. Overcoming T cell exhaustion in infection and cancer. Trends Immunol [Internet]. 2015;36(4):1–12. Available from: http://dx.doi.org/10.1016/j.it.2015.02.008

42. Wherry EJ. T cell exhaustion. Nat Immunol [Internet]. 2011;12(6):492–9. Available from: http://dx.doi.org/10.1038/ni.2035

43. Quigley M, Pereyra F, Nilsson B, Porichis F, Fonseca C, Eichbaum Q, et al. Transcriptional analysis of HIV-specific CD8+ T cells shows that PD-1 inhibits T cell function by upregulating BATF. Nat Med [Internet]. 2010;16(10):1147–51. Available from: http://dx.doi.org/10.1038/nm.2232

44. Chang JT, Wherry EJ, Goldrath AW. Molecular regulation of effector and

memory T cell differentiation. Nat Immunol [Internet]. 2014;15(12):1104–15. Available from: http://www.nature.com/doifinder/10.1038/ni.3031

45. Wherry EJ, Blattman JN, Murali-krishna K, Most R Van Der, Ahmed R. Viral Persistence Alters CD8 T-Cell Immunodominance and Tissue Distribution and Results in Distinct Stages of Functional Impairment Viral Persistence Alters CD8 T-Cell Immunodominance and Tissue Distribution and Results in Distinct Stages of Functional Im. J Virol. 2003;77(8):4911–3927.

46. Hanahan D, Weinberg RA. The hallmarks of cancer. Cell [Internet]. 2000;100(1):57–70. Available from: http://www.ncbi.nlm.nih.gov/pubmed/10647931

47. Houston A, O'Connell J. The Fas signalling pathway and its role in the pathogenesis of cancer. Curr Opin Pharmacol. 2004;4(4):321–6.

48. Westphal D, Dewson G, Czabotar PE, Kluck RM. Molecular biology of Bax and Bak activation and action. Biochim Biophys Acta - Mol Cell Res [Internet]. 2011;1813(4):521–31. Available from: http://dx.doi.org/10.1016/j.bbamcr.2010.12.019

49. Hassin D, Garber OG, Meiraz A, Schiffenbauer YS, Berke G. Cytotoxic T lymphocyte perforin and Fas ligand working in concert even when Fas ligand lytic action is still not detectable. Immunology [Internet]. 2011 Jun [cited 2013 Nov 12];133(2):190–6. Available from: http://www.pubmedcentral.nih.gov/articlerender.fcgi?artid=3088981&tool=pmcentrez&rendertype=abstract

50. Kaiserman D, Bird CH, Sun J, Matthews A, Ung K, Whisstock JC, et al. The major human and mouse granzymes are structurally and functionally divergent. J Cell Biol. 2006;175(4):619–30.

51. Lieberman J. The ABCs of granule-mediated cytotoxicity: new weapons in the arsenal. Nat Rev Immunol [Internet]. 2003 May [cited 2013 Nov 16];3(5):361–70. Available from: http://www.ncbi.nlm.nih.gov/pubmed/12766758

52. Sutton VR, Davis JE, Cancilla M, Johnstone RW, Ruefli a a, Sedelies K, et al. Initiation of apoptosis by granzyme B requires direct cleavage of bid, but not direct granzyme B-mediated caspase activation. J Exp Med [Internet]. 2000 Nov 20;192(10):1403–14. Available from: http://www.pubmedcentral.nih.gov/articlerender.fcgi?artid=2193191&tool=pmcentrez&rendertype=abstract

53. Metkar SS, Wang B, Ebbs ML, Kim JH, Lee YJ, Raja SM, et al. Granzyme B activates procaspase-3 which signals a mitochondrial amplification loop for maximal apoptosis. J Cell Biol [Internet]. 2003 Mar 17 [cited 2013 Dec 3];160(6):875–85. Available from: http://www.pubmedcentral.nih.gov/articlerender.fcgi?artid=2173758&tool

=pmcentrez&rendertype=abstract

54. Dotiwala F, Mulik S, Polidoro RB, Ansara JA, Burleigh BA, Walch M, et al. Killer lymphocytes use granulysin, perforin and granzymes to kill intracellular parasites. Nat Med. 2016;22(2):210–6.

55. Walch M, Dotiwala F, Mulik S, Thiery J, Kirchhausen T, Clayberger C, et al. Cytotoxic Cells Kill Intracellular Bacteria through Granulysin-Mediated Delivery of Granzymes. Cell [Internet]. 2014 Jun [cited 2014 Jun 5];157(6):1309–23. Available from: http://linkinghub.elsevier.com/retrieve/pii/S0092867414005923

56. Law RHP, Lukoyanova N, Voskoboinik I, Caradoc-Davies TT, Baran K, Dunstone MA, et al. The structural basis for membrane binding and pore formation by lymphocyte perforin. Nature [Internet]. 2010 Nov 18 [cited 2012 Mar 20];468(7322):447–51. Available from: http://www.ncbi.nlm.nih.gov/pubmed/21037563

57. Keefe D, Shi L, Feske S, Massol R, Navarro F, Kirchhausen T, et al. Perforin triggers a plasma membrane-repair response that facilitates CTL induction of apoptosis. Immunity [Internet]. 2005 Sep [cited 2012 Mar 23];23(3):249–62. Available from: http://www.ncbi.nlm.nih.gov/pubmed/16169498

58. Thiery J, Keefe D, Boulant S, Boucrot E, Walch M, Martinvalet D, et al. Perforin pores in the endosomal membrane trigger the release of endocytosed granzyme B into the cytosol of target cells. Nat Immunol [Internet]. 2011 Aug [cited 2014 Aug 8];12(8):770–7. Available from: http://www.pubmedcentral.nih.gov/articlerender.fcgi?artid=3140544&tool=pmcentrez&rendertype=abstract

59. Lopez JA, Susanto O, Jenkins MR, Lukoyanova N, Sutton VR, Law RHPP, et al. Perforin forms transient pores on the target cell plasma membrane to facilitate rapid access of granzymes during killer cell attack. Blood [Internet]. 2013 Apr 4 [cited 2013 Nov 22];121(14):2659–68. Available from: http://www.ncbi.nlm.nih.gov/pubmed/23377437

60. Pipkin ME, Lieberman J. Delivering the kiss of death: progress on understanding how perforin works. Curr Opin Immunol. 2007;19(3):301–8.

61. Smyth MJ, Street SEA, Trapani JA. Cutting edge: granzymes A and B are not essential for perforin-mediated tumor rejection. J Immunol [Internet]. 2003 Jul 15;171(2):515–8. Available from: http://www.jimmunol.org/cgi/doi/10.4049/jimmunol.171.2.515

62. Kägi D, Ledermann B, Bürki K, Seiler P, Odermatt B, Olsen KJ, et al. Cytotoxicity mediated by T cells and natural killer cells is greatly impaired in perforin-deficient mice. Nature [Internet]. 1994;369(6475):31–7. Available from:

http://www.nature.com/doifinder/10.1038/369031a0

63. van den Broek ME, Kägi D, Ossendorp F, Toes R, Vamvakas S, Lutz WK, et al. Decreased tumor surveillance in perforin-deficient mice. J Exp Med [Internet]. 1996 Nov 1;184(5):1781–90. Available from: http://www.ncbi.nlm.nih.gov/pubmed/8920866

64. Stepp SE, Dufourcq-Lagelouse R, Le Deist F, Bhawan S, Certain S, Mathew PA, et al. Perforin gene defects in familiar hemophagocytic lymphohistiocytosis. Science (80-). 1999;286(5446):1957–9.

65. Matloubian M, Suresh M, Glass A, Galvan M, Chow K, Whitmire JK, et al. A role for perforin in downregulating T-cell responses during chronic viral infection. J Virol [Internet]. 1999 Mar;73(3):2527–36. Available from: http://www.ncbi.nlm.nih.gov/pubmed/9971838

66. Katano H, Cohen JI. Perforin and lymphohistiocytic proliferative disorders. Br J Haematol [Internet]. 2005 Mar;128(6):739–50. Available from: http://doi.wiley.com/10.1111/j.1365-2141.2004.05305.x

67. Aivazian D, Stern LJ. Phosphorylation of T cell receptor ζ is regulated by a lipid dependent folding transition. Nat Struct Biol. 2000;7(11):1023–6.

68. Kim ST, Takeuchi K, Sun ZYJ, Touma M, Castro CE, Fahmy A, et al. The αβ T cell receptor is an anisotropic mechanosensor. J Biol Chem. 2009;284(45):31028–37.

69. Liu B, Chen W, Evavold BD, Zhu C. Accumulation of dynamic catch bonds between TCR and agonist peptide-MHC triggers T cell signaling. Cell [Internet]. 2014 Apr 10 [cited 2014 Jul 10];157(2):357–68. Available from: http://www.cell.com/article/S0092867414003419/fulltext

70. Ritter AT, Asano Y, Stinchcombe JC, Dieckmann NMG, Chen BC, Gawden-Bone C, et al. Actin Depletion Initiates Events Leading to Granule Secretion at the Immunological Synapse. Immunity [Internet]. 2015;42(5):864–76. Available from: http://dx.doi.org/10.1016/j.immuni.2015.04.013

71. Bashour KT, Gondarenko A, Chen H, Shen K, Liu X, Huse M, et al. CD28 and CD3 have complementary roles in T-cell traction forces. Proc Natl Acad Sci [Internet]. 2014 Jan 27 [cited 2014 Jan 30];111(6):2241–6. Available from: http://www.ncbi.nlm.nih.gov/pubmed/24469820

72. O'Connor RS, Hao X, Shen K, Bashour K, Akimova T, Hancock WW, et al. Substrate Rigidity Regulates Human T Cell Activation and Proliferation. J Immunol [Internet]. 2012;189(3):1330–9. Available from: http://www.jimmunol.org/cgi/doi/10.4049/jimmunol.1102757

73. Judokusumo E, Tabdanov E, Kumari S, Dustin ML, Kam LC. Mechanosensing in T lymphocyte activation. Biophys J [Internet].

2012;102(2):L5–7. Available from: http://dx.doi.org/10.1016/j.bpj.2011.12.011

74. BURNET M. Cancer-A Biological Approach. Br Med J [Internet]. 1957 Apr 6;1(5022):779–86. Available from: http://www.ncbi.nlm.nih.gov/pubmed/13404306%0Ahttp://www.pubmedcentral.nih.gov/articlerender.fcgi?artid=PMC1973174

75. Shankaran V, Ikeda H, Bruce AT, White JM, Swanson PE, Old LJ, et al. IFNγ, and lymphocytes prevent primary tumour development and shape tumour immunogenicity. Nature. 2001;410(6832):1107–11.

76. Dunn GP, Bruce AT, Ikeda H, Old LJ, Schreiber RD. Cancer immunoediting: From immunosurveillance to tumor escape. Nat Immunol. 2002;3(11):991–8.

77. Quail DF, Joyce JA. Microenvironmental regulation of tumor progression and metastasis. Nat Med [Internet]. 2013 Nov 1;19(11):1423–37. Available from: http://www.nature.com/articles/nm.3394

78. Gasteiger G, Hemmers S, Firth MA, Le Floc'h A, Huse M, Sun JC, et al. IL-2–dependent tuning of NK cell sensitivity for target cells is controlled by regulatory T cells. J Exp Med [Internet]. 2013 Jun 3;210(6):1167–78. Available from: http://www.jem.org/lookup/doi/10.1084/jem.20122462

79. Bates GJ, Fox SB, Han C, Leek RD, Garcia JF, Harris AL, et al. Quantification of regulatory T cells enables the identification of high-risk breast cancer patients and those at risk of late relapse. J Clin Oncol. 2006;24(34):5373–80.

80. Fu J, Xu D, Liu Z, Shi M, Zhao P, Fu B, et al. Increased Regulatory T Cells Correlate With CD8 T-Cell Impairment and Poor Survival in Hepatocellular Carcinoma Patients. Gastroenterology [Internet]. 2007 Jun;132(7):2328–39. Available from: http://linkinghub.elsevier.com/retrieve/pii/S0016508507006282

81. Frey DM, Droeser RA, Viehl CT, Zlobec I, Lugli A, Zingg U, et al. High frequency of tumor-infiltrating FOXP3 + regulatory T cells predicts improved survival in mismatch repair-proficient colorectal cancer patients. Int J Cancer [Internet]. 2010;2643. Available from: http://doi.wiley.com/10.1002/ijc.24989

82. Harding FA, McArthur JG, Gross JA, Raulet DH, Allison JP. CD28-mediated signalling co-stimulates murine T cells and prevents induction of anergy in T-cell clones. Nature [Internet]. 1992 Apr 16;356(6370):607–9. Available from: http://www.nature.com/doifinder/10.1038/356607a0

83. Krummel MF, Allison JP. CD28 and CTLA-4 have opposing effects on the response of T cells to stimulation. J Exp Med [Internet]. 1995 Aug

1;182(2):459–65. Available from: http://jem.rupress.org/content/182/2/459

84. Walunas TL, Lenschow DJ, Bakker CY, Linsley PS, Freeman GJ, Green JM, et al. CTLA-4 can function as a negative regulator of T cell activation. Immunity [Internet]. 1994 Aug 1;1(5):405–13. Available from: http://www.ncbi.nlm.nih.gov/pubmed/21934098

85. Leach DR, Krummel MF, Allison JP. Enhancement of Antitumor Immunity by CTLA-4 Blockade. Science (80-) [Internet]. 1996;271(5256):1734–6. Available from: http://www.sciencemag.org/cgi/doi/10.1126/science.271.5256.1734

86. Freeman GJ, Long AJ, Iwai Y, Bourque K, Chernova T, Nishimura H, et al. Engagement of the PD-1 immunoinhibitory receptor by a novel B7 family member leads to negative regulation of lymphocyte activation. J Exp Med [Internet]. 2000 Oct 2;192(7):1027–34. Available from: http://www.jem.org/lookup/doi/10.1084/jem.192.7.1027

87. Sheppard K-A, Fitz LJ, Lee JM, Benander C, George JA, Wooters J, et al. PD-1 inhibits T-cell receptor induced phosphorylation of the ZAP70/CD3zeta signalosome and downstream signaling to PKCtheta. FEBS Lett [Internet]. 2004 Sep 10;574(1–3):37–41. Available from: http://www.ncbi.nlm.nih.gov/pubmed/15358536

88. Hui E, Vale RD. In vitro membrane reconstitution of the T-cell receptor proximal signaling network. Nat Struct Mol Biol [Internet]. 2014;21(2):133–42. Available from: http://dx.doi.org/10.1038/nsmb.2762

89. Wolchok JD, Chiarion-Sileni V, Gonzalez R, Rutkowski P, Grob J-J, Cowey CL, et al. Overall Survival with Combined Nivolumab and Ipilimumab in Advanced Melanoma. N Engl J Med [Internet]. 2017;NEJMoa1709684. Available from: http://www.nejm.org/doi/10.1056/NEJMoa1709684

90. Wei SC, Levine JH, Cogdill AP, Zhao Y, Anang NAAS, Andrews MC, et al. Distinct Cellular Mechanisms Underlie Anti-CTLA-4 and Anti-PD-1 Checkpoint Blockade. Cell [Internet]. 2017;170(6):1120–1133.e17. Available from: http://dx.doi.org/10.1016/j.cell.2017.07.024

91. Larkin J, Chiarion-Sileni V, Gonzalez R, Grob JJ, Cowey CL, Lao CD, et al. Combined Nivolumab and Ipilimumab or Monotherapy in Untreated Melanoma. N Engl J Med [Internet]. 2015;373(1):23–34. Available from: http://www.nejm.org/doi/10.1056/NEJMoa1504030

92. Nishino M, Ramaiya NH, Hatabu H, Hodi FS. Monitoring immune-checkpoint blockade: response evaluation and biomarker development. Nat Rev Clin Oncol [Internet]. 2017;14(11):655–68. Available from: http://www.nature.com/doifinder/10.1038/nrclinonc.2017.88

93. Wherry EJ, Kurachi M. Molecular and cellular insights into T cell exhaustion. Nat Rev Immunol [Internet]. 2015;15(8):486–99. Available from: http://www.nature.com/doifinder/10.1038/nri3862

94. Maxwell R, Jackson CM, Lim M. Clinical Trials Investigating Immune Checkpoint Blockade in Glioblastoma. Curr Treat Options Oncol. 2017;18(8).

95. Srivastava S, Riddell SR. Chimeric Antigen Receptor T Cell Therapy: Challenges to Bench-to-Bedside Efficacy. J Immunol [Internet]. 2018;200(2):459–68. Available from: http://www.jimmunol.org/lookup/doi/10.4049/jimmunol.1701155

96. Porter DL, Levine BL, Kalos M, Bagg A, June CH. Chimeric antigen receptor-modified T cells in chronic lymphoid leukemia. N Engl J Med [Internet]. 2011 Aug 25 [cited 2015 Jan 5];365(8):725–33. Available from: http://www.pubmedcentral.nih.gov/articlerender.fcgi?artid=3387277&tool=pmcentrez&rendertype=abstract

97. Grupp SA, June CH. Adoptive Cellular Therapy. In: Dranoff G, editor. Cancer Immunology and Immunotherapy [Internet]. Berlin, Heidelberg: Springer Berlin Heidelberg; 2011. p. 149–72. Available from: https://doi.org/10.1007/82_2010_94

98. Tran E, Turcotte S, Gros A, Robbins PF, Lu Y, Dudley ME, et al. Cancer immunotherapy based on mutation-specific CD4+ T cells in a patient with epithelial cancer. Science [Internet]. 2014 May 9 [cited 2014 Jul 10];344(6184):641–5. Available from: http://www.ncbi.nlm.nih.gov/pubmed/24812403

99. Brudno JN, Kochenderfer JN. Chimeric antigen receptor T-cell therapies for lymphoma. Nat Rev Clin Oncol [Internet]. 2018;15(1):31–46. Available from: http://dx.doi.org/10.1038/nrclinonc.2017.128

100. Morgan RA, Yang JC, Kitano M, Dudley ME, Laurencot CM, Rosenberg SA. Case Report of a Serious Adverse Event Following the Administration of T Cells Transduced With a Chimeric Antigen Receptor Recognizing ERBB2. Mol Ther [Internet]. 2010 Apr;18(4):843–51. Available from: http://dx.doi.org/10.1038/mt.2010.24

101. Bonifant CL, Jackson HJ, Brentjens RJ, Curran KJ. Toxicity and management in CAR T-cell therapy. Mol Ther - Oncolytics [Internet]. 2016;3(February):16011. Available from: http://dx.doi.org/10.1038/mto.2016.11

102. Roybal KT, Rupp LJ, Morsut L, Walker WJ, McNally KA, Park JS, et al. Precision Tumor Recognition by T Cells with Combinatorial Antigen-Sensing Circuits. Cell. 2016;164(4):770–9.

103. Ingber DE. Cellular mechanotransduction: putting all the pieces together again. FASEB J [Internet]. 2006;20(7):811–27. Available from: http://eutils.ncbi.nlm.nih.gov/entrez/eutils/elink.fcgi?dbfrom=pubmed&id=16705083&retmode=ref&cmd=prlinks%5Cnfile:///Users/LizMacari/Library/Application Support/Papers2/Articles/2006/Schlueter/The FASEB Journal 2006 Schlueter.pdf%5Cnpapers2://publication/

104. Orr AW, Helmke BP, Blackman BR, Schwartz MA. Mechanisms of mechanotransduction. Dev Cell. 2006;10(1):11–20.

105. Stinchcombe JC, Griffiths GM. Secretory mechanisms in cell-mediated cytotoxicity. Annu Rev Cell Dev Biol [Internet]. 2007 Jan [cited 2014 Dec 15];23:495–517. Available from: http://www.ncbi.nlm.nih.gov/pubmed/17506701

106. Bertrand F, Muller S, Roh K-H, Laurent C, Dupre L, Valitutti S. An initial and rapid step of lytic granule secretion precedes microtubule organizing center polarization at the cytotoxic T lymphocyte/target cell synapse. Proc Natl Acad Sci [Internet]. 2013;110(15):6073–8. Available from: http://www.pnas.org/cgi/doi/10.1073/pnas.1218640110

107. Le Floc'h A, Huse M. Molecular mechanisms and functional implications of polarized actin remodeling at the T cell immunological synapse. Cell Mol Life Sci [Internet]. 2015 Feb;72(3):537–56. Available from: http://link.springer.com/10.1007/s00018-014-1760-7

108. Bunnell SC, Kapoor V, Trible RP, Zhang W, Samelson LE. Dynamic actin polymerization drives T cell receptor-induced spreading: A role for the signal transduction adaptor LAT. Immunity. 2001;14(3):315–29.

109. Grakoui a, Bromley SK, Sumen C, Davis MM, Shaw a S, Allen PM, et al. The immunological synapse: a molecular machine controlling T cell activation. Science. 1999;285(5425):221–7.

110. Husson J, Chemin K, Bohineust A, Hivroz C, Henry N. Force generation upon T cell receptor engagement. PLoS One. 2011;6(5).

111. Beal AM, Anikeeva N, Varma R, Cameron TO, Vasiliver-Shamis G, Norris PJ, et al. Kinetics of Early T Cell Receptor Signaling Regulate the Pathway of Lytic Granule Delivery to the Secretory Domain. Immunity [Internet]. 2009;31(4):632–42. Available from: http://dx.doi.org/10.1016/j.immuni.2009.09.004

112. Ostergaard HL, Kane KP, Mescher MF, Clark WR. Cytotoxic T lymphocyte mediated lysis without release of serine esterase. Nature [Internet]. 1987;330(6143):71–2. Available from: http://www.nature.com/nature/journal/v330/n6143/abs/330071a0.html%5Cnhttp://www.ncbi.nlm.nih.gov/pubmed/3118212

113. Babich A, Li S, O'Connor RS, Milone MC, Freedman BD, Burkhardt JK.

F-actin polymerization and retrograde flow drive sustained PLCγ1 signaling during T cell activation. J Cell Biol. 2012;197(6):775–87.

114. Jacobelli J, Chmura SA, Buxton DB, Davis MM, Krummel MF. A single class II myosin modulates T cell motility and stopping, but not synapse formation. Nat Immunol. 2004;5(5):531–8.

115. Yi J, Wu XS, Crites T, Hammer JA. Actin retrograde flow and actomyosin II arc contraction drive receptor cluster dynamics at the immunological synapse in Jurkat T cells. Mol Biol Cell [Internet]. 2012;23(5):834–52. Available from: http://www.molbiolcell.org/cgi/doi/10.1091/mbc.E11-08-0731

116. Hammer JA, Burkhardt JK. Controversy and consensus regarding myosin II function at the immunological synapse. Curr Opin Immunol [Internet]. 2013;25(3):300–6. Available from: http://dx.doi.org/10.1016/j.coi.2013.03.010

117. Liu X, Kapoor TM, Chen JK, Huse M. Diacylglycerol promotes centrosome polarization in T cells via reciprocal localization of dynein and myosin II. Proc Natl Acad Sci [Internet]. 2013;110(29):11976–81. Available from: http://www.pnas.org/cgi/doi/10.1073/pnas.1306180110

118. Huang HW, Chen FY, Lee MT. Molecular mechanism of peptide-induced pores in membranes. Phys Rev Lett. 2004;92(19):1–4.

119. Lee M-T, Hung W-C, Chen F-Y, Huang HW. Mechanism and kinetics of pore formation in membranes by water-soluble amphipathic peptides. Proc Natl Acad Sci [Internet]. 2008;105(13):5087–92. Available from: http://www.pnas.org/cgi/doi/10.1073/pnas.0710625105

120. Polozov I V., Anantharamaiah GM, Segrest JP, Epand RM. Osmotically induced membrane tension modulates membrane permeabilization by class L amphipathic helical peptides: Nucleation model of defect formation. Biophys J [Internet]. 2001;81(2):949–59. Available from: http://dx.doi.org/10.1016/S0006-3495(01)75753-0

121. Engler AJ, Sen S, Sweeney HL, Discher DE. Matrix Elasticity Directs Stem Cell Lineage Specification. Cell. 2006;126(4):677–89.

122. Chan CE, Odde DJ. Traction dynamics of filopodia on compliant substrates. Science (80-). 2008;322(5908):1687–91.

123. Hui KL, Balagopalan L, Samelson LE, Upadhyaya A. Cytoskeletal forces during signaling activation in Jurkat T-cells. Mol Biol Cell [Internet]. 2015;26(4):685–95. Available from: http://www.molbiolcell.org/cgi/doi/10.1091/mbc.E14-03-0830

124. Lo CM, Wang HB, Dembo M, Wang YL. Cell movement is guided by the rigidity of the substrate. Biophys J [Internet]. 2000;79(1):144–52.

Available from: http://dx.doi.org/10.1016/S0006-3495(00)76279-5

125. Oakes PW, Patel DC, Morin NA, Zitterbart DP, Fabry B, Reichner JS, et al. Neutrophil morphology and migration are affected by substrate elasticity. Blood. 2009;114(7):1387–95.

126. Houk AR, Jilkine A, Mejean CO, Boltyanskiy R, Dufresne ER, Angenent SB, et al. Membrane tension maintains cell polarity by confining signals to the leading edge during neutrophil migration. Cell [Internet]. 2012;148(1–2):175–88. Available from: http://dx.doi.org/10.1016/j.cell.2011.10.050

127. Lee C-Y, Herant M, Heinrich V. Target-specific mechanics of phagocytosis: protrusive neutrophil response to zymosan differs from the uptake of antibody-tagged pathogens. J Cell Sci [Internet]. 2011;124(7):1106–14. Available from: http://jcs.biologists.org/cgi/doi/10.1242/jcs.078592

128. Masters TA, Pontes B, Viasnoff V, Li Y, Gauthier NC. Plasma membrane tension orchestrates membrane trafficking, cytoskeletal remodeling, and biochemical signaling during phagocytosis. Proc Natl Acad Sci [Internet]. 2013;110(29):11875–80. Available from: http://www.pnas.org/cgi/doi/10.1073/pnas.1301766110

129. Wakatsuki T, Schwab B, Thompson NC, Elson EL. Effects of cytochalasin D and latrunculin B on mechanical properties of cells. J Cell Sci. 2001;114(Pt 5):1025–36.

130. Rak GD, Mace EM, Banerjee PP, Svitkina T, Orange JS. Natural Killer cell lytic granule secretion occurs through a pervasive actin network at the immune synapse. PLoS Biol. 2011;9(9).

131. Dai J, Sheetz MP. Mechanical properties of neuronal growth cone membranes studied by tether formation with laser optical tweezers. Biophys J [Internet]. 1995;68(3):988–96. Available from: http://dx.doi.org/10.1016/S0006-3495(95)80274-2

132. Comrie WA, Babich A, Burkhardt JK. F-actin flow drives affinity maturation and spatial organization of LFA-1 at the immunological synapse. J Cell Biol. 2015;208(4):475–91.

133. Natkanski E, Lee W-Y, Mistry B, Casal A, Molloy JE, Tolar P. B Cells Use Mechanical Energy to Discriminate Antigen Affinities. Science (80-) [Internet]. 2013 Jun 28;340(6140):1587–90. Available from: http://www.sciencemag.org/cgi/doi/10.1126/science.1237572

134. Stinchcombe JC, Griffiths GM. Secretory Mechanisms in Cell-Mediated Cytotoxicity. Annu Rev Cell Dev Biol [Internet]. 2007;23(1):495–517. Available from: http://www.annualreviews.org/doi/10.1146/annurev.cellbio.23.090506.12

3521

135. Woodsworth DJ, Dunsing V, Coombs D. Design Parameters for Granzyme-Mediated Cytotoxic Lymphocyte Target-Cell Killing and Specificity. Biophys J [Internet]. 2015;109(3):477–88. Available from: http://dx.doi.org/10.1016/j.bpj.2015.06.045

136. Feinerman O, Jentsch G, Tkach KE, Coward JW, Hathorn MM, Sneddon MW, et al. Single-cell quantification of IL-2 response by effector and regulatory T cells reveals critical plasticity in immune response. Mol Syst Biol [Internet]. 2010 Nov 30 [cited 2013 Aug 14];6:437. Available from: http://www.pubmedcentral.nih.gov/articlerender.fcgi?artid=3010113&tool=pmcentrez&rendertype=abstract

137. Müller AJ, Filipe-Santos O, Eberl G, Aebischer T, Späth GF, Bousso P. CD4+ T Cells Rely on a Cytokine Gradient to Control Intracellular Pathogens beyond Sites of Antigen Presentation. Immunity [Internet]. 2012 Jun; Available from: http://linkinghub.elsevier.com/retrieve/pii/S1074761312002282

138. Sanderson NSR, Puntel M, Kroeger KM, Bondale NS, Swerdlow M, Iranmanesh N, et al. Cytotoxic immunological synapses do not restrict the action of interferon-γ to antigenic target cells. Proc Natl Acad Sci U S A [Internet]. 2012 Apr 30 [cited 2012 May 12];109(20):7835–40. Available from: http://www.ncbi.nlm.nih.gov/pubmed/22547816

139. Diz-Muñoz A, Fletcher DA, Weiner OD. Use the force: Membrane tension as an organizer of cell shape and motility. Trends Cell Biol. 2013;23(2):47–53.

140. Dustin ML, Chakraborty AK, Shaw AS. Understanding the structure and function of the immunological synapse. Cold Spring HarbPerspectBiol. 2010;2(1943–0264 (Electronic)):a002311.

141. Brown ACN, Oddos S, Dobbie IM, Alakoskela JM, Parton RM, Eissmann P, et al. Remodelling of cortical actin where lytic granules dock at Natural Killer cell immune synapses revealed by super-resolution microscopy. PLoS Biol. 2011;9(9).

142. Paszek MJ, Zahir N, Johnson KR, Lakins JN, Rozenberg GI, Gefen A, et al. Tensional homeostasis and the malignant phenotype. Cancer Cell. 2005;8(3):241–54.

143. Rabinovich GA, Gabrilovich D, Sotomayor EM. Immunosuppressive Strategies that are Mediated by Tumor Cells. Annu Rev Immunol [Internet]. 2007;25(1):267–96. Available from: http://www.annualreviews.org/doi/10.1146/annurev.immunol.25.022106.141609

144. Guck J, Schinkinger S, Lincoln B, Wottawah F, Ebert S, Romeyke M, et

al. Optical deformability as an inherent cell marker for testing malignant transformation and metastatic competence. Biophys J. 2005;88(5):3689–98.

145. Hou HW, Li QS, Lee GYH, Kumar AP, Ong CN, Lim CT. Deformability study of breast cancer cells using microfluidics. Biomed Microdevices. 2009;11(3):557–64.

146. Xu W, Mezencev R, Kim B, Wang L, McDonald J, Sulchek T. Cell Stiffness Is a Biomarker of the Metastatic Potential of Ovarian Cancer Cells. PLoS One. 2012;7(10).

147. Sage PT, Varghese LM, Martinelli R, Sciuto TE, Kamei M, Dvorak AM, et al. Antigen Recognition Is Facilitated by Invadosome-like Protrusions Formed by Memory/Effector T Cells. J Immunol [Internet]. 2012;188(8):3686–99. Available from: http://www.jimmunol.org/cgi/doi/10.4049/jimmunol.1102594

148. Ueda H, Morphew MK, McIntosh JR, Davis MM. CD4+ T-cell synapses involve multiple distinct stages. Proc Natl Acad Sci [Internet]. 2011;108(41):17099–104. Available from: http://www.pnas.org/cgi/doi/10.1073/pnas.1113703108

149. Quann EJ, Merino E, Furuta T, Huse M. Localized diacylglycerol drives the polarization of the microtubule-organizing center in T cells. Nat Immunol. 2009;10(6):627–35.

150. Thiery J, Walch M, Jensen DK, Martinvalet D, Lieberman J. Isolation of cytotoxic T cell and NK granules and purification of their effector proteins. Curr Protoc Cell Biol [Internet]. 2010 Jun [cited 2014 Feb 12];Chapter 3:Unit3.37. Available from: http://www.ncbi.nlm.nih.gov/pubmed/20521234

151. Dobrzanski MJ, Reome JB, Dutton RW. Therapeutic effects of tumor-reactive type 1 and type 2 CD8+ T cell subpopulations in established pulmonary metastases. J Immunol [Internet]. 1999 Jun 1;162(11):6671–80. Available from: http://www.ncbi.nlm.nih.gov/pubmed/10352285

152. Brown DM, Fisher TL, Wei C, Frelinger JG, Lord EM. Tumours can act as adjuvants for humoral immunity. Immunology [Internet]. 2001 Apr;102(4):486–97. Available from: http://doi.wiley.com/10.1046/j.1365-2567.2001.01213.x

153. Locke FL, Zha Y, Zheng Y, Driessens G, Gajewski TF. Conditional deletion of PTEN in peripheral T cells augments TCR-mediated activation but does not abrogate CD28 dependency or prevent anergy induction. J Immunol [Internet]. 2013;191(4):1677–85. Available from: http://www.pubmedcentral.nih.gov/articlerender.fcgi?artid=3759681&tool=pmcentrez&rendertype=abstract%5Cnhttp://www.ncbi.nlm.nih.gov/pubmed/23851688

154. Platt RJ, Chen S, Zhou Y, Yim MJ, Swiech L, Kempton HR, et al. CRISPR-Cas9 knockin mice for genome editing and cancer modeling. Cell [Internet]. 2014;159(2):440–55. Available from: http://dx.doi.org/10.1016/j.cell.2014.09.014

155. Lesche R, Groszer M, Gao J, Wang Y, Messing A, Sun H, et al. Cre/loxP-mediated inactivation of the murine Pten tumor suppressor gene. Genesis. 2002;32(2):148–9.

156. Kim EH, Sullivan JA, Plisch EH, Tejera MM, Jatzek A, Choi KY, et al. Signal Integration by Akt Regulates CD8 T Cell Effector and Memory Differentiation. J Immunol [Internet]. 2012;188(9):4305–14. Available from: http://www.jimmunol.org/cgi/doi/10.4049/jimmunol.1103568

157. Finlay DK, Sinclair L V, Feijoo C, Waugh CM, Hagenbeek TJ, Spits H, et al. Phosphoinositide-dependent kinase 1 controls migration and malignant transformation but not cell growth and proliferation in PTEN-null lymphocytes. J Exp Med. 2009;206(11):2441–54.

158. Jameson SC. Maintaining the norm: T-cell homeostasis. Nat Rev Immunol [Internet]. 2002 Aug;2(8):547–56. Available from: http://www.nature.com/articles/nri853

159. Sabatini DM, Erdjument-Bromage H, Lui M, Tempst P, Snyder SH. RAFT1: A mammalian protein that binds to FKBP12 in a rapamycin-dependent fashion and is homologous to yeast TORs. Cell. 1994;78(1):35–43.

160. Saxton RA, Sabatini DM. mTOR Signaling in Growth, Metabolism, and Disease. Cell [Internet]. 2017;168(6):960–76. Available from: http://dx.doi.org/10.1016/j.cell.2017.02.004

161. Boyman O, Krieg C, Homann D, Sprent J. Homeostatic maintenance of T cells and natural killer cells. Cell Mol Life Sci. 2012;69(10):1597–608.

162. Mazurier F, Fontanellas A, Salesse S, Taine L, Landriau S, Moreau-Gaudry F, et al. A novel immunodeficient mouse model--RAG2 x common cytokine receptor gamma chain double mutants--requiring exogenous cytokine administration for human hematopoietic stem cell engraftment. J Interferon Cytokine Res [Internet]. 1999 May;19(5):533–41. Available from: http://www.liebertonline.com/doi/abs/10.1089/107999099313983

163. Araki K, Turner AP, Shaffer VO, Gangappa S, Keller SA, Bachmann MF, et al. mTOR regulates memory CD8 T-cell differentiation. Nature [Internet]. 2009;460(7251):108–12. Available from: http://www.nature.com/doifinder/10.1038/nature08155

164. Zhang X, Sun S, Hwang I, Tough DF, Sprent J. Potent and selective stimulation of memory-phenotype CD8+ T cells in vivo by IL-15.

Immunity [Internet]. 1998;8(5):591–9. Available from: http://www.ncbi.nlm.nih.gov/pubmed/9620680

165. Sawa Y, Arima Y, Ogura H, Kitabayashi C, Jiang JJ, Fukushima T, et al. Hepatic Interleukin-7 Expression Regulates T Cell Responses. Immunity [Internet]. 2009;30(3):447–57. Available from: http://dx.doi.org/10.1016/j.immuni.2009.01.007

166. Chen CC, Jeon SM, Bhaskar PT, Nogueira V, Sundararajan D, Tonic I, et al. FoxOs Inhibit mTORC1 and Activate Akt by Inducing the Expression of Sestrin3 and Rictor. Dev Cell [Internet]. 2010;18(4):592–604. Available from: http://dx.doi.org/10.1016/j.devcel.2010.03.008

167. Luo CT, Liao W, Dadi S, Toure A, Li MO. Graded Foxo1 activity in Treg cells differentiates tumour immunity from spontaneous autoimmunity. Nature [Internet]. 2014;529(7587):121–36. Available from: http://www.pubmedcentral.nih.gov/articlerender.fcgi?artid=4522873&tool=pmcentrez&rendertype=abstract%5Cnhttp://www.ncbi.nlm.nih.gov/pubmed/24378538%5Cnhttp://www.nature.com/doifinder/10.1038/nature16486

168. Shaner NC, Lin MZ, McKeown MR, Steinbach PA, Hazelwood KL, Davidson MW, et al. Improving the photostability of bright monomeric orange and red fluorescent proteins. Nat Methods. 2008;5(6):545–51.

169. Fellmann C, Hoffmann T, Sridhar V, Hopfgartner B, Muhar M, Roth M, et al. An Optimized microRNA Backbone for Effective Single-Copy RNAi. Cell Rep [Internet]. 2013;5(6):1704–13. Available from: http://linkinghub.elsevier.com/retrieve/pii/S2211124713006876

170. Haeussler M, Schönig K, Eckert H, Eschstruth A, Mianné J, Renaud JB, et al. Evaluation of off-target and on-target scoring algorithms and integration into the guide RNA selection tool CRISPOR. Genome Biol [Internet]. 2016;17(1):1–12. Available from: http://dx.doi.org/10.1186/s13059-016-1012-2

171. Shalem O, Sanjana NE, Hartenian E, Shi X, Scott DA, Mikkelsen TS, et al. Genome-scale CRISPR-Cas9 knockout screening in human cells. Science (80-). 2014;343(6166):84–7.

172. Sanjana NE, Shalem O, Zhang F. Improved vectors and genome-wide libraries for CRISPR screening. Nat Methods [Internet]. 2014;11(8):783–4. Available from: http://dx.doi.org/10.1038/nmeth.3047

173. Ringer P, Weißl A, Cost AL, Freikamp A, Sabass B, Mehlich A, et al. Multiplexing molecular tension sensors reveals piconewton force gradient across talin-1. Nat Methods. 2017;14(11):1090–6.

174. Wu J, Lewis AH, Grandl J. Touch, Tension, and Transduction - The Function and Regulation of Piezo Ion Channels. Trends Biochem Sci

[Internet]. 2017;42(1):57–71. Available from: http://dx.doi.org/10.1016/j.tibs.2016.09.004

175. Opsahl LR, Webb WW. Transduction of membrane tension by the ion channel alamethicin. Biophys J [Internet]. 1994 Jan;66(1):71–4. Available from: http://dx.doi.org/10.1016/S0006-3495(94)80751-9

176. Baitsch L, Legat A, Barba L, Marraco SA, Rivals JP, Baumgaertner P, et al. Extended co-expression of inhibitory receptors by human CD8 T-cells depending on differentiation, antigen-specificity and anatomical localization. PLoS One. 2012;7(2):1–10.

177. Lin S-J, Peacock CD, Bahl K, Welsh RM. Programmed death-1 (PD-1) defines a transient and dysfunctional oligoclonal T cell population in acute homeostatic proliferation. J Exp Med [Internet]. 2007;204(10):2321–33. Available from: http://www.jem.org/lookup/doi/10.1084/jem.20062150